12-2010

Mitochondrial Regulation of Arterial Contractility

Damodaran Narayanan
University of Tennessee Health Science Center

Mitochondrial Regulation of Arterial Contractility

DOI
10.21007/etd.cghs.2010.0223

MITOCHONDRIAL REGULATION OF ARTERIAL CONTRACTILITY

A Dissertation
Presented for
The Graduate Studies Council
The University of Tennessee
Health Science Center

In Partial Fulfillment
Of the Requirements for the Degree
Doctor of Philosophy
From The University of Tennessee

By
Damodaran Narayanan
December 2010

DEDICATION

I dedicate this dissertation to my parents Narayanan Deenadayalan and Lakshmi Narayanan for their endless love and support.

ACKNOWLEDGMENTS

I would like to thank my advisor Dr. Jonathan H. Jaggar for the motivation, intellectual guidance, encouragement, support, and many opportunities he has offered during my Ph.D. training. He has taught me how to think scientifically and present my research professionally. I am extremely grateful to him for the graduate education he has provided me and for instilling in me the qualities of a good scientific investigator.

I extend my gratitude to my dissertation advisory committee members Drs. Charles W. Leffler, Rennolds S. Ostrom, Radhakrishna Rao, and Christopher M. Waters for their valuable guidance, assistance, and suggestions throughout my project. Special thanks to Dr. Lawrence M. Pfeffer for his advice, guidance, and constructive criticism.

I would like to show my appreciation for all the members of Dr. Jaggar's laboratory for their help and suggestions. I would like to thank Dr. Lidia Gardner for her technical advice. I also like to thank late Mr. Gerwin and Mrs. Gerwin for awarding me the Graduate Scholarship, which motivated me a lot. Thanks to the American Heart Association for awarding me the predoctoral fellowship.

I would also like to thank Mr. Larry Tague, Ms. Shirley Hancock and the ETD group for help in formatting this dissertation. I sincerely thank all my friends and colleagues in Memphis for their support and camaraderie over the years.

I would like to thank the University of Tennessee Health Science Center for providing me with the opportunity to pursue graduate education. I am also grateful to the administrative staff of the Department of Physiology and the College of Graduate Health Science for all their help and cooperation.

I express my sincere gratitude and appreciation to Mr. N.V. Reddy for his inspiration. I am forever indebted to my father, mother, and brother for their unconditional love, patience, and support during my graduate education. Finally, I would like to thank God for everything that I have achieved today.

ABSTRACT

Rationale: Physiological functions of mitochondria in contractile arterial smooth muscle cells are poorly understood. Mitochondria can uptake calcium (Ca^{2+}), but intracellular Ca^{2+} signals that regulate mitochondrial Ca^{2+} concentration ($[Ca^{2+}]_{mito}$) and physiological functions of changes in $[Ca^{2+}]_{mito}$ in arterial smooth muscle cells are unclear.

Objective: Identify Ca^{2+} signals that regulate $[Ca^{2+}]_{mito}$, examine the significance of changes in $[Ca^{2+}]_{mito}$, and test the hypothesis that $[Ca^{2+}]_{mito}$ controls functional ion channel transcription in smooth muscle cells of resistance-size cerebral arteries.

Methods and Results: Endothelin-1 (ET-1) activated Ca^{2+} waves and elevated global Ca^{2+} concentration ($[Ca^{2+}]_i$) via inositol 1,4,5-triphosphate receptor (IP_3R) activation. IP_3R-mediated sarcoplasmic reticulum (SR) Ca^{2+} release increased $[Ca^{2+}]_{mito}$ and induced mitochondrial depolarization, which stimulated mitochondrial reactive oxygen species (mitoROS) generation that elevated cytosolic ROS. In contrast, a global $[Ca^{2+}]_i$ elevation did not alter $[Ca^{2+}]_{mito}$, mitochondrial potential, or mitoROS generation. ET-1 stimulated nuclear translocation of nuclear factor kappa B (NF-κB) p50 subunit and ET-1-induced IP_3R-mediated mitoROS elevated NF-κB-dependent transcriptional activity. ET-1 elevated voltage-dependent Ca^{2+} ($Ca_V1.2$) channel expression, leading to an increase in both pressure (myogenic tone)- and depolarization-induced vasoconstriction. Baseline $Ca_V1.2$ expression and the ET-1-induced elevation in $Ca_V1.2$ expression were both reduced by IP_3R inhibition, mitochondrial electron transport chain block, antioxidant treatment, and NF-κB subunit knockdown, leading to vasodilation.

Conclusions: IP_3R-mediated SR Ca^{2+} release elevates $[Ca^{2+}]_{mito}$, which induces mitoROS generation. MitoROS activate NF-κB, which stimulates $Ca_V1.2$ channel transcription. Thus, mitochondria sense IP_3R-mediated SR Ca^{2+} release to control NF-κB-dependent $Ca_V1.2$ channel expression in arterial smooth muscle cells, thereby modulating arterial contractility.

TABLE OF CONTENTS

LIST OF FIGURES

LIST OF ABBREVIATIONS

ψ_m	Mitochondrial membrane potential
ADP	Adenosine 5'-diphosphate
Ang II	Angiotensin II
ANT	Adenine nucleotide translocase
AP-1	Activator protein 1
ATP	Adenosine 5'-triphosphate
ATPase	Adenosine 5'-triphosphatase
Ba^{2+}	Barium
BES	N,N-bis(2-hydroxyethyl)-2-aminoethanesulfonic acid
BH_4	Tetrahydrobiopterin
BSA	Bovine serum albumin
Ca^{2+}	Calcium
$[Ca^{2+}]_i$	Intracellular Ca^{2+} concentration
$[Ca^{2+}]_{mito}$	Mitochondrial Ca^{2+} concentration
cADPR	Cyclic ADP ribose
CaM	Calmodulin
$Ca_V1.2$	L-type voltage-dependent Ca^{2+} channel
CCCP	Carbonyl cyanide 3-chlorophenylhydrazone
Cl^-	Chloride
Cl_{Ca} channel	Ca^{2+}-activated Cl^- channel
CM-H_2DCFDA	5-(and-6)-chloromethyl-2',7'-dichlorodihydrofluorescein diacetate
cpYFP	Circularly permuted YFP
CREB	Cyclic AMP response element-binding protein
CT	Fluorescence threshold
CYP450	Cytochrome P450
CypD	Cyclophilin D
DAG	Diacylglycerol
DCF	Dichlorofluorescin
DMEM	Dulbecco's modified eagle medium
eNOS	Endothelial NOS
ER	Endoplasmic reticulum
ET-1	Endothelin-1
ETC	Electron transport chain
F	Fluorescence
F_0	Baseline fluorescence
FBS	Fetal bovine serum
FKBP	FK-506 binding protein
GFP	Green fluorescent protein
gp91ds-tat	$gp91^{phox}$ docking sequence peptide conjugated to tat
gp91scrm-tat	Scrambled $gp91^{phox}$ peptide conjugated to tat
H^+	Hydrogen
H_2DCF	Dichlorodihydrofluorescein
H_2O_2	Hydrogen peroxide

HEK293 cells	Human embryonic kidney 293 cells
HGPRT	Hypoxanthine-guanine phosphoribosyltransferase
HIF-1α	Hypoxia-inducible factor-1 alpha
HOCl	Hypochlorous acid
I_{Cat}	Non-selective cation current
IκB	I kappa B
IKK	IκB kinase
IL	Interleukin
iNOS	Inducible NOS
IP_3	Inositol 1,4,5-triphosphate
$[IP_3]_i$	Intracellular IP_3 concentration
IP_3R	IP_3 receptor
K^+	Potassium
K_{Ca} channel	Large conductance Ca^{2+}-activated potassium channel
kDa	Kilodalton
MCP-1	Monocyte chemoattractant protein-1
MCU	Mitochondrial Ca^{2+} uniporter
Mg^{2+}	Magnesium
mitoROS	Mitochondrial reactive oxygen species
MLC20	Myosin light chains
Mn^{2+}	Manganese
mNCX	Mitochondrial Na^+/Ca^{2+} exchanger
MnTMPyP	Manganese (III) tetrakis(1-methyl-4-pyridyl)porphyrin
mPTP	Mitochondrial permeability transition pore
Na^+	Sodium
NAADP	Nicotinic acid adenine dinucleotide phosphate
NADH	Nicotinamide adenine dinucleotide
NCX	Plasma membrane Na^+/Ca^{2+} exchanger
NE	Norepinephrine
NF-κB	Nuclear factor kappa B
NF-κB-p-Luc	Firefly luciferase vectors under the control of an NF-κB promoter
NFAT	Nuclear factor of activated T cell
NLS	Nuclear localization signal
NO	Nitric oxide
NOS	NO synthase
nNOS	Neuronal NOS
O_2	Molecular oxygen
$O_2^{-}\cdot$	Superoxide
OH·	Hydroxyl radical
ONOO·	Peroxynitrite
p105	NF-κB p105 subunit
p105siRNA	siRNA directed against NF-κB p105 subunit
p105scrm	Scrambled siRNA
p50	NF-κB p50 subunit
PBS	Phosphate-buffered saline
PDGF	Platelet-derived growth factor

Pi	Inorganic phosphate
PIP_2	Phosphatidylinositol 4,5-biphosphate
PK	Protein kinase
PKCα	Protein kinase C alpha
PKCδ	Protein kinase C delta
PLC	Phospholipase C
PLN	Phospholamban
PMCA	Plasma membrane Ca^{2+}-ATPase
PSS	Physiological salt solution
$QH\cdot$	Ubisemiquinone radical intermediate
RaM	Rapid uptake mode
RNaseA	Ribonuclease A
ROCC	Receptor-operated Ca^{2+} channel
ROS	Reactive oxygen species
Rps5	Ribosomal protein subunit 5
RT-PCR	Real-time polymerase chain reaction
RyR	Ryanodine-sensitive Ca^{2+} channel
S1P	Sphingosine-1-phosphate
SCaMPER	Sphingolipid Ca^{2+}-release-mediating protein of ER
SERCA	Sarcoplasmic/endoplasmic reticulum Ca^{2+} ATPase
siRNA	Small interfering RNA
SOCC	Store-operated Ca^{2+} channel
SOD	Superoxide dismutase
Sr^{2+}	Strontium
SR	Sarcoplasmic reticulum
STIM1	Stromal interaction molecule 1
TBS	Tris-buffered solution
TBS-T	TBS with 0.1% tween-20
TMRM	Tetramethylrhodamine methyl ester
TNF-α	Tumor necrosis factor-alpha
TRP channel	Transient receptor potential channel
UQ	Ubiquinone
UTP	Uridine 5'-triphosphate
VDAC	Voltage-dependent anion channel
VDCC	Voltage-dependent Ca^{2+} channel
VEGF	Vascular endothelial growth factor
XDH	Xanthine dehydrogenase
XeC	Xestospongin C.
XO	Xanthine oxidase
YFP	Yellow fluorescent protein
$^1O_2$	Singlet oxygen
17-ODYA	17-octadecynoic acid

CHAPTER 1. INTRODUCTION*

1.1. Ca^{2+} Signaling in Vascular Smooth Muscle Cells

Calcium (Ca^{2+}) is a highly versatile signal transduction element in almost every cell type, controlling a wide variety of functions (Berridge, 2001; Bootman *et al.*, 2001; Berridge, 2004). Ca^{2+} translates an array of extracellular stimuli, including hormones, neurotransmitters, and growth factors into distinct intracellular functions, varying from contraction to secretion, and from survival to differentiation. Under resting conditions, cytosolic Ca^{2+} concentration ($[Ca^{2+}]_i$) is maintained at ~100 nM, whereas the extracellular medium and intracellular stores contain more than 1 mM (Rizzuto & Pozzan, 2006). The difference in concentrations permits stimulation of rapid Ca^{2+} signals, to regulate various cellular responses. Under resting conditions, $[Ca^{2+}]_i$ is influenced by the regulation of several processes, which either introduce Ca^{2+} into or remove Ca^{2+} from the entire cytosol or a localized region of the cytosol (Bootman *et al.*, 2001). Stimuli that elevate $[Ca^{2+}]_i$ cause Ca^{2+} influx from extracellular space and/or Ca^{2+} release from internal sources. Most of this Ca^{2+} is bound to buffers, whereas a small proportion of the Ca^{2+} binds to effector elements, leading to stimulation of numerous Ca^{2+}-dependent processes (Berridge *et al.*, 1998). Removal of Ca^{2+} from the cytosol occurs via various plasma membrane exchangers, which extrude Ca^{2+} into the extracellular space, or intracellular pumps, which recycle Ca^{2+} back into organelles (Berridge *et al.*, 1998). Interplay between these opposing processes is responsible for the maintenance of $[Ca^{2+}]_i$ and modulation of Ca^{2+}-dependent functions (Bootman *et al.*, 2001).

To influence different cellular functions, Ca^{2+} signals are flexibly and precisely regulated with regard to space, time, and amplitude (Berridge *et al.*, 1998). Spatial distribution of Ca^{2+} signals occur due to differences in Ca^{2+}sources, including Ca^{2+} entry from extracellular medium through plasma membrane ion channels, and Ca^{2+} release from internal stores (Berridge *et al.*, 2003). Diffusion of Ca^{2+} from one cellular compartment to another, and localization of a Ca^{2+} signal to a specific cellular region also contribute to spatial heterogeneity. Temporal organization of Ca^{2+} signals occurs by modulation of the frequency of Ca^{2+} signals, leading to variations in intensity and nature of cellular process (Berridge *et al.*, 2003). Changes in amplitude or concentration of Ca^{2+} also serve to differentially influence specific functions. The spatiotemporal organization of Ca^{2+} signals influences the diversity of Ca^{2+} signals, controls recruitment of different intracellular components, and regulation of specific cellular functions (Berridge, 2001; Bootman *et al.*, 2001; Berridge, 2004).

* Portions of this chapter adapted with permission. Narayanan D, Xi Q, Pfeffer LM, & Jaggar JH (2010). Mitochondria control functional $Ca_V1.2$ expression in smooth muscle cells of cerebral arteries. *Circ Res* **107**, 631-641.

1.2. Ca^{2+} Transport Mechanisms across Plasma Membrane

Ca^{2+} entry from the extracellular medium occurs through plasma membrane ion channels in response to a wide variety of stimuli, including membrane depolarization, stretch, noxious stimuli, extracellular agonists, intracellular messengers, and the depletion of intracellular stores (Berridge *et al.*, 2003). Under physiological conditions, the membrane potential of smooth muscle cells from resistance-size arteries is ~45 mV (Knot & Nelson, 1998). The negative membrane potential, coupled with a high extracellular Ca^{2+} concentration creates a considerable electrochemical gradient across the plasma membrane, which drives Ca^{2+} entry through ion channels on the plasma membrane. Based on the mechanism of activation, several different types of Ca^{2+} influx channels have been found in vascular smooth muscle cells – voltage-dependent Ca^{2+} channels (VDCCs), receptor-operated Ca^{2+} channels (ROCCs), and store-operated Ca^{2+} channels (SOCCs) (Bootman *et al.*, 2001). Two Ca^{2+} efflux mechanisms that exist are the plasma membrane Ca^{2+}-adenosine 5'-triphosphatase (ATPase) (PMCA) and sodium (Na^+)/Ca^{2+} exchanger (NCX).

1.2.1. Voltage-dependent Ca^{2+} channels

VDCCs open in response to membrane depolarization, permitting rapid Ca^{2+} entry to regulate numerous physiological functions, including excitation–contraction coupling, excitation-secretion coupling, neurotransmitter release, gene expression, and hormone secretion (Halling *et al.*, 2005; Liao *et al.*, 2005). VDCCs are hetero-oligomeric protein complexes, composed of an α_1 subunit in association with auxiliary β, $\alpha_2\delta$, and γ subunits (Liao *et al.*, 2005). The 190-250 kilodalton (kDa) α_1 subunit is the autonomous pore-forming subunit, comprising four membrane-spanning domains, with each domain consisting of six transmembrane segments (S1–S6) (Liao *et al.*, 2005). The S4 segment contains three to five positively charged amino acids and serves as the voltage sensor of the channel (Liao *et al.*, 2005). The α_1 subunit also contains binding sites for dihydropyridines. An intracellular β subunit, a transmembrane, disulfide-linked $\alpha_2\delta$ subunit, and a γ subunit interact with the α_1 subunit to regulate its expression and characteristics, such as activity and membrane trafficking of the channel (Liao *et al.*, 2005). Based on the homology of their sequences, VDCCs are classified into three families - Ca_V1 (L-type), Ca_V2 (P/Q-, N-, and R-type), and Ca_V3 (T-type) (Catterall, 2000; Ertel *et al.*, 2000). VDCC α_1 subunits are encoded by ten genes. Based on the α_1 subunit, there are four types of Ca_V1 channels. $Ca_V1.1$ (α_{1S}) expressed in skeletal muscle cells, $Ca_V1.2$ (α_{1C}) expressed in heart, vascular, and visceral smooth muscle cells, $Ca_V1.3$ (α_{1D}) expressed in brain, and $Ca_V1.4$ (α_{1F}) expressed in the retina (Ertel *et al.*, 2000).

$Ca_V1.2$ channel is the major VDCC isoform and the primary Ca^{2+} entry pathway expressed in vascular smooth muscle cells (Gollasch & Nelson, 1997). Molecular diversity of $Ca_V1.2$ channels is achieved by alternative gene splicing and transcriptional regulation by different promoters in the 5' flanking regions of α_{1C} gene. This has given rise to exon 1a, exon 1b, and exon 1c in the N-terminus of α_{1C} subunit of $Ca_V1.2$ in vascular smooth muscle cells (Cheng *et al.*, 2007). The α_{1C} subunit of $Ca_V1.2$ is

synthesized as a ~240 kDa protein which is proteolytically cleaved in its C-terminal domain by enzymes, including calpain to yield ~190 and 50 kDa products (Gerhardstein *et al.*, 2000). The 50 kDa C-terminal product reassociates with the 190 kDa channel to form the fully functional $Ca_V1.2$ channel.

Activation of $Ca_V1.2$ channels by membrane depolarization, leads to Ca^{2+} influx, $[Ca^{2+}]_i$ elevation, and vasoconstriction (Berridge, 2001; Cheng *et al.*, 2007). Ca^{2+} influx also stimulates Ca^{2+} release from intracellular stores. In small, resistance-sized arteries and arterioles, $Ca_V1.2$ channels are essential for myogenic tone development and blood pressure regulation (Cheng *et al.*, 2007). Hypertension is associated with an elevation in arterial smooth muscle cell $Ca_V1.2$ expression, which leads to increased Ca^{2+} influx, $[Ca^{2+}]_i$ elevation, and vasoconstriction (Wang *et al.*, 2006). L-type Ca^{2+} channel blockers are widely used to treat hypertension because of their ability to reduce arterial smooth muscle cell contractility (Triggle, 2006).

Vascular smooth muscle cells also express $Ca_V1.3$, $Ca_V2.1$, $Ca_V3.1$, and $Ca_V3.2$ channels. Ca^{2+} influx through these channels make a minor contribution to $[Ca^{2+}]_i$ in vascular smooth muscle cells.

1.2.2. Store-operated Ca^{2+} channels

SOCCs are plasma membrane, non-selective, cation channels that are activated in response to depletion of intracellular Ca^{2+} stores (Bootman *et al.*, 2001). Although, the precise mechanisms are presently unclear, there exist two major theories which attempt to elucidate the activation mechanism of SOCCs. According to these schemes, SOCCs are activated by either a conformational coupling between Ca^{2+} channels on the SR and those on the plasma membrane, or SR Ca^{2+} depletion stimulates a second messenger, which activates plasma membrane Ca^{2+} channels (Bootman *et al.*, 2001).

The molecular identities of SOCCs are presently unclear. Many of the SOCCs are speculated to belong to the large transient receptor potential (TRP) channel family, which were first identified in Drosophila (Beech *et al.*, 2004). The mammalian TRP channel superfamily that is subdivided into 7 families, is encoded by at least 28 different genes (Beech *et al.*, 2004). Vascular smooth muscle cells express at least members of three TRP families, including TRPC (1, 3, 4, 5, 6, and 7), TRPM (2, 4, 7, and 8), and TRPV (2 and 4) (Earley & Brayden, 2010). TRP channels, which are permeable to Ca^{2+}, Na^+, potassium (K^+), and magnesium (Mg^{2+}), regulate multiple functions in arterial smooth muscle cells, including membrane potential, $[Ca^{2+}]_i$, contractility, and proliferation (Beech *et al.*, 2004; Adebiyi *et al.*, 2010). Recent studies have identified two other proteins, including Orai1 and stromal interaction molecule (STIM)1 which regulate store-operated Ca^{2+} entry in smooth muscle cells (Guibert *et al.*, 2008). Orai1 is a plasma membrane protein which has been suggested to be the pore subunit of store-operated current (Guibert *et al.*, 2008). STIM1 is primarily an endoplasmic reticulum (ER) membrane protein but it is also present in the plasma membrane (Guibert *et al.*, 2008). Few studies have suggested that SOCCs comprise an assembly of proteins, including

TRPC, STIM1 and Orai1 present in the plasma membrane (Guibert *et al.*, 2008).

In smooth muscle cells, the regulation, ion selectivity, and conductance of store-operated cation currents differ in anatomically diverse blood vessels (Xi *et al.*, 2008). In rat cerebral artery smooth muscle cells, the preparation used in this study, there is very little evidence for SOCCs. Ca^{2+} depletion of sarcoplasmic reticulum (SR) by thapsigargin, an SR Ca^{2+} ATPase inhibitor (Lytton *et al.*, 1991) resulted in vasoconstriction at 60 mm Hg but not at 20 mm Hg of intravascular pressure, indicating that SR Ca^{2+} depletion-induced current is pressure-dependent (Xi *et al.*, 2008). SR Ca^{2+} depletion has been suggested to constrict cerebral arteries by inhibiting Ca^{2+} sparks and large conductance Ca^{2+}-activated K^+ (K_{Ca}) channels, which are activated by an elevation in intravascular pressure (Xi *et al.*, 2008).

1.2.3. Receptor-operated Ca^{2+} channels

ROCCs comprise a range of structurally and functionally diverse channels that exist in many cells, including vascular smooth muscle cells (Bootman *et al.*, 2001). They are Ca^{2+}-permeable, non-selective, cation channels activated by the binding of an agonist to the extracellular domain (Bootman *et al.*, 2001). In vascular smooth muscle cells, a wide variety of agonists, including adenosine 5'-triphosphate (ATP), serotonin, norepinephrine (NE), acetylcholine, endothelin-1 (ET-1), vasopressin, glutamate, and angiotensin II (Ang II) activate ROCCs, and induce Ca^{2+} entry (Large, 2002). Apart from the P2X1 receptor, an ATP-gated cation channel, other receptor-operated currents are likely to be mediated via G-protein-coupled receptors, and some through tyrosine kinases (Large, 2002). In guinea pig aorta, NE-induced Ca^{2+} influx was only partially blocked by Ca^{2+} channel blockers (Gouw *et al.*, 1990). In rat cultured aortic smooth muscle cells, ATP, Ang II, and vasopressin cause $^{45}Ca^{2+}$ influx that is independent of membrane depolarization and unaffected by Ca^{2+} channel antagonists, but reduced by phospholipase C (PLC) inhibitors (Ruegg *et al.*, 1989).

Several TRP channels, including TRPC4, TRPC5, and heteromultimeric complex of TRPC6 and TRPC7 can be activated by various stimuli, such as vasopressin (Plant & Schaefer, 2003; Earley, 2006; Maruyama *et al.*, 2006) suggesting that TRP channels could also act as ROCCs.

1.2.4. Other Ca^{2+} entry channels

Apart from VDCCs, SOCCs, and ROCCs, Ca^{2+} influx could occur through other pathways. One example is the stretch-activated cation channels which allow Ca^{2+} entry and regulate cell contractility (Bootman *et al.*, 2001; Hill *et al.*, 2001). In isolated vascular smooth muscle cells, longitudinal stretch activates a non-selective, inward cation conductance (Hill *et al.*, 2001). Therefore, it is accepted that stretch activation contributes to membrane depolarization, leading to activation of VDCCs (Hill *et al.*, 2001). Mechanical disturbance of cell membranes also releases factors that modulate the

activity of stretch-activated channels (Hill *et al.*, 2001). Second messengers, including fatty acids, arachidonic acid metabolites, diacylglycerol (DAG), and cyclic nucleotides have been suggested to activate channels by regulating ion channel gating (Hill *et al.*, 2001).

1.2.5. Plasma membrane Ca^{2+}-ATPases

PMCA extrude Ca^{2+} from cytosol to the extracellular compartment using energy derived from ATP hydrolysis to pump Ca^{2+} against the steep electrochemical gradient (Berridge, 2001). The C-terminus contains a calmodulin (CaM)-binding domain, which acts as an autoinhibitory domain and maintains the pump in an inactive state (Sanders, 2001). Binding of CaM removes the inhibition and stimulates pump activity (Sanders, 2001). Phosphorylation by protein kinases, including protein kinase A (PKA) and G (PKG) also reduces autoinhibition and facilitates Ca^{2+} transport (Sanders, 2001).

Four isoforms of PMCAs (1-4) are widely expressed (Bootman *et al.*, 2001). Vascular smooth muscle cells express PMCA1 and PMCA4 (Abramowitz *et al.*, 2000). PMCA4b inhibits neuronal nitric oxide synthase (nNOS), by binding of its C-terminus to the PDZ domain of nNOS (Schuh *et al.*, 2001). Transgenic mice overexpressing PMCA4b in vascular smooth muscle cells are associated with elevated peripheral blood pressure due to inhibition of nNOS activity (Gros *et al.*, 2003). Mesenteric arteries from these transgenic mice display more prominent myogenic response and elevated responses to vasoconstrictors, including phenylephrine and prostaglandin $F_{2\alpha}$ (Gros *et al.*, 2003). PMCAs localize in caveolae of visceral smooth muscle cells, endothelial cells, and rat cardiomyocytes, but whether similar localization occurs in vascular smooth muscle cells is unclear.

1.2.6. Plasma membrane Na^+/Ca^{2+} exchanger

NCX is an integral plasma membrane protein which counter-transports Ca^{2+} in exchange for Na^+, utilizing the Na^+ gradient across the plasma membrane, generated by the Na^+/K^+-ATPase (NKA), as an energy source (Bootman *et al.*, 2001). The mammalian NCX family comprises three isoforms NCX (1-3) with numerous splice variants. Vascular smooth muscle cells predominantly expresses NCX1.3 and NCX1.7 (Quednau *et al.*, 1997). NCXs function either to pump one molecule of Ca^{2+} out (forward mode) of cells, or into cells (reverse mode) in exchange for three molecules of Na^+. NCX activity is regulated by membrane potential, ATP, and transmembrane gradients of Na^+ and Ca^{2+} (Iwamoto *et al.*, 2005). In vascular smooth muscle cells, NCXs are colocalized with NKA on the plasma membrane near the SR, suggesting that NCX/NKA can functionally operate with SERCA (Ishida & Paul, 2005). Under physiological conditions, high extracellular Na^+ concentration stimulates NCX to pump Ca^{2+} out of cells. Cardiovascular diseases, including hypertension are associated with improper functioning of NCX. High salt diet inhibits NKA, leading to elevated submembrane Na^+ levels, resulting in NCX functioning in the reverse mode. Ca^{2+} influx through NCX increases

$[Ca^{2+}]_i$ and may contribute to salt-sensitive hypertension (Iwamoto *et al.*, 2005). Aortic smooth muscle cells from spontaneously hypertensive rats are associated with elevated NCX1 expression and enhanced Ang II-induced Ca^{2+} efflux via NCX (Ishida & Paul, 2005).

1.3. Intracellular Ca^{2+} Stores

Cytosol of smooth muscle cell is packed with myofilaments and intermediate filaments, occupying up to 90% of the cell volume with the intracellular organelles sharing the remaining space (Wray & Burdyga, 2010). Intracellular stores contain a high Ca^{2+} concentration, and release Ca^{2+} into the cytosol upon stimulation and opening of Ca^{2+} channels on their membrane. SR, a rich reticular network, which occupies ~5% of cell volume, is the major intracellular Ca^{2+} source (Wray & Burdyga, 2010). Apart from the SR, mitochondria can store and release Ca^{2+}.

1.3.1. Sarcoplasmic reticulum

In vascular smooth muscle cells, Ca^{2+} release from the SR occurs through inositol 1,4,5-triphosphate (IP_3) receptors (IP_3R) and ryanodine-sensitive Ca^{2+} release (RyR) channels. Ca^{2+} release from these channels are regulated by a collection of messengers, including Ca^{2+}, IP_3, cyclic ADP ribose (cADPR), nicotinic acid adenine dinucleotide phosphate (NAADP), and sphingosine-1-phosphate (S1P), that operate on both the luminal and cytosolic surfaces of the channel (Berridge *et al.*, 2003). Sarcoplasmic/endoplasmic reticulum Ca^{2+} ATPase (SERCA), which is located on the SR membrane pumps Ca^{2+} from the cytosol into the SR (Inesi, 1987).

1.3.1.1. Ryanodine-sensitive Ca^{2+} release channels

RyR channels specifically bind the plant alkaloid ryanodine, which is the reason for its name (Jaggar *et al.*, 2000). Three molecularly distinct RyR isoforms (1-3), encoded by distinct genes, are present in a variety of tissues (Jaggar *et al.*, 2000). RyR1 is expressed primarily in skeletal muscle, whereas RyR2 and RyR3 are found in cardiac muscle and brain, respectively (Jaggar *et al.*, 2000). All three RyR isoforms are expressed in smooth muscles of pulmonary and systemic vessels, with variations in the type and the relative proportion of each being tissue- and species-dependent (Wray & Burdyga, 2010). In rat cerebral artery smooth muscle cells, RyR2 is the predominant isoform (Vaithianathan *et al.*, 2010).

Each of these isoforms exists as a homotetramer with the subunits surrounding a central Ca^{2+} pore (Jaggar *et al.*, 2000; Wray & Burdyga, 2010). The subunits are associated with FK-506-binding protein (FKBP), a regulatory protein. The pore-forming, membrane-spanning regions are localized to the C-terminus (Wray & Burdyga, 2010). The cytosolic N-terminus, which is the modulatory region, contains phosphorylation sites

and binding sites for Ca^{2+}, adenine nucleotides, CaM, and FKBP. RyRs are approximately twice as large as IP_3R (Wray & Burdyga, 2010). Because of their massive size, RyR is suitable for sudden and large release of SR Ca^{2+} (Wray & Burdyga, 2010).

The principal endogenous modulator of RyR activity is Ca^{2+}, which upon binding can activate or inhibit the channels. Low cytosolic Ca^{2+} concentrations (nM to μM) activate RyR, whereas high cytosolic Ca^{2+} concentrations (μM to mM) inhibit RyRs (Bootman *et al.*, 2001). Similarly, ryanodine at low concentrations (1-10 μM) locks RyRs into a long-lived subconductance state, leading to Ca^{2+} release over a prolonged period of time and eventually SR Ca^{2+} depletion. At high concentrations (~100 μM), ryanodine irreversibly inhibits RyR channel opening. RyR channels have to be activated for ryanodine to bind to them (Bootman *et al.*, 2001). Millimolar concentrations of caffeine activate RyRs by increasing the sensitivity of RyRs to Ca^{2+}, resulting in basal Ca^{2+} concentrations to become activatory and stimulate further Ca^{2+} release (Bootman *et al.*, 2001). Changes in the SR luminal Ca^{2+} concentration, which is ~1 mM can activate RyRs (Bootman *et al.*, 2001). Activation of SERCA, which is responsible for maintaining SR Ca^{2+} load, activates RyR by increasing luminal Ca^{2+} concentration (Bootman *et al.*, 2001). cADPR is an endogenous cellular messenger that causes RyR-mediated SR Ca^{2+} release. The precise mechanism by which cADPR activates RyR is unclear. It has been suggested that cADPR binds to the inhibitory protein FKBP, resulting in increasing the open probability of RyR (Bootman *et al.*, 2001). cADPR could also activate SERCA, leading to an increase in SR Ca^{2+} load, resulting in RyR activation (Lukyanenko *et al.*, 2001). RyR channels can also be regulated by several protein kinases and phosphatases, including PKA, protein kinase C (PKC), PKG, CaM kinase II, and protein phosphatase 1 (Jaggar *et al.*, 2000; Bootman *et al.*, 2001; Wray & Burdyga, 2010).

1.3.1.2. Inositol 1,4,5-triphosphate receptors

Binding of ligands, including hormones, and growth factors to plasma membrane G_q protein-coupled receptors activates PLC, leading to hydrolysis of phosphatidylinositol 4,5-biphosphate (PIP_2) to produce IP_3 and DAG (Bootman *et al.*, 2001). IP_3 binds to IP_3R-gated Ca^{2+} channels on the SR, leading to Ca^{2+} release. DAG serves as an intracellular messenger to activate PKC (Bootman *et al.*, 2001).

Distinct genes encode each of the three IP_3R isoforms (1-3) (Wray & Burdyga, 2010). IP_3R isoforms, which are structurally and functionally related, differ in their sensitivities to destruction by intracellular proteases, with IP_3R1 and IP_3R3 being more susceptible to breakdown than IP_3R2 (Wray & Burdyga, 2010). IP_3Rs are extensively expressed in brain and other tissues including vascular smooth muscles. In vascular smooth muscles, IP_3R density is ~100 times less than that in the brain, and the stoichiometric ratio of IP_3Rs to RyRs is 3-4:1 (Wray & Burdyga, 2010). Smooth muscle cells express multiple IP_3R isoforms (Zhao *et al.*, 2008; Wray & Burdyga, 2010). IP_3R1 has been found in rat aorta, basilar, and mesenteric arteries, whereas IP_3R2 and IP_3R3 have been detected in basilar artery and a cell line derived from rat aorta, respectively

(Wray & Burdyga, 2010). IP_3R1 is the predominant isoform expressed in smooth muscle cells of resistance-size cerebral arteries (Zhao *et al.*, 2008).

IP_3Rs are tetrameric, with a monomeric mass of ~300 kDa, containing ~2700 amino acids (Wray & Burdyga, 2010). IP_3Rs can form either homo- or hetero-tetramer, although reports suggesting IP_3R as a heterotetramer complex have been derived from cell lines (Patterson *et al.*, 2004). The IP_3R structure can be divided to two regions. The C-terminal end of IP_3R contains the Ca^{2+} channel region, which shares sequence homology with that of the RyR (Patterson *et al.*, 2004). The C-terminal region consists of six membrane-spanning helices with the C-terminus projecting into the cytosol (Patterson *et al.*, 2004). The N-terminal region which also extends to the cytosol, contains the IP_3-binding site (Patterson *et al.*, 2004). The modulatory domain, which contains binding sites for Ca^{2+}, nucleotides, CaM, and protein kinases is located between the ligand-binding domain and the channel pore (Patterson *et al.*, 2004).

The principal mechanism which results in IP_3R-mediated SR Ca^{2+} release, is the interaction of IP_3 with IP_3R (Bootman *et al.*, 2001). IP_3 produced at the plasma membrane is highly mobile and diffuses in the cytosol to bind IP_3R on the SR membrane (Bootman *et al.*, 2001). Binding of IP_3 induces a conformational change in IP_3R, resulting in channel opening and release of Ca^{2+}, which is stored at high concentrations in the SR (Patterson *et al.*, 2004). Although binding of IP_3 is essential for IP_3R activation, Ca^{2+} concentration at their cytosolic side also regulate IP_3R activity, thereby permitting IP_3R-mediated Ca^{2+} release to regulate further Ca^{2+} release (Patterson *et al.*, 2004). Binding of IP_3 increases the IP_3R sensitivity to Ca^{2+}, which has a biphasic action (Patterson *et al.*, 2004). At low IP_3 levels (<100 nM), IP_3Rs are stimulated by Ca^{2+} concentrations between 100 and 300 nM, whereas inhibited by cytosolic Ca^{2+} concentrations >1 μM (Worley *et al.*, 1987; Bootman *et al.*, 2001). At high IP_3 levels (>100 nM), very high Ca^{2+} concentration is required to induce inhibition of IP_3R (Berridge, 2001). Ca^{2+}-dependence of IP_3R activity is important for the generation of complex patterns of Ca^{2+} signals seen. SR luminal Ca^{2+} can also regulate IP_3R activity, whereby a reduced SR Ca^{2+} load, leads to a decrease in IP_3-induced Ca^{2+} release (Patterson *et al.*, 2004). In permeabilized hepatocytes, IP_3R is inactivated by IP_3, and this effect is enhanced by cytosolic Ca^{2+}, suggesting that IP_3 and Ca^{2+} inhibit IP_3R, resulting in limiting the IP_3R-mediated SR Ca^{2+} release (Hajnoczky & Thomas, 1994). Certain SR luminal proteins, including calreticulin and calnexin, which are Ca^{2+}-binding proteins are also known to interact with IP_3R and regulate their activity (Berridge, 2001). IP_3R activity can also be modulated by other signaling pathways, including phosphorylation by PKA, PKC, PKG, and CaM kinase II (Bootman *et al.*, 2001).

In smooth muscle cells of resistance-size cerebral arteries, IP_3R1 activation also induces physical coupling of the N-terminus of IP_3R1 and the C-terminus of plasma membrane TRPC3 channel, leading to non-selective cation current (I_{Cat}) activation. IP_3R-dependent I_{Cat} activation produces membrane depolarization, $Ca_V1.2$ channel activation, and global $[Ca^{2+}]_i$ elevation (Xi *et al.*, 2008; Zhao *et al.*, 2008; Adebiyi *et al.*, 2010). This is an additional mechanism by which IP_3R activation contributes to global $[Ca^{2+}]_i$ elevation in arterial smooth muscle cells.

1.3.1.3. Sarcoplasmic/endoplasmic reticulum Ca^{2+}ATPases

Three mammalian isoforms of SERCA (1-3) exist and splice variants have been reported in each of the isoforms (Rizzuto *et al.*, 1993). SERCA2a, 2b, and 3 are the isoforms expressed in vascular smooth muscle cells, with SERCA2b being the major isoform (Wu *et al.*, 2001; Ishida & Paul, 2005).

SERCA transports two molecules of Ca^{2+} into the SR using the energy from the hydrolysis of one molecule of ATP (Inesi, 1987). Counter-transport of two or three hydrogen (H^+) ions into the cytosol ensures partial charge balancing (Levy *et al.*, 1990). In smooth muscle cells, the locations of Ca^{2+} release and re-uptake by the SERCA on the SR membrane are spatially separated (Floyd & Wray, 2007). Ca^{2+}-binding proteins in the SR lumen regulate SERCA activity to attain a free Ca^{2+} concentration of ~500 μM. In uterine smooth muscle cells, overloading the SR with Ca^{2+} did not alter, whereas reducing SR Ca^{2+} load, inhibited IP_3-induced Ca^{2+} signals, suggesting that the ability of SR to store Ca^{2+} is finite (Floyd & Wray, 2007).

Phospholamban (PLN) endogenously inhibits SERCA through direct protein-protein interactions by lowering its apparent Ca^{2+} affinity (Wray & Burdyga, 2010). PLN is phosphorylated by PKA or CaM kinase, leading to removal of the inhibition, resulting in an increase in SERCA activity (Ishida & Paul, 2005; Wray & Burdyga, 2010). Sarcolipin, a PLN homolog, which inhibits SERCA by lowering its apparent Ca^{2+} affinity, is expressed in skeletal and cardiac muscles, but not in smooth muscle cells (Vangheluwe *et al.*, 2005). SERCA activity is also controlled by regulators such as insulin-receptor substrate 1/2, the Ca^{2+}-binding protein S100A1, acylphosphatase, and the antiapoptotic protein Bc1-2 (Wray & Burdyga, 2010).

1.3.2. Mitochondria

Intracellular Ca^{2+} signaling is also regulated by mitochondria which accumulate and retain Ca^{2+}. Electron transport chain (ETC) complexes present on the inner mitochondrial membrane transfer electrons to molecular oxygen during oxidative phosphorylation. The electron transfer is coupled with translocation of protons into the intermembrane space, which creates and sustains the mitochondrial membrane potential (ψ_m) which is ~150-200 mV more negative than the cytosol (McCarron *et al.*, 2006). This difference in potential between the cytosol and mitochondrial matrix, drives Ca^{2+} transport into the mitochondria (McCarron *et al.*, 2006). Mitochondria act as a local, spatial buffering system, by regulating Ca^{2+} signals which arise from the SR or plasma membrane in many cells, including smooth muscle cells. Mitochondrial Ca^{2+} uptake occurs via the voltage-dependent anion channel (VDAC), mitochondrial Ca^{2+} uniporter (MCU), and rapid uptake mode (RaM) (Gunter *et al.*, 2000). The mitochondrial permeability transition pore (mPTP) and the mitochondrial Na^+/Ca^{2+} exchanger (mNCX) extrude Ca^{2+} from the mitochondrial matrix to the cytosol (Gunter *et al.*, 2000).

1.3.2.1. Voltage-dependent anion channel

Ca^{2+} transit through the outer mitochondrial membrane occurs through VDAC, the most abundant protein on the outer mitochondrial membrane. Mammals have three distinct VDAC isoforms (1-3). VDAC is an anion-selective channel, fully opened at low potential (<20–30 mV), but switches to cation selectivity at higher potentials ("closed" state) (Colombini, 2004). In the resting condition, VDAC is closed and exhibits higher permeability to Ca^{2+}, rather than in the opened state (Tan & Colombini, 2007). In HeLa cells and skeletal myotubes, VDAC overexpression enhanced Ca^{2+} transport from SR into the mitochondrial matrix (Rapizzi *et al.*, 2002). VDAC activity is regulated by several factors, including nicotinamide adenine dinucleotide (NADH), Bcl-2 proteins, chaperones, and cytoskeletal elements (Rizzuto *et al.*, 2009).

1.3.2.2. Mitochondrial Ca^{2+} uniporter

MCU is a highly selective ion channel located on the inner mitochondrial membrane that transports Ca^{2+} from the cytosol into the mitochondrial matrix (Rizzuto *et al.*, 2000). MCU has both an activation site as well as a transport site (Gunter & Pfeiffer, 1990). MCU activation stimulates Ca^{2+} influx into the mitochondrial matrix due to the negative ψ_m (Rizzuto *et al.*, 2000). MCU has low sensitivity to Ca^{2+} and is activated by Ca^{2+} concentrations >3 μM (K_m ~10 μM) in the inter membrane space (Poburko *et al.*, 2004). The velocity of Ca^{2+} uptake is near zero for external $[Ca^{2+}]_i$ <200-300 nM (Poburko *et al.*, 2004). $[Ca^{2+}]_i$ regulates MCU activity in a biphasic manner (Montero *et al.*, 2004; Moreau *et al.*, 2006). Studies in HeLa cells suggested that MCU activation by Ca^{2+} is mediated by the activation of Ca^{2+}-dependent CaM and subsequently, CaM kinase II (Montero *et al.*, 2004). Following activation, cytosolic Ca^{2+} elevation inactivates the MCU and limits mitochondrial Ca^{2+} uptake. This biphasic regulation of MCU activity by cytosolic Ca^{2+} occurs with MCU activation and Ca^{2+} uptake occurring with a time constant of ~6 seconds, while the Ca^{2+}-dependent MCU inactivation occurs with a time constant of ~17 seconds. This mechanism permits oscillations in mitochondrial Ca^{2+} concentrations ($[Ca^{2+}]_{mito}$), but prevents excessive Ca^{2+} uptake when $[Ca^{2+}]_i$ elevation is prolonged (Moreau *et al.*, 2006). Different PKC isoforms have been suggested to participate in the cytosolic Ca^{2+}-mediated regulation of MCU activity (Rizzuto *et al.*, 2009). Overexpression of uncoupling proteins, including UCP2 and UCP3 in an endothelial cell line enhanced mitochondrial Ca^{2+} uptake, and small interfering RNA (siRNA)-mediated knockdown decreased MCU activity and mitochondrial Ca^{2+} sequestration, suggesting that uncoupling proteins could be essential components of MCU (Trenker *et al.*, 2007). MCU activity is inhibited by ruthenium red and its related compound Ru360, and adenine nucleotides (ATP>ADP>AMP) (Rizzuto *et al.*, 2009).

1.3.2.3. Rapid uptake mode

Ca^{2+} pulses of physiological concentration (~400 nM) more effectively induce mitochondrial Ca^{2+} uptake compared to a steady $[Ca^{2+}]_i$ for the same overall time

(Rizzuto *et al.*, 2000; Rizzuto *et al.*, 2009). RaM is a mechanism by which large amounts of Ca^{2+} are transported in short pulses at least 300 times faster than through the MCU (Rizzuto *et al.*, 2000). The activity, identity, and regulation of RaM remains poorly understood. It is speculated that RaM transports Ca^{2+} only for a brief period during the initial part of the pulse, followed by inactivation induced by binding of Ca^{2+} to an external site (Rizzuto *et al.*, 2009). RaM exhibits a high initial Ca^{2+} uptake velocity, and its steady-state uptake is inhibited at $[Ca^{2+}]_i$ >150-180 nM (Gunter & Gunter, 2001), suggesting that RaM functions in resting conditions to maintain basal $[Ca^{2+}]_{mito}$ (Poburko *et al.*, 2004).

1.3.2.4. Mitochondrial permeability transition pore

Mitochondria accumulate Ca^{2+} in the presence of adenine nucleotides. Depletion of adenine nucleotides in the presence of oxidants stimulates Ca^{2+} overload in the mitochondrial matrix. Ca^{2+} overload triggers opening of mPTP, a high conductance, non-selective channel located in the inner-outer contact sites of the mitochondrial membranes (Rizzuto *et al.*, 2000; Rizzuto *et al.*, 2009). Several factors, including high $[Ca^{2+}]_{mito}$, mitochondrial depolarization, oxidative stress, adenine nucleotide depletion, and a high concentration of inorganic phosphate (Pi) stimulate mPTP opening (Duchen, 2000a; Rizzuto *et al.*, 2009). mPTP opening is stimulated by Ca^{2+} influx into the mitochondrial matrix which binds to a site on the mPTP (Rizzuto *et al.*, 2009). In the presence of high Ca^{2+} concentrations, cyclophilin D (CypD) binds to the inner mitochondrial membrane and to adenine nucleotide translocase (ANT), thus inhibiting ATP/adenosine 5'-diphosphate (ADP) binding and inducing mPTP opening (Rizzuto *et al.*, 2009). mPTP opening is inhibited by cyclosporine A, and ions such as Mg^{2+}, strontium (Sr^{2+}), and manganese (Mn^{2+}) (Rizzuto *et al.*, 2009). The molecular identity of mPTP is unclear with studies speculating it to be a multi-protein complex comprising VDAC, ANT, and CypD, while others indicate that inhibiting one or more of these components does not affect mPTP activity (Duchen, 2000a; Rizzuto *et al.*, 2009). Apoptosis which causes loss of mitochondrial components is associated with mPTP opening (Chang & Yang, 2000; Rizzuto *et al.*, 2009). Reversible mPTP openings have been observed both in individual isolated mitochondria (Huser *et al.*, 1998) and in intact cells (Petronilli *et al.*, 1999). However, it is unclear whether mPTP can function as a physiological mitochondrial Ca^{2+} release channel (Bernardi & Petronilli, 1996).

1.3.2.5. Mitochondrial Na^+/Ca^{2+} exchanger

mNCX mediates physiological Ca^{2+} cycling out of the mitochondrial matrix (Rizzuto *et al.*, 2000). One molecule of Ca^{2+} is transported out of the mitochondria for every three molecules of Na^+ transported in (Rizzuto *et al.*, 2000). Difference in Na^+ concentration between the cytosol and mitochondria causes Na^+ influx into the mitochondrial matrix. Na^+ influx drives Ca^{2+} efflux out of the mitochondria into the cytosol. mNCX is inhibited by ions such as Sr^{2+}, barium (Ba^{2+}), Mg^{2+} or Mn^{2+}, ruthenium red, and drugs, including antimycin A, amiloride, trifluoperazine, diltiazem,

verapamil, clonazepam, bepridil and CGP37157 (Rizzuto *et al.*, 2009). mNCX is inhibited by protonophores which disrupt ψ_m, indicating that mNCX activity is regulated by the difference in potential between the cytosol and mitochondria (Rizzuto *et al.*, 2000). Studies done in cultured vascular smooth muscle cells have found that CGP-37157, a selective mNCX inhibitor, increased resting $[Ca^{2+}]_{mito}$ indicating that mNCX contributes to mitochondrial Ca^{2+} efflux in smooth muscle cells (Poburko *et al.*, 2004).

1.3.3. Other intracellular stores

NAADP is formed from β-$NADP^+$ and β-NAD^+ by ADP ribosyl cyclases which also produce cADPR (Berridge, 2001). Unlike cADPR, NAADP does not activate RyR, but stimulates Ca^{2+} release from an internal store, which is distinct from the SR because Ca^{2+} depletion of SR does not affect NAADP-mediated Ca^{2+} release (Bootman *et al.*, 2001). The mechanism(s) behind NAADP-mediated Ca^{2+} release and the channel identity remains unclear (Clapham, 1995).

Sphingolipids, including sphingosylphosphorylcholine and S1P stimulate Ca^{2+} release in several different cell types (Bootman *et al.*, 2001). Sphingolipid-derived messengers are believed to be responsible for agonist-induced SR Ca^{2+} signals that are generated independently of IP_3R or RyR (Berridge *et al.*, 2003). The exact mechanism for S1P-mediated Ca^{2+} release is unclear. The identity of the S1P receptor is believed to be the sphingolipid Ca^{2+}-release-mediating protein of ER (SCaMPER), a 20 kDa protein with a transmembrane domain (Bootman *et al.*, 2001). In rat cerebral artery smooth muscle cells, plasma membrane S1P receptors activate PLC, leading to IP_3R and RyR activation, resulting in Ca^{2+} release (Yatomi, 2006).

1.4. Cytosolic Ca^{2+} Signals

In arterial smooth muscle cells, four principal Ca^{2+} signaling modalities have been described: "Global intracellular Ca^{2+}", "Ca^{2+} sparks", "Ca^{2+} sparklets", and "Ca^{2+} waves". These Ca^{2+} signals differ with respect to spatial localization, temporal kinetics, and amplitude properties (Jaggar *et al.*, 2000; Lee *et al.*, 2002; Wray *et al.*, 2005). Several factors, including Ca^{2+} sensitivity and proximity to the source of a Ca^{2+} signal, influence whether proteins detect local or global Ca^{2+} signals (Jaggar, 2007).

1.4.1. Global intracellular Ca^{2+}

Global $[Ca^{2+}]_i$ is the spatially averaged cytosolic $[Ca^{2+}]_i$. In arterial smooth muscle cells, an elevation in global $[Ca^{2+}]_i$ occurs because of Ca^{2+} influx through plasma membrane Ca^{2+} channels and Ca^{2+} release from the SR through IP_3R channels (Jaggar *et al.*, 2000; Zhao *et al.*, 2008). Either of these events which produce an initial rise in global $[Ca^{2+}]_i$ can be further enhanced by RyR-mediated Ca^{2+} release via a Ca^{2+}-induced Ca^{2+} release mechanism (Bolton *et al.*, 2004). In addition to these mechanisms, IP_3R

activation induces Ca^{2+} influx through plasma membrane TRPC3 channels, resulting in a further elevation in global $[Ca^{2+}]_i$ (Adebiyi *et al.*, 2010). A nanomolar elevation in global $[Ca^{2+}]_i$ regulates cell contractility by modulating Ca^{2+}/CaM-dependent myosin light chain (MLC) kinase activity (Nelson *et al.*, 1988; Brayden & Nelson, 1992; Endo, 2006). Ca^{2+} binds CaM and the Ca^{2+}-CaM complex activates MLC kinase which phosphorylates MLC20. MLC20 is bound to the myosin head near the neck, and prevents it from interacting with actin. MLC20 phosphorylation by MLC kinase activates the myosin head, initiating contraction. A reduction in global $[Ca^{2+}]_i$ leads to MLC20 dephosphorylation by MLC phosphatase, resulting in vasodilation (Jaggar, 2001; Endo, 2006).

Ca^{2+} influx through $Ca_V1.2$ channels is the major contributor to global $[Ca^{2+}]_i$ in arterial smooth muscle cells. Therefore, membrane potential, a key regulator of $Ca_V1.2$ channel activation, influences global $[Ca^{2+}]_i$ (Knot & Nelson, 1998). In cerebral artery smooth muscle cells under physiological conditions, the membrane potential is ~-45 mV, and global $[Ca^{2+}]_i$ is ~193 nM (Knot & Nelson, 1998; Cheranov & Jaggar, 2004; Zhao *et al.*, 2008). Small changes in membrane potential result in significant changes to Ca^{2+} influx through $Ca_V1.2$ channels, global $[Ca^{2+}]_i$, and arterial diameter. Membrane depolarization from -45 mV by ~9 mV elevates global $[Ca^{2+}]_i$ by ~45 nM and constricts the artery by about 25%. In arterial smooth muscle cells, the entire range of global $[Ca^{2+}]_i$ which is from ~120 to 350 nM, and arterial diameter from fully dilated to maximally constricted state, is associated with membrane potentials from -65 to -25 mV (Knot & Nelson, 1998).

1.4.2. Ca^{2+} sparks

Ca^{2+} sparks are localized, intracellular Ca^{2+} transients that occur due to the activation of RyR channels on the SR (Cheng *et al.*, 1993; Nelson *et al.*, 1995; Jaggar *et al.*, 2000). In resting arterial smooth muscle cells, the Ca^{2+} spark frequency is very low (~1 Hz in rat cerebral artery), and the spatial spread (full width at half maximal amplitude) is only ~2-3 μm (Jaggar *et al.*, 2000). A single Ca^{2+} spark does not alter global $[Ca^{2+}]_i$ significantly in arterial smooth muscle cells (Wellman & Nelson, 2003). However, Ca^{2+} sparks can produce a rapid, local elevation in $[Ca^{2+}]_i$ and activate Ca^{2+}-sensitive proteins. One of the targets for Ca^{2+} sparks is the plasma membrane K_{Ca} channel (Jaggar *et al.*, 2000). Ca^{2+} sparks generate a micromolar $[Ca^{2+}]_i$ elevation near the release site, which activates many plasma membrane K_{Ca} channels, causing a transient K_{Ca} current (Jaggar *et al.*, 2000; Perez *et al.*, 2001; Zhuge *et al.*, 2002). K_{Ca} channel, which has a low Ca^{2+} affinity would not be activated by global $[Ca^{2+}]_i$ changes (Perez *et al.*, 2001). Ca^{2+} spark-activated K_{Ca} current induces membrane hyperpolarization, which reduces $Ca_V1.2$ activity, causing global $[Ca^{2+}]_i$ reduction and vasodilation (Nelson *et al.*, 1995; Jaggar *et al.*, 2000). Therefore, in small resistance-size arteries, RyR, K_{Ca}, and $Ca_V1.2$ channels form a functional unit that provides a negative feedback mechanism for the regulation of vascular tone and blood pressure (Jaggar *et al.*, 2000).

RyR channels also form signaling complex with TRPV4 and K_{Ca} channels in rat

cerebral artery smooth muscle cells, and produce membrane hyperpolarization and vasodilation (Earley *et al.*, 2005). In smooth muscle cells of pulmonary arteries and portal vein, Ca^{2+} sparks activate Ca^{2+}-activated chloride (Cl_{Ca}) channels, leading to chloride (Cl^-) efflux and membrane depolarization (Wang *et al.*, 1992; Hogg *et al.*, 1993). Rat pulmonary artery smooth muscle cells express both K_{Ca} and Cl_{Ca} channels, giving rise to mixed K^+ and Cl^- efflux.

1.4.3. Ca^{2+} waves

Ca^{2+} waves are intracellular Ca^{2+} transients that propagate across the whole cell along the longitudinal axis (Jaggar *et al.*, 2000; Jaggar & Nelson, 2000). Ca^{2+} wave generation requires: 1) a stimulus that activates Ca^{2+} channels, initiating Ca^{2+} release; 2) regenerative Ca^{2+} release propagating across the cell; 3) Ca^{2+} clearance from the cytosol; 4) refilling of intracellular Ca^{2+} stores; and 5) reactivation of Ca^{2+} release channels (Lee *et al.*, 2005).

In resting arterial smooth muscle cells, Ca^{2+} wave frequency is low (Jaggar & Nelson, 2000). Vasoconstrictors, including ET-1, NE, phenylephrine, uridine 5'-triphosphate (UTP), and vasopressin stimulate Ca^{2+} waves in smooth muscle cells of rat tail artery, portal vein, mesenteric and cerebral arteries (Boittin *et al.*, 1999; Jaggar & Nelson, 2000; Mauban *et al.*, 2001; Lamont & Wier, 2004; Dai *et al.*, 2007). Elevating the agonist concentration increases the frequency but not the amplitude of Ca^{2+} waves (Shimamura *et al.*, 1999; Lee *et al.*, 2002). Intravascular pressure elevation increases Ca^{2+} wave frequency via increasing IP_3 synthesis and activating RyR channels (Jaggar, 2001). Blocking SERCA abolishes Ca^{2+} waves, suggesting the requirement of Ca^{2+} release from intracellular Ca^{2+} stores (Lee *et al.*, 2002). Ca^{2+} waves could occur by activation of both RyR and IP_3Rs, with the relative involvement of each varying in different smooth muscle cells. In rat portal vein smooth muscle cells, an anti-IP_3R antibody blocked NE-induced Ca^{2+} waves (Boittin *et al.*, 1999). Vasoconstrictor-induced Ca^{2+} waves are also abolished by ryanodine (Blatter & Wier, 1992; Lamont & Wier, 2004). In rat pulmonary artery smooth muscle cells, NAADP initiated Ca^{2+} waves, which were blocked by ryanodine but not by xestospongin C (XeC), an IP_3R inhibitor (Gafni *et al.*, 1997), suggesting that NAADP-mediated RyR activation results in Ca^{2+} waves (Boittin *et al.*, 2002). During a Ca^{2+} wave, intracellular stores release Ca^{2+} and need to be refilled by extracellular Ca^{2+} influx to maintain the ongoing wave (Lee *et al.*, 2005). In rat cerebral arteries, diltiazem, a $Ca_V1.2$ channel inhibitor blocked Ca^{2+} influx and reduced Ca^{2+} waves (Jaggar, 2001). The oscillatory feature of Ca^{2+} waves implicates repetitive $[Ca^{2+}]_i$ increase due to Ca^{2+} release from intracellular stores, and $[Ca^{2+}]_i$ decrease due to both a reduction in Ca^{2+} release and removal of cytosolic Ca^{2+} (Aalkjaer & Nilsson, 2005).

Presently, the physiological function of Ca^{2+} waves is poorly understood. In rat mesenteric arteries, adrenergic stimulation using vasoconstrictors, including phenylephrine and NE elevated asynchronous propagating wave-like Ca^{2+} transients which induced vasoconstriction (Miriel *et al.*, 1999; Mauban *et al.*, 2001; Lamont &

Wier, 2004) and synchronous spatially uniform Ca^{2+} transients which caused oscillatory vasomotion (Mauban *et al.*, 2001; Lamont & Wier, 2004). In rat cerebral arteries, alkalinizing external pH (Heppner *et al.*, 2002) or increasing intravascular pressure from 10 to 60 mm Hg (Jaggar, 2001) elevated Ca^{2+} wave frequency, but Ca^{2+} waves do not appear to significantly contribute to the global $[Ca^{2+}]_i$ elevation required for vasoconstriction (Jaggar, 2001; Heppner *et al.*, 2002). Therefore, it is unclear if Ca^{2+} waves influence vascular contractility with reports suggesting that activation of a large Ca^{2+} wave frequency can induce constriction, while others indicate that Ca^{2+} waves and oscillations do not contribute to contractile Ca^{2+} (Jaggar, 2007). Apart from contractility, Ca^{2+} waves have been suggested to regulate gene expression in cultured mouse cerebral artery segments (Wilkerson *et al.*, 2006). IP_3R-mediated Ca^{2+} waves induced nuclear translocation of proliferating cell nuclear antigen, a transcriptional regulator resulting in smooth muscle cell proliferation (Wilkerson *et al.*, 2006).

1.4.4. Ca^{2+} sparklets

Ca^{2+} sparklets are intracellular subsarcolemmal Ca^{2+} transients generated by Ca^{2+} influx through one or several tightly clustered VDCCs, causing a local high $[Ca^{2+}]_i$ elevation near the Ca^{2+} channel (Amberg *et al.*, 2007). In cerebral artery smooth muscle cells, Ca^{2+} sparklets occur due to the activation of $Ca_V1.2$ channels (Navedo *et al.*, 2005; Navedo *et al.*, 2006). There are two modes of Ca^{2+} sparklet activity in arterial smooth muscle cells. Low activity Ca^{2+} sparklets occure due to random, brief openings of L-type Ca^{2+} channels (Navedo *et al.*, 2006). Persistent Ca^{2+} sparklets occur due to small clusters of L-type Ca^{2+} channels operating in a high activity mode, generating sites of constant Ca^{2+} influx (Navedo *et al.*, 2006). Persistent Ca^{2+} sparklets occur as a result of AKAP150, a scaffolding protein, which targets PKC alpha (PKCα) to specific regions of the plasma membrane, leading to Ca^{2+} channel activation, Ca^{2+} influx, and global $[Ca^{2+}]_i$ elevation (Navedo *et al.*, 2008). Calcineurin, which is associated with AKAP150, inhibits PKCα and Ca^{2+} sparklets (Navedo *et al.*, 2008). Membrane depolarization increases the occurrence of both modes of Ca^{2+} sparklets, resulting in an elevation in local and global $[Ca^{2+}]_i$ (Santana & Navedo, 2009). Ca^{2+} sparklet activity is increased in arterial smooth muscle cells during hypertension, resulting in activation of the transcription factor nuclear factor of activated T cell (NFAT) c3 (Nieves-Cintron *et al.*, 2008). Ca^{2+} sparklet activity is also elevated via a PKA-dependent pathway in cerebral artery smooth muscle cells during hyperglycemia (Navedo *et al.*, 2010).

1.5. Mitochondria in Vascular Smooth Muscle Cells

1.5.1. Electron transport chain and ATP synthesis

Mitochondrial ETC consists of four proteins called Complexes I (NADH-ubiquinone oxidoreductase), II (succinate dehydrogenase), III (cytochrome bc_1), and IV (cytochrome c oxidase) (Fernie *et al.*, 2004). Electrons are transferred from the strongly

reducing products (NADH, succinate) of the citric acid cycle through the ETC complexes to molecular oxygen (O_2) (Fernie *et al.*, 2004). Coenzymes ubiquinone (UQ), which is in the lipid membrane and cytochrome c, which is in the intermembrane space regulate the electron transfer between the ETC complexes (Fernie *et al.*, 2004). Complex I transfers electrons from the Kreb's cycle product NADH to UQ, which also receives electrons from complex II (Fernie *et al.*, 2004). UQ transfers electrons from Complexes I and II to III, and cytochrome c transfers electrons from Complex III to IV (Fernie *et al.*, 2004). Complex IV uses the electrons to reduce O_2 to water. Energy obtained as a result of electron transfer through the ETC complexes is coupled to pump protons from the mitochondrial matrix to the intermembrane space by complexes I and IV, and by UQ at complexes I, II, and III (Fernie *et al.*, 2004). Proton pumping creates an electrochemical proton gradient across the inner mitochondrial membrane (Fernie *et al.*, 2004). ATP synthase uses the H^+ flow down the gradient back into the matrix to stimulate ATP production from ADP and Pi (Fernie *et al.*, 2004).

1.5.2. Mitochondrial membrane potential

The proton gradient that is physiologically generated across the inner mitochondrial membrane by the respiratory chain activity is responsible for the maintenance of ψ_m (Gunter *et al.*, 2000). ψ_m is ~150-180 mV more negative compared to the cytosol (Gunter *et al.*, 2000). Kinetics of ATP synthase follows a sigmoidal pattern in response to increase in ψ_m, reaching a plateau phase when ψ_m ~50 mV more negative compared to the cytosol, suggesting that ATP synthesis is regulated primarily by the availability of the substrates ADP and Pi and not by ψ_m in the physiological range (Brookes, 2005). ψ_m maintenance is essential for the normal functioning of mitochondria. Transport of ions and metabolites into and out of the mitochondria is regulated predominantly by ψ_m (Brookes, 2005). According to Nernst equation, equilibrium would be reached only if $[Ca^{2+}]_{mito}$ is 10^6 times that of $[Ca^{2+}]_i$ (Graier *et al.*, 2007). Uncouplers, including carbonyl cyanide 3-chlorophenylhydrazone (CCCP), which disrupt the proton gradient across the inner mitochondrial membrane, reduce the driving force for Ca^{2+}, resulting in strongly diminishing mitochondrial Ca^{2+} uptake (Graier *et al.*, 2007).

1.5.3. Spatial proximity between SR and mitochondria

To reconcile the low mitochondrial affinity for Ca^{2+} at physiological $[Ca^{2+}]_i$, mitochondria may be exposed to Ca^{2+} microdomains, such as intracellular Ca^{2+} stores, permitting localized mitochondrial Ca^{2+} uptake to occur (Rizzuto *et al.*, 2009). In HeLa cells, imaging green fluorescent protein (GFP) constructs targeted to the SR and mitochondria has revealed that ~5-20 % of the mitochondrial surface is in close apposition to the SR (Rizzuto *et al.*, 2009). Conventional thin section transmission electron microscopy studies indicate that mitochondria are located in close proximity (~10-25 nm) to the SR in many cell types, including arterial smooth muscle cells (Rizzuto *et al.*, 1999; Duchen, 2000b; Szado *et al.*, 2003; Rizzuto *et al.*, 2009).

To achieve effective local Ca^{2+} signaling between the SR and mitochondria, the SR Ca^{2+} release sites and the mitochondrial Ca^{2+} uptake channels should be present at the interface area (Hajnoczky *et al.*, 2000). Distribution of the IP_3Rs and RyRs is not homogenous on the SR membrane (Hajnoczky *et al.*, 2000). In cardiac muscle cells, ~90% of the SR Ca^{2+} release channels are located very close to mitochondria (Sharma *et al.*, 2000). A high density of IP_3R1 and IP_3R2 exist on regions of the SR which face the mitochondria (Takei *et al.*, 1992; Simpson *et al.*, 1997). MCU is exclusively localized in the regions of contact between the mitochondria and ER (Hajnoczky *et al.*, 2000).

In addition to being in close proximity to each other, SR and mitochondria may be physically tethered to one another to sustain local communication during continuous organelle movement and reorganization (Hajnoczky *et al.*, 2000; Csordas & Hajnoczky, 2009). The SR-mitochondria physical coupling is established via several anchoring proteins, including dynamin-like protein-1 (Pitts *et al.*, 1999), glucose-regulated protein 75 (Szabadkai *et al.*, 2006), sigma-1 receptor (Hayashi & Su, 2007), and mitofusin-2 (De Brito & Scorrano, 2008). Since both SR and mitochondria bind to microtubules/actin filaments, cytoskeletal proteins may also offer additional physical support to the SR-mitochondria associations (Spat *et al.*, 2008). Therefore, the spatial distribution of SR and mitochondria, and the physical coupling between them may provide a strong platform for efficient local communication.

Not all the mitochondria are in close proximity to the SR. Some mitochondria may be isolated or relatively far from the SR, resulting in them either not or poorly responding to SR Ca^{2+} release (Hajnoczky *et al.*, 2000). There may also exist substantial heterogeneity among different mitochondria in the efficacy of Ca^{2+} uptake with differences in MCU activation, driving force, rate, and peak of Ca^{2+} uptake (Rizzuto *et al.*, 2004). Therefore, a sub-population of mitochondria may be exposed to $[Ca^{2+}]_i$ much higher than other mitochondria in the same cell (McCarron *et al.*, 2006).

1.5.4. Interplay between mitochondria and cytosolic Ca^{2+} signals

Ca^{2+} transport pathways of the mitochondria consist of high velocity, ψ_m-driven uptake mechanisms which are activated by local $[Ca^{2+}]_i$ elevations, and slow, easily saturable, concentration-dependent efflux systems, which are only mildly stimulated by $[Ca^{2+}]_{mito}$ elevations. Therefore, mitochondria accumulate Ca^{2+} during rapid, local $[Ca^{2+}]_i$ elevations and slowly release it back into the cytosol (Rizzuto *et al.*, 2000). This permits the mitochondria to alter spatio-temporal patterns of global and local Ca^{2+} signaling (Rizzuto *et al.*, 2000; Xi *et al.*, 2005). The physiological range of arterial smooth muscle cell global $[Ca^{2+}]_i$ is ~100-300 nM. Local Ca^{2+} signals elevate Ca^{2+} into the micromolar concentration range, which is sufficient for mitochondrial Ca^{2+} uptake because *in vitro* K_d for Ca^{2+} of MCU is ~10-20 μM (Gunter & Pfeiffer, 1990; Perez *et al.*, 2001). SR Ca^{2+} release due to the activation of IP_3R-gated Ca^{2+}-release channels caused a micromolar increase in the local cytosolic $[Ca^{2+}]_i$ and Ca^{2+} uptake by localized mitochondria (Rizzuto *et al.*, 1993; Duchen *et al.*, 1998; Hajnoczky *et al.*, 2002). In rat pulmonary artery smooth muscle cells, cytosolic Ca^{2+} oscillations due to SR Ca^{2+} release resulted in

$[Ca^{2+}]_{mito}$ oscillations (Drummond & Tuft, 1999). In cardiac smooth muscle cells, local SR Ca^{2+} release via RyR channels elicited miniature $[Ca^{2+}]_{mito}$ elevations termed "Ca^{2+} marks", and transient mitochondrial depolarizations termed "flickers" (Duchen *et al.*, 1998; Pacher *et al.*, 2002).

Vascular smooth muscle cell mitochondria can in turn feedback to alter the activity of Ca^{2+} channels which produce the local Ca^{2+} signals (Cheranov & Jaggar, 2004; Poburko *et al.*, 2004; Chalmers *et al.*, 2007). In particular, mitochondria regulate IP_3R and RyR channel activity, and in turn influence the propagation of Ca^{2+} waves and generation of Ca^{2+} sparks, respectively (Lee *et al.*, 2002; Wellman & Nelson, 2003). Mitochondria can regulate these SR Ca^{2+} release channels by buffering local $[Ca^{2+}]_i$, controlling ATP synthesis, via reactive oxygen species (ROS) signaling, and cADPr metabolism (Poburko *et al.*, 2004; Xi *et al.*, 2005; Chalmers *et al.*, 2007). RyR and IP_3R are sensitive to cADPr and ATP, respectively (Bezprozvanny & Ehrlich, 1995; Sitsapesan *et al.*, 1995), and both channels have distinct Ca^{2+}-sensitive stimulating and inhibiting sites. By influencing channel modulators and by buffering $[Ca^{2+}]_i$, mitochondria can regulate both the Ca^{2+} sensitivity and the duration of opening of RyR and IP_3R. In various cell types, including vascular smooth muscle cells, mitochondria affect RyR channel activity and influence the frequency and amplitude of Ca^{2+} sparks (Pacher *et al.*, 2002; Xi *et al.*, 2005). In cerebral artery smooth muscle cells, mitochondrial depolarization-induced ROS elevation activated Ca^{2+} sparks, leading to K_{Ca} channel stimulation, resulting in vasodilation (Xi *et al.*, 2005). In pulmonary and mesenteric artery smooth muscle cells, mitochondria increased both Ca^{2+} spark frequency and amplitude, resulting in increased Cl_{Ca} current (Wang *et al.*, 2003). Mitochondrial regulation of IP_3R activity has been reported in colonic and arterial smooth muscle cells (McCarron & Muir, 1999; Sward *et al.*, 2002). In rat tail artery smooth muscle cells, mitochondrial inhibitors increased the frequency and decreased the amplitude of IP_3R-mediated $[Ca^{2+}]_i$ oscillations (Sward *et al.*, 2002). Mitochondria can also regulate SR Ca^{2+} refilling by controlling ATP synthesis and modulating Ca^{2+} efflux via mNCX (Landolfi *et al.*, 1998; Arnaudeau *et al.*, 2001). In vascular smooth muscle cells, mitochondria regulate the activity of several plasma membrane ion channels, including SOCCs, VDCCs, K_{Ca}, and Cl_{Ca} channels (Poburko *et al.*, 2004). Mitochondria influence plasma membrane channel activity by buffering local subplasmalemmal Ca^{2+} gradients, which activate or inhibit channels and also through regulation of SR Ca^{2+} refilling, which dictates the activity of SOCCs (Poburko *et al.*, 2004). Therefore, the activity of mitochondria may regulate and be influenced by Ca^{2+} signals in smooth muscle cells.

1.5.5. Role of mitochondria in vascular smooth muscle cells

In vascular smooth muscle cells, the physiological role of mitochondria apart from their energy-generating function is unclear. Mitochondria provide an efficient system for buffering cytosolic Ca^{2+} changes, thereby controlling a variety of mitochondrial events, including ATP synthesis, mPTP opening, and mitochondrial ROS (mitoROS) generation. However, the physiological consequences of these $[Ca^{2+}]_{mito}$ elevation-mediated events are poorly understood.

Mitochondrial dysfunction is associated with several pathological conditions of the vasculature, including apoptosis, migration, remodeling, and glycation (Lee *et al.*, 2008; Birukov, 2009; Wang *et al.*, 2009; Ahn *et al.*, 2010). Few studies have examined the role of mitochondria in regulating physiological functions of vascular smooth muscle cells. In cerebral artery smooth muscle cells, mitoROS activate Ca^{2+} sparks and stimulate K_{Ca} channels, resulting in vasodilation (Xi *et al.*, 2005). Cold-induced constriction of cutaneous arteries is mediated through mitoROS generation (Bailey *et al.*, 2005). During hypoxia, mitochondria in pulmonary artery smooth muscle cells act as oxygen sensors and stimulate redox-sensitive transcription factors (Schumacker, 2003; Sato *et al.*, 2005). Therefore, there is very minimal information available about the role of mitochondria in mediating normal physiological processes other than ATP synthesis in vascular smooth muscle cells.

1.6. Reactive Oxygen Species in Vascular Smooth Muscle Cells

In physiological or pathological conditions, O_2 is converted into highly reactive oxygen-derived molecules and free radicals, called reactive oxygen species (ROS) that interact with reducible compounds. There are different species of ROS, including hydrogen peroxide (H_2O_2), superoxide anion ($O^{2-}\cdot$), hydroxyl radical ($OH\cdot$). nitric oxide (NO), peroxynitrite ($ONOO\cdot$), hypochlorous acid (HOCl), and singlet oxygen ($^1O_2$) (Mueller *et al.*, 2005; Gloire *et al.*, 2006). $O^{2-}\cdot$ and H_2O_2 are the two major species of ROS produced in cells. $O^{2-}\cdot$ through reaction with NO generates $ONOO\cdot$. $OH\cdot$ is produced from H_2O_2 in a Fenton reaction (Turrens, 2003).

1.6.1. Cellular sources of ROS

Multiple sources generate ROS, including mitochondrial ETC complexes, NAD(P)H oxidase, cytochrome P450 (CYP450), xanthine oxidoreductase, NO synthase (NOS), cyclooxygenases, and lipoxygenases (Irani, 2000; Turrens, 2003; Wong *et al.*, 2003; Mueller *et al.*, 2005; Clempus & Griendling, 2006). The major sources of ROS in vascular smooth muscle cells are mitochondrial ETC and NAD(P)H oxidase (Mueller *et al.*, 2005).

1.6.1.1. Mitochondrial ETC complexes

Mitochondrial ETC is a major source of $O^{2-}\cdot$ and H_2O_2 in most tissues, including vascular smooth muscle cells (Mueller *et al.*, 2005; Clempus & Griendling, 2006). Under normal metabolic conditions, electron leakage occurs during transfer between complexes, resulting in the incomplete reduction of ~1–5% of total O_2 consumed, to produce $O^{2-}\cdot$ (Mueller *et al.*, 2005). Mitochondrial $O^{2-}\cdot$ production occurs primarily at ETC complexes I and III (Mueller *et al.*, 2005). The main source of $O^{2-}\cdot$ in mitochondria is the ubisemiquinone radical intermediate ($QH\cdot$), which is formed from UQ at complex III (Brookes *et al.*, 2004). $QH\cdot$ formation occurs under two conditions: 1) an increase in

$QH\cdot$ concentration when ETC is inhibited distally, and 2) an increased rate of $QH\cdot$ production when ETC functions faster (Brookes *et al.*, 2004). Therefore, both stimulation and inhibition of mitochondrial ETC elevate mitochondrial $O^{2-}\cdot$ generation.

Mitochondrial superoxide dismutase converts $O^{2-}\cdot$ to H_2O_2 (Clempus & Griendling, 2006). Since $O^{2-}\cdot$ generation is non-enzymatic, the rate of mitoROS production is directly proportional to the rate of metabolism (Brookes, 2005). MitoROS generation is regulated primarily by the redox state of the ETC complexes, which is controlled by the ψ_m and the proton gradient (Brookes, 2005; Xi *et al.*, 2005). Several other stimuli, including mitochondrial Ca^{2+} uptake (Wolin *et al.*, 2005), and mPTP opening (Wang *et al.*, 2008a) stimulate mitoROS production in cell types, including vascular smooth muscle cells. MitoROS regulates several physiological and pathological signaling pathways, including cell cycle, cell proliferation, apoptosis, metalloproteinase function, protein phosphorylation, dephosphorylation, Ca^{2+} signaling, vascular contractility, and transcription factors (Brookes *et al.*, 2004; Xi *et al.*, 2005).

1.6.1.2. NAD(P)H oxidase

NAD(P)H oxidases are multiprotein complexes consisting of the $p22^{phox}$ subunit bound to the catalytic subunit Nox (known as $gp91^{phox}$ in phagocytes) (Touyz *et al.*, 2002; Mueller *et al.*, 2005; Paravicini & Touyz, 2006; Parfenova & Leffler, 2008; Basuroy *et al.*, 2009). In addition to the membrane-bound Nox/$p22^{phox}$ complex, there are three cytosolic subunits, including Rac1, $p47^{phox}$ and $p67^{phox}$, which are recruited to the membrane upon activation (Abo *et al.*, 1991; Ambasta *et al.*, 2004; Basuroy *et al.*, 2009). The catalytic subunit in vascular smooth muscle cells is either Nox1, Nox2, or Nox4 (Mueller *et al.*, 2005; Paravicini & Touyz, 2006). Nox1 expression levels, which are low in vascular smooth muscle cells, can be induced by stimuli such as platelet-derived growth factor (PDGF), Ang II, and serum (Lassegue & Clempus, 2003). Nox2 is expressed in endothelial and adventitial cells of large arteries and in vascular smooth muscle cells of smaller resistance-size arteries (Wang *et al.*, 1998; Gorlach *et al.*, 2000; Touyz *et al.*, 2002; Parfenova & Leffler, 2008; Basuroy *et al.*, 2009). Nox4 is constitutively expressed and active in vascular smooth muscle and endothelial cells (Ago *et al.*, 2004; Hilenski *et al.*, 2004; Basuroy *et al.*, 2009).

Activation of NAD(P)H oxidase results in the assembly of the cytosolic and membrane-bound subunits to form an enzyme complex (Lassegue & Clempus, 2003; Mueller *et al.*, 2005). NAD(P)H oxidase produces $O^{2-}\cdot$ by the transfer of two electrons from NAD(P)H to O_2 (Paravicini & Touyz, 2006). Vasoactive hormones (Ang II), growth factors (PDGF), and mechanical stimuli (shear stress) activate NAD(P)H oxidase in vascular smooth muscle cells (Mueller *et al.*, 2005).

1.6.1.3. Cytochrome P450

Membrane-bound microsomal monooxygenase system is present in the SR of most tissues, including vascular smooth muscle cells (Zangar *et al.*, 2004). It contains CYP450 enzymes which oxygenate exogenous and endogenous compounds. NAD(P)H-CYP450 reductase transfers two electrons to CYP450 resulting in activation of O_2, leading to monooxygenation of substrates (Zangar *et al.*, 2004). The efficiency with which electrons are transferred from NAD(P)H to CYP450 for substrate oxygenation is not tightly regulated, resulting in ROS production (Gorsky *et al.*, 1984; Blanck *et al.*, 1991). Therefore, continuous generation of $O^{2-}\cdot$ and H_2O_2 by CYP450, as a result of NAD(P)H consumption occurs both in the presence and absence of substrates (Kuthan & Ullrich, 1982; Zangar *et al.*, 2004).

1.6.1.4. Xanthine oxidoreductase

The xanthine oxidoreductase system exists as xanthine dehydrogenase (XDH) and xanthine oxidase (XO) (Mueller *et al.*, 2005). XDH transfers electrons from hypoxanthine and xanthine to NAD^+ to produce NADH and uric acid (Harrison, 2002). XO forms $O^{2-}\cdot$ and H_2O_2 by transferring electron from NADH and uric acid to O_2 (Harrison, 2002). Therefore, the relative cellular amounts of XDH and XO determine the ROS produced (Mueller *et al.*, 2005). Several stimuli, including tumor necrosis factor alpha (TNF-α), and $ONOO^-\cdot$ convert XDH to XO, and thereby increase ROS production in vascular smooth muscle cells (Friedl *et al.*, 1989; Sakuma *et al.*, 1997).

1.6.1.5. Nitric oxide synthases

There are three NOS isoforms, namely endothelial NOS (eNOS) and nNOS, which are constituvely expressed, and inducible NOS (iNOS) (Kibbe *et al.*, 1999). Under normal conditions, NOS transfers electrons to L-arginine in the presence of cofactor tetrahydrobiopterin (BH_4) to yield NO (Mueller *et al.*, 2005).

eNOS activity is regulated by $[Ca^{2+}]_i$ between ~100 and 500 nM, which permits CaM binding and its activation (Forstermann *et al.*, 1994). In pathological conditions, including hypertension, elevated levels of $O^{2-}\cdot$ oxidize BH_4 , thereby uncoupling eNOS, which transfers electron to O_2 instead of L-arginine to produce additional $O^{2-}\cdot$ (Mueller *et al.*, 2005).

In addition to eNOS-derived NO production in endothelial cells, NO generation in vascular smooth muscle cells occurs via iNOS (Griendling & FitzGerald, 2003). iNOS generates 100-1000-fold more NO than eNOS and nNOS (Kibbe *et al.*, 1999). iNOS is expressed in conditions where smooth muscle cells change from a contractile to a proliferative phenotype in response to cellular stress, inflammatory states, and arterial injury (Kibbe *et al.*, 1999; Griendling & FitzGerald, 2003).

1.6.1.6. Cyclooxygenases and lipoxygenases

Cyclooxygenases and lipoxygenases metabolize arachidonic acid. $O^{2-\cdot}$ production occurs due to the hydroperoxidase activity of the enzymes via side-chain reactions that are dependent upon the presence of a suitable reducing substrate, either NADH or NAD(P)H (Wong *et al.*, 2003). Like cyclooxygenases, lipoxygenases can produce $O^{2-\cdot}$ in the presence of either NADH or NAD(P)H (Lotzer *et al.*, 2005).

1.6.2. Antioxidant mechanisms

Cells have developed defensive antioxidant mechanisms to eliminate excess ROS from cell compartments and extracellularly. The antioxidant mechanisms include superoxide dismutase (SOD), catalase, thioredoxin, glutathione peroxidases and peroxiredoxins (Karihtala & Soini, 2007). In human cells, three different types of SODs are expressed, including cytosolic copper-zinc SOD, mitochondrial manganese SOD and extracellular SOD (Karihtala & Soini, 2007). All three SODs dismutate two $O^{2-\cdot}$ anions to H_2O_2 and O_2 (Karihtala & Soini, 2007). Catalase, thioredoxin, glutathione peroxidases, and peroxiredoxins reduce H_2O_2 to water and O_2 (Karihtala & Soini, 2007). When cellular production of ROS overwhelms its antioxidant capacity, a state of oxidative stress is reached leading to serious cellular injuries and contributing to the pathogenesis of several diseases.

1.6.3. ROS regulation of vascular smooth muscle cell functions

When generated in optimal concentrations, ROS can act as second messengers in regulating signal transduction pathways, leading to regulation of cellular responses in a variety of cell types and conditions, including cytokine, growth factor and hormone treatments, ion transport, transcription, neuromodulation, and apoptosis (Lander, 1997; Hensley *et al.*, 2000). Distinct properties of different species of ROS determine their capability of stimulating diverse signaling pathways, which may then lead to convergent or divergent consequences. $O^{2-\cdot}$ and $OH\cdot$ are very reactive, have short half-lives and therefore, are unlikely to mediate effects distant from where they are produced (Paravicini & Touyz, 2006). The negative charge on $O^{2-\cdot}$ prevents it from crossing cellular membranes, except through ion channels (Paravicini & Touyz, 2006). H_2O_2 is comparatively more stable, has a greater diffusion radius than $O^{2-\cdot}$ and $OH\cdot$, and is able to diffuse across membranes and between cells (Paravicini & Touyz, 2006). Therefore, different species of ROS are capable of regulating multiple signaling pathways, depending on their reactivity and stability (Paravicini & Touyz, 2006).

In arterial smooth muscle cells, several ligands, including Ang II, ET-1, and PDGF, mechanical stress, and hypoxia increase ROS production (Griendling *et al.*, 1994; Nishio & Watanabe, 1997; Xi *et al.*, 2005; Clempus & Griendling, 2006; Paravicini & Touyz, 2006). ROS exert their effects through interaction with and regulating the functions of multiple cellular components, including ion channels, protein kinases and

phosphatases, transcription factors, and cell cycle proteins (Clempus & Griendling, 2006; Paravicini & Touyz, 2006).

In vascular smooth muscle cells, ROS regulate several processes, including contractility, hypertrophy, hyperplasia, migration, differentiation, secretion of inflammatory cytokines, gene expression, extracellular matrix protein deposition, activation of matrix metalloproteinases, and inflammation (Clempus & Griendling, 2006; Paravicini & Touyz, 2006). ROS stimulate smooth muscle cell hypertrophy and hyperplasia by regulating the activity of redox-sensitive kinases and phosphatases, which lead to c-Src activation (Clempus & Griendling, 2006). Several vasoactive ligands, including PDGF, insulin-like growth factor-1, thrombin, vascular endothelial growth factor (VEGF), and monocyte chemoattractant protein-1 (MCP-1) induce redox-dependent migration of vascular smooth muscle cells (Clempus & Griendling, 2006). ROS mediate smooth muscle cell differentiation from a native, contractile to an invasive, proliferative phenotype in response to arterial injury (Clempus & Griendling, 2006). Arterial contractility is controlled by ROS by regulating functions of ion channels, including K_{Ca} channels (Xi *et al.*, 2005; Clempus & Griendling, 2006; Paravicini & Touyz, 2006). In addition, ROS also influence gene expression by activating redox-sensitive transcription factors.

ROS modulate the activity of redox-sensitive transcription factors, including activator protein (AP)-1, nuclear factor kappa B (NF-κB), cyclic AMP response element-binding protein (CREB), hypoxia-inducible factor-1 alpha (HIF-1α), peroxisome proliferator-activated receptors, NF-E2-related factor-2 (Nrf2), Gax, and gut-enriched kruppel-like factor in vascular smooth muscle cells (Clempus & Griendling, 2006; Gloire *et al.*, 2006). ROS regulation of transcription factor activity occurs via direct and indirect mechanisms (Kunsch & Medford, 1999). Direct mechanism involves oxidation of the transcription factor, leading to alteration of its activity (Kunsch & Medford, 1999). ROS can also indirectly control transcription factor function by regulating its post-translational modifications (phosphorylation or dephosphorylation) via redox-sensitive kinases and phosphatases (Kunsch & Medford, 1999). Both mechanisms alter several properties of transcription factors, including cellular localization, DNA binding, and recruitment of activators and/or repressors (Kunsch & Medford, 1999). Vasoconstrictors, including Ang II induce expression of genes, including MCP-1 and interleukin (IL)-6 through ROS-dependent NF-κB activation (Chen *et al.*, 1998; Han *et al.*, 1999). Therefore, ROS regulate both physiological and pathological functions in vascular smooth muscle cells.

1.7. NF-κB in Vascular Smooth Muscle Cells

1.7.1. NF-κB family of proteins

NF-κB proteins comprise structurally-related eukaryotic transcription factors that regulate gene expression and control a large number of cellular processes, including immune and inflammatory responses, cellular growth, and apoptosis. NF-κB proteins

regulate gene expression by binding to *cis*-acting κB sites in the promoter regions. In mammals, there are five NF-κB/REL genes, NF-κB1, NF-κB2, RELA, c-REL and RELB (Chen & Greene, 2004; Hayden & Ghosh, 2008). The NF-κB family of transcription factors contains five members: NF-κB1 (p105/p50), NF-κB2 (p100/p52), RelA (p65), RelB, and c-Rel (Chen & Greene, 2004; Hayden & Ghosh, 2008). NF-κB proteins are related through the presence of a highly conserved Rel homology domain in their N-terminal region (Chen & Greene, 2004; Hayden & Ghosh, 2008). The Rel homology domain which contains a nuclear localization sequence is involved in DNA binding, dimerization with other NF-κB proteins, and interaction with the inhibitory I kappa B (IκB) proteins (Chen & Greene, 2004; Hayden & Ghosh, 2008). p105 and p100 are processed to generate the DNA binding subunits p50 and p52, respectively. p105 and p100 proteins contain ankyrin repeats, as well as glycine-rich regions in their C-terminal regions. The glycine-rich regions are essential for co-translational processing of p105 to p50 and post-translational processing of p100 to p52 by the ubiquitin-proteasome pathway (Chen & Greene, 2004; Hayden & Ghosh, 2008). In addition to the Rel homology domain, p65, c-Rel, and RelB contain transactivation domains in their C-teminal region. Transactivation domains interact with various parts of the transcription apparatus to regulate gene expression (Chen & Greene, 2004; Hayden & Ghosh, 2008). p50 and p52 proteins contain the Rel homology domains but lack the transactivation domains. NF-κB proteins are expressed in a cell- and tissue-specific manner (Chen & Greene, 2004; Hayden & Ghosh, 2008). p50 and p65 are ubiquitously expressed, whereas NF-κB2, Rel-B, and c-Rel are specifically expressed in lymphoid tissues (Hayden & Ghosh, 2008).

NF-κB proteins dimerize to form homo- or hetero-dimers, which produce specific responses to different stimuli and diverse effects on transcription. The most often observed NF-κB complexes in cells are the p50-p65 and p52-RelB heterodimers (Sun & Andersson, 2002). Homodimers of p50 and p52 act as transcriptional repressors (Sun & Andersson, 2002). Presence of different NF-κB homo- and hetero-dimers determines which dimers control transcription. Therefore, depending on the dimer, transcriptional activity is either stimulated or inhibited (Sun & Andersson, 2002).

1.7.2. NF-κB activation pathways

There are two modes of signaling pathways, including the "classical/canonical" pathway and the "alternative/non-canonical" pathway, each of which lead to the translocation of NF-κB dimers from the cytosol to the nucleus (Bonizzi & Karin, 2004). NF-κB activated by each of these pathways regulate the transcription of distinct target genes (Bonizzi & Karin, 2004; Chen & Greene, 2004; Hayden & Ghosh, 2008).

1.7.2.1. Classical/Canonical pathway

The prototypical NF-κB complex comprising the p50-p65 heterodimer is bound to IκB which masks the nuclear localization signal (NLS) of p65 and causes cytosolic

retention of NF-κB (Bonizzi & Karin, 2004). Activation occurs when signalsome containing the IκB kinases (IKKs), including IKKα, IKKβ, and IKKγ phosphorylates IκB on serine residues 32 and 36 (Karin, 1999). IκB phosphorylation leads to IκB dissociation from the inactive NF-κB/IκB complex (Karin, 1999). Dissociated IκB is ubiquitinated and degraded by the 26S proteasome complex (Karin, 1999). IκB degradation unmasks the NLS on p65, leading to nuclear translocation of activated NF-κB and DNA binding (Karin, 1999).

1.7.2.2. Alternative/Non-canonical pathway

Certain stimuli, including B-cell activating factor and CD40 activate NF-κB-inducing kinase and IKKα, leading to NF-κB2 (p100) phosphorylation (Senftleben *et al.*, 2001). p100 phosphorylation leads to its ubiquitination, and is proteolytically processed by the 26S proteasome to yield p52 (Lin *et al.*, 1998). This pathway principally involves the p52-RelB heterodimer as opposed to the p50-p65 heterodimer produced by the canonical pathway (Senftleben *et al.*, 2001; Chen & Greene, 2004).

Upon nuclear translocation, NF-κB regulates gene expression by recruiting additional transcriptional activators and/or repressors, which contain κB consensus sequences (5'-GGGRNYYYCC-3', where R is a purine, Y is a pyrimidine, and N is any nucleic acid) (Chen & Greene, 2004). One of the target genes that is always stimulated by NF-κB is IκBα, which is depleted during the events of NF-κB activation (Chen & Greene, 2004). IκBα expression results in translocating the nuclear NF-κB back to the cytosol, thereby terminating the transcriptional regulation (Chen & Greene, 2004).

1.7.3. Mechanisms of NF-κB activation

NF-κB is activated by a range of stimuli, including various pro-inflammatory cytokines, growth factors, DNA-damaging agents, and viral proteins. The cellular events underlying NF-κB activation consists of IKK activation and IκBα degradation (classical pathway) or the post-translational processing of p100 to p52 (alternative pathway) (Sun & Andersson, 2002). With regard to vascular biology, various stimuli including TNF-α, IL-1, advanced glycation end products, hyperglycemia, mechanical stress, ROS, and hypoxia/reperfusion activate NF-κB (De Martin *et al.*, 2000). ROS activates NF-κB in vascular smooth muscle cells and other cell types (Asehnoune *et al.*, 2004; Bubici *et al.*, 2006; Miller, Jr. *et al.*, 2007). In addition, mitoROS activate NF-κB in several cell types, including in cultured vascular smooth muscle cells, skeletal muscle myotubes, and cultured macrophages (Li *et al.*, 1999; Chandel *et al.*, 2000; Lee *et al.*, 2008). The mechanism through which ROS activate NF-κB appears to involve the activity of IKKs, including IKKα and IKKβ (Gloire *et al.*, 2006).

1.7.4. Regulation of vascular function by NF-κB

NF-κB is constitutively activated and inactivated in arterial smooth muscle cells and is essential for the regulation of a variety of vascular functions, including smooth muscle cell proliferation, angiogenesis, and induction of cytokines (Asehnoune *et al.*, 2004; Bubici *et al.*, 2006; Clempus & Griendling, 2006; Miller, Jr. *et al.*, 2007). In arterial smooth muscle cells, NF-κB regulates expression of genes, including vascular cell adhesion molecule-1, IL-1, and c-*myc* (Bourcier *et al.*, 1997; Detmer *et al.*, 2001). NF-κB also induces expression of anti-apoptotic genes, leading to protection during abnormal proliferation (De Martin *et al.*, 2000). The physiological NF-κB-dependent gene expression may be exaggerated in pathological situations, resulting in damage to the vessel wall and impaired vascular cell function (De Martin *et al.*, 2000). High levels of NF-κB are present in arterial smooth muscle cells of arteriosclerotic intimal lesions (De Martin *et al.*, 2000).

Previous reports in cultured arterial smooth muscle cells have suggested that NF-κB plays an important role in regulating gene expression and proliferation (Landry *et al.*, 1997). NF-κB is also involved in regulating gene transcription of ion channels, including amiloride-sensitive Na^+ channel, small conductance Ca^{2+}-activated K^+ channel, and TRPC1 channel (Baines *et al.*, 2002; Paria *et al.*, 2006; Kye *et al.*, 2007) in several cell types, including cultured aortic smooth muscle cells. In pathological states, NF-κB activation has been shown to upregulate ET_B receptor expression in arterial smooth muscle cells, leading to enhanced contraction (Xu *et al.*, 2008). However, the physiological functions and mechanisms of regulation of NF-κB in contractile arterial smooth muscle cells are poorly understood. In this study, we have examined the physiological regulation of arterial contractility by NF-κB-dependent ion channel expression.

1.8. Transcriptional Regulation of $Ca_V1.2$ Expression

$Ca_V1.2$ channels are expressed in heart, vascular, and visceral smooth muscle cells (Ertel *et al.*, 2000). The α_{1C} subunit of human $Ca_V1.2$ is encoded by the CACNA1C gene, which is located in the distal region of chromosome 12 (Tang *et al.*, 2004). CACNA1C contains 55 exons, of which 15 are subjected to alternative splicing, generating 40 reported splice variations, expressed in different tissues (Tang *et al.*, 2004). In smooth muscle cells, alternatively splicing has been reported in exons 1, 8, and 9 in smooth muscle cells, and in exons 1, 8, 31, and 32 in cardiac muscle (Liao *et al.*, 2005). CACNA1C transcription is regulated by different promoters in cardiac muscle and smooth muscle cells (Dai *et al.*, 2002; Saada *et al.*, 2003). CACNA1C transcription is driven by promoters upstream of exon 1a and 1b in cardiac muscle and smooth muscle cells, respectively (Dai *et al.*, 2002; Saada *et al.*, 2003). The promoter driving α_{1C} expression in cardiac muscle has binding sites for several transcription factors, including myocyte enhancer factor-2, Nkx2.5, NFAT, and CREB (Dai *et al.*, 2002). The promoter region of α_{1C} in human colonic smooth muscle cells has 2 binding sites for CREB, which upregulates transcription, and 3 binding sites for NF-κB which represses transcription

(Shi *et al.*, 2005; Shi *et al.*, 2007). The identity of the transcription factors which bind to the promoter region of α_{1C} in vascular smooth muscle cells are unknown. It is poorly understood if transcription factors regulating α_{1C} gene expression in visceral and vascular smooth muscle cells are similar or different. In rat renal arteries, global $[Ca^{2+}]_i$ elevation increased $Ca_V1.2$ protein expression (Pesic *et al.*, 2004). In coronary artery smooth muscle cells, PKC delta (PKCδ) increased $Ca_V1.2$ protein levels (Maddali *et al.*, 2005). Although these studies report an increase in $Ca_V1.2$ protein levels, little is known about the transcriptional regulation of $Ca_V1.2$ α_{1C} gene in vascular smooth muscle cells.

1.9. Unresolved Issues

Smooth muscle cells from small, resistance-size arteries generate multiple types of local and global Ca^{2+} signals. Physiological functions of vasoconstrictor-induced Ca^{2+} signals, specifically Ca^{2+} waves in smooth muscle cells of resistance-size arteries are poorly understood (Miriel *et al.*, 1999; Jaggar, 2001; Mauban *et al.*, 2001; Heppner *et al.*, 2002; Lamont & Wier, 2004; Jaggar, 2007). Elevation in intracellular $[Ca^{2+}]_i$ induces mitochondrial Ca^{2+} uptake (Poburko *et al.*, 2004; Chalmers *et al.*, 2007), but identity of the intracellular Ca^{2+} signal(s) that regulate $[Ca^{2+}]_{mito}$ in arterial smooth muscle cells is unclear. Physiological functions of changes in $[Ca^{2+}]_{mito}$ and mitoROS in arterial smooth muscle cells are also poorly understood. Similarly, stimuli that cause mitochondrial depolarization and generate mitoROS in arterial smooth muscle cells are unclear (Rizzuto *et al.*, 1999; Duchen, 2000b; Szado *et al.*, 2003; Poburko *et al.*, 2004). Also, little is known about the mechanisms that regulate NF-κB activity in contractile arterial smooth muscle cells. $Ca_V1.2$ channels are the major Ca^{2+} entry pathway for smooth muscle cells of resistance-size arteries and are essential for myogenic tone development and blood pressure regulation (Cheng *et al.*, 2007). However, the transcriptional regulation of $Ca_V1.2$ gene expression in vascular smooth muscle cells is unclear.

This study aimed to determine the Ca^{2+} signaling mechanisms that regulate $[Ca^{2+}]_{mito}$ and to investigate the physiological functions of changes in $[Ca^{2+}]_{mito}$ in smooth muscle cells of resistance-size cerebral arteries in their native, contractile phenotype.

CHAPTER 2. HYPOTHESIS

2.1. Goal

The unifying goal of this study was to test the hypothesis that ET-1-induced IP_3R-mediated SR Ca^{2+} release elevates $[Ca^{2+}]_{mito}$ and mitoROS generation, which activates NF-κB, leading to transcription of $Ca_V1.2$ channels and vasoconstriction.

2.2. Specific Aims

2.2.1. Aim 1

To test the hypothesis that ET-1-induced IP_3R-mediated SR Ca^{2+} release elevates $[Ca^{2+}]_{mito}$ leading to mitochondrial depolarization.

Regulation of local and global Ca^{2+} signals by ET-1 was studied. Mechanisms by which ET-1 regulate $[Ca^{2+}]_{mito}$ and ψ_m were examined in arterial smooth muscle cells. ET-1 regulation of local and global Ca^{2+} signals was studied in intact arteries using fluo-4, a Ca^{2+}-sensitive fluorescent dye and rapid confocal imaging. $[Ca^{2+}]_{mito}$ was measured in smooth muscle cells of intact arteries using confocal imaging of 2mt8CG2, a mitochondria-targeted, genetically-encoded Ca^{2+} indicator. ψ_m was studied by measuring TMRM fluorescence in isolated cerebral artery smooth muscle cells.

2.2.2. Aim 2

To investigate the hypothesis that ET-1-induced $[Ca^{2+}]_{mito}$ elevation and mitochondrial depolarization elevate mitoROS production, which activates NF-κB.

The importance of ET-1-induced $[Ca^{2+}]_{mito}$ elevation and mitochondrial depolarization in the mitoROS elevation was examined. The contributions of ET-1-induced IP_3R-mediated SR Ca^{2+} release and mitoROS elevation in mediating NF-κB activation in arterial smooth muscle cells were also studied. MitoROS and cytosolic ROS were measured in smooth muscle cells of intact arteries using genetically-encoded fluorescent ROS indicators targeted to the mitochondria and cytosol, respectively. ROS measurements obtained using genetically-encoded fluorescent ROS indicators were confirmed using 5-(and-6)-chloromethyl-2',7'-dichlorodihydrofluorescein diacetate, acetyl ester (CM-H_2DCFDA) and laser-scanning confocal microscopy. ET-1 regulation of endogenous NF-κB activity was evaluated by using immunofluorescence to study nuclear translocation of activated NF-κB in smooth muscle cells of intact arteries. Transcriptional activity of NF-κB was measured by using luciferase reporter gene assays, which was also used to support results obtained in immmunofluorescence experiments.

2.2.3. Aim 3

To explore the hypothesis that NF-κB, activated by ET-1-induced mitoROS elevation, stimulates $Ca_v1.2$ transcription, leading to vasoconstriction.

Mechanisms by which ET-1 elevates $Ca_V1.2$ channel expression were investigated. The importance of ET-1-induced mitoROS elevation and NF-κB activation in regulating $Ca_V1.2$ expression in smooth muscle cells of cerebral arteries was studied. $Ca_V1.2$ mRNA and protein levels were quantified by real-time polymerase chain reaction (RT-PCR) and Western blotting, respectively. Pressurized artery diameter measurements were used to assess the functional effects of the ET-1-induced elevation in $Ca_V1.2$ expression.

CHAPTER 3. MATERIALS AND METHODS*

3.1. Vertebrate Animal Subjects

3.1.1. Justification of animal use

Male Sprague-Dawley rats (200–250 g body wt) (12-14 weeks of age) were purchased from Harlan-Teklad Laboratories (Ewing, IL). Rats were chosen for this study because diameter regulation by intravascular pressure, physiological functions of $Ca_V1.2$ channels, and vasoconstrictor-induced modulation of local and global Ca^{2+} signals are best described in rats. Therefore, rats were the most appropriate species in which to conduct this study. All experimental methodologies were carried out *ex vivo* on appropriate tissues collected from rats immediately following euthanasia. The number of animals used for a given experiment varied based on specific experimental design, variability of the measurements of the parameter in question, and the absolute difference among groups. For biochemical techniques such as Western blotting, it was usual for more than one rat to be used per experimental observation since the arteries used in this study gave smaller protein yields compared to other samples such as rat brain. For non-biochemical techniques used herein, one rat was typically used per experimental number. In functional studies, more than one drug was tested in a single experiment, either alone, or in combination with other modulators, which increased the experimental observations obtained per animal.

3.1.2. Information on veterinary care

Research was conducted in accordance with the Guide for Care and Use of Laboratory Animals, and the provisions of the Animal Welfare Act (USDA) and all other applicable federal and state laws and regulations. Protocols were reviewed and approved by IACUC. The University of Tennessee maintains an AAALAC-accredited facility that is staffed by three full-time veterinarians, two of whom are board-certified in laboratory animal care. The Department of Comparative Medicine (DCM) was responsible for husbandry and veterinary care for all vertebrate animals on campus. Animals were housed by species and health status to minimize infectious disease problems.

* Portions of this chapter adapted with permission. Narayanan D, Xi Q, Pfeffer LM, & Jaggar JH (2010). Mitochondria control functional $Ca_V1.2$ expression in smooth muscle cells of cerebral arteries. *Circ Res* **107**, 631-641.

3.1.3. Euthanasia

3.1.3.1. Procedure for limiting animal discomfort, distress, pain, and injury

All experiments were performed using cerebral arteries isolated from rat brain after euthanization. Rats were rendered pliant (immobile but visibly breathing) with CO_2 introduced directly into a specially designed housing chamber, prior to euthanasia by sodium pentobarbital injection. Care was taken at all times to minimize distress to rats during the euthanization process.

3.1.3.2. Method of euthanasia

Rats were euthanized by intraperitoneal injection of sodium pentobarbital solution (150 mg/kg) (Vortech Pharmaceuticals, Dearborn, MI). This method induces euthanasia smoothly and it is consistent with the recommendations of the American Veterinary Medical Association Panel on Euthanasia (American Veterinary Medical Association Panel on Euthanasia, 2001). Overdose of sodium pentobarbital causes rapid unconsciousness, followed by respiratory arrest through paralysis of the diaphragm and collapse of the lungs. The drug then suppresses cardiac activity, thus causing death. A new syringe and small needle was used with each animal to reduce injection trauma. Animal expiration was confirmed by cessation of spontaneous reflex movement to toe/skin pinch, absence of respiration, heartbeat, and corneal reflex. After confirmation of expiration, the rats were euthanized by decapitation and the brain removed, for dissection/removal of cerebral arteries.

3.2. Tissue Preparation

The brain was removed and placed into ice-cold (4°C) HEPES-buffered physiological salt solution (PSS) containing (in mM): 134 NaCl, 6 KCl, 2 $CaCl_2$, 1 $MgCl_2$, 10 HEPES, and 10 glucose (with pH adjusted to 7.4 with NaOH). Posterior cerebral, middle cerebral, and cerebellar arteries (~50–200 μm diameter) were removed from the brain. The arteries were cleaned of connective tissue. Care was taken while cleaning to avoid stretching and damage to the arteries. The cleaned arteries were placed in a petri dish containing 4°C HEPES-buffered PSS. Intact artery segments and enzymatically isolated smooth muscle cells were harvested on the day of experimentation. Enzymatically isolated smooth muscle cells were used for colocalization studies and ψ_m measurements. For all other experiments, intact artery segments were used.

3.3. Endothelial Denudation

When appropriate, endothelial layer of the arterial wall was removed. Briefly, the artery segments (1–2 mm in length) were cannulated at one end in a perfusion chamber (Living Systems Instrumentation, Burlington, VT). Following cannulation at one end, an air bubble was gently introduced into the arterial lumen for 2 minutes. After 2 minutes, PSS was flushed through the lumen. This approach of endothelial denudation has been shown to be effective in previous studies (Xi *et al.*, 2005; Adebiyi *et al.*, 2008; Zhao *et al.*, 2008).

3.4. Isolation of Arterial Smooth Muscle Cells

3.4.1. Preparation of solutions used for smooth muscle cell isolation

Isolated cerebral arteries were placed for 15 minutes in a Ca^{2+}-free solution containing (in mM): 55 NaCl, 80 sodium glutamate, 5.6 KCl, 2 $MgCl_2$, 10 HEPES, and 10 glucose (with pH adjusted to 7.4 with NaOH). 3 glass vials were rinsed with KOH and washed thoroughly with distilled water. Papain (0.7 mg/ml) and dithioerythreitol (1 mg/ml) were dissolved in enzyme solution (Ca^{2+}-free solution containing bovine serum albumin (BSA) (1 mg/ml)). Collagenases F and H were added to enzyme solution supplemented with $CaCl_2$ (100 μM) in a ratio of 2:1 (1 mg/ml total collagenase). Vials containing papain and collagenase solutions were warmed to 37°C for 10 minutes prior to transferring arteries into them.

3.4.2. Dissociation of smooth muscle cells

3.4.2.1. Freshly dissociated cerebral arteries

Cerebral arteries were placed into vial containing prewarmed papain solution and incubated for 12 minutes at 37°C. Then, the arteries were immediately transferred to a vial containing prewarmed collagenase solution and incubated for 9 minutes at 37°C. Arteries were subsequently washed in three petri dishes containing ice-cold Ca^{2+}-free solution for 10 min, to remove the enzymes from the arteries. The rinsed arteries were transferred to a vial containing Ca^{2+}-free solution and triturated gently using three polished glass pasteur pipettes of progressively decreasing diameter of their opening. The trituration process gently dissociates the smooth muscle cells from the arteries. Smooth muscle cells were used for experimentation within 8 hours of dissociation.

3.4.2.2. Reverse-permeabilized arteries

To deliver expression vectors into smooth muscle cells of intact arteries, reverse permeabilization procedure (described in detail in section 3.8) was used. Reverse-permeabilized arteries were then placed in Dulbecco's Modified Eagle Medium (DMEM)/F-12 culture medium (Cellgro, Manassas, VA) supplemented with penicillin/streptomycin (1%) (Cellgro, Manassas, VA) and placed in a 74% N_2/21% O_2/5% CO_2 incubator at 37°C for 4 days prior to use to allow expression of the genes of interest. After 4 days, smooth muscle cells were isolated and used for colocalization experiments. The protocol for dissociation of smooth muscle cells from reverse-permeabilized arteries was similar to that used for dissociating smooth muscle cells from freshly isolated arteries. The durations of papain and collagenase treatments were reduced to 9 and 7 minutes at 37°C, respectively.

3.5. Laser-Scanning Confocal Ca^{2+} Imaging

3.5.1. Fluo-4 AM loading

Endothelium-denuded cerebral artery segments were cannulated on 10-15 mm length borosilicate rectangular tubing (external dimensions: 220 × 40 μm) (internal dimensions: 200 × 20 μm, wall thickness: 20 μm) (Friedrich & Dimmock Inc., Millville, NJ). Branches were removed from cerebral artery segments to provide a flat surface for imaging. Cannulated arteries were incubated in the dark in HEPES-buffered PSS containing fluo-4 AM (10 μM) (Molecular Probes, Invitrogen, Eugene, OR) and 0.05% Pluronic F-127 (Molecular Probes, Invitrogen, Eugene, OR) for 1 hour at room temperature. To allow indicator de-esterification, the cannulated arteries were then placed for 30 minutes at room temperature in 30 mM K^+ solution containing (in mM): 110 NaCl, 30 KCl, 10 HEPES, 2 $CaCl_2$, 1 $MgCl_2$, and 10 glucose (with pH adjusted to 7.4 with NaOH). 30 mM K^+ solution depolarizes smooth muscle cells to ~-40 mV, which is similar to the membrane potential of cerebral arteries pressurized to 60 mmHg (Jaggar *et al.*, 1998; Jaggar & Nelson, 2000; Jaggar, 2001).

3.5.2. Imaging protocol

Intracellular Ca^{2+} signals in cerebral artery smooth muscle cells were imaged using a Noran Oz laser-scanning confocal microscope (Noran Instruments, Middleton, WI) with a 60X water-immersion objective (numerical aperture=1.2) attached to a Nikon TE300 microscope by illuminating with a krypton-argon laser at 488 nm and collecting emitted light >500 nm. Sequential planar images (256 × 240 pixels, 56.3 × 52.8 μm) of each region of the arterial wall containing ~8-10 smooth muscle cells were recorded every 16.6 ms (60 Hz) for 10 seconds. In each artery, 2-3 different regions of smooth muscle cells were scanned for each condition. The same area of artery was scanned only once to avoid any laser-induced changes in Ca^{2+} signaling. Ca^{2+} spark frequency, Ca^{2+}

wave frequency and global $[Ca^{2+}]_i$ were analyzed offline using custom software written with IDL 5.3 (Research Systems Inc., Boulder, CO) kindly provided by Dr. M. T. Nelson (University of Vermont, Burlington, VT). The full 10-second acquisition period of each image stack was analyzed to measure Ca^{2+} sparks, Ca^{2+} waves, and global $[Ca^{2+}]_i$.

3.5.3. Analysis of cytosolic Ca^{2+}signals

3.5.3.1. Detection of Ca^{2+} sparks and Ca^{2+} waves

Ca^{2+} sparks were detected by dividing fluorescence (F) in an area 1.54 μm × 1.54 μm (7 × 7 pixels, 2.37 μm^2) in individual smooth muscle cells in each image by a baseline fluorescence (F_0) that was determined by averaging 10 images without Ca^{2+} spark activity. The entire area of each image was analysed to detect Ca^{2+} sparks. A Ca^{2+} spark was defined as a localized rapid increase in F/F_0>1.2 (Jaggar *et al.*, 2000).

Ca^{2+} waves were detected by placing 2.2 × 2.2 μm (10 × 10 pixel, 4.84 μm^2) boxes in individual smooth muscle cells, and refer to an elevation in F/F_0>1.3 that was monitored for >200 milliseconds and propagated for more than 20 μm.

3.5.3.2. Calculation of Ca^{2+} spark and wave frequency, and global $[Ca^{2+}]_i$

Changes in Ca^{2+} spark frequency, Ca^{2+} wave frequency, and global $[Ca^{2+}]_i$ in response to pharmacological manipulation were determined in paired arteries. For each condition, Ca^{2+} spark and wave frequency for a region was calculated by dividing the number of Ca^{2+} sparks or waves detected in that region by the time of acquisition. Ca^{2+} spark and wave frequency per cell was calculated by dividing the frequency for each region by the number of smooth muscle cells in that region. Ca^{2+} spark and Ca^{2+} wave frequency, and global $[Ca^{2+}]_i$ that were obtained from smooth muscle cells of multiple regions of the same artery were averaged, giving data under each condition. Global F/F_0 for a given condition was calculated as the mean pixel value of 100 different images acquired over 10 seconds. Global $[Ca^{2+}]_i$ was calculated using the following equation: $[Ca^{2+}]_i = KR/\{K/([Ca^{2+}]_{rest} + 1 - R)\}$, where K is the apparent affinity of fluo-4 AM for Ca^{2+} (770 nM) (Cheranov & Jaggar, 2004), R is the fractional fluorescence increase (F/F_0), and $[Ca^{2+}]_{rest}$ is $[Ca^{2+}]_i$ at F_0 (193 nM) (Cheranov & Jaggar, 2004). Changes in global $[Ca^{2+}]_i$ were calculated from a control value previously determined using fura-2 (Cheranov & Jaggar, 2004). Arterial Ca^{2+} signal values were then averaged generating mean data. In results, n (experimental number) refers to the number of arteries from which data were obtained under each condition.

3.6. Genetically-Encoded Fluorescent Indicators

3.6.1. 2mt8CG2

pMITO-2mt8CG2 vector encoding 2mt8CG2, a genetically-encoded, mitochondria-targeted, fluorescent Ca^{2+} indicator (Griesbeck *et al.*, 2001; Filippin *et al.*, 2005) was a kind gift from Dr. Tullio Pozzan (University of Padua, Italy). pMITO-2mt8CG2 was constructed as follows: firstly, CaM, the Ca^{2+} probe was inserted into the backbone of yellow fluorescent protein (YFP) in place of Tyr^{145} (Griesbeck *et al.*, 2001). YFP-tagged CaM was then inserted in-frame with two copies of the first 36 amino acids of subunit VIII of human cytochrome c oxidase (ETC complex IV), a mitochondrial specific protein (Filippin *et al.*, 2005). 2mt8CG2 targets to mitochondria via cytochrome c oxidase subunit expression (Filippin *et al.*, 2005). Upon mitochondrial localization, Ca^{2+} in the mitochondrial matrix binds to CaM and causes a conformational change in YFP, leading to a change in fluorescence (Filippin *et al.*, 2005). 2mt8CG2 has a K_d for Ca^{2+} of ~5.3 μM (Griesbeck *et al.*, 2001). Therefore, 2mt8CG2 is not capable of detecting changes in global $[Ca^{2+}]_i$, which is usually in the nanomolar range (Rizzuto & Pozzan, 2006).

3.6.2. mt-cpYFP

pShuttle-CMV vector encoding mt-cpYFP, a genetically-encoded, mitochondria-targeted, fluorescent $O_2^{-}\cdot$ indicator was a kind gift from Dr. Heping Cheng (Peking University, China). mt-cpYFP comprises a circularly permuted YFP (cpYFP) that selectively detects $O_2^{-}\cdot$, the major ROS generated by the mitochondrial ETC (Wang *et al.*, 2008a). mt-cpYFP localizes to mitochondria using subunit IV of cytochrome C oxidase targeting sequence (Wang *et al.*, 2008a). *In vitro* experiments have suggested that fluorescence changes of cpYFP are highly selective to $O_2^{-}\cdot$ levels since its fluorescence is unchanged by H_2O_2 and $ONOO\cdot$, and is decreased by $OH\cdot$ and NO (Wang *et al.*, 2008a).

3.6.3. HyPer-CYTO

pHyPer-Cyto vector encoding HyPer-CYTO, a genetically-encoded cytosolic fluorescent H_2O_2 indicator was purchased from Axxora, Evrogen (San Diego, CA). HyPer comprises a cpYFP inserted into the regulatory domain of *Escherichia Coli* OxyR, a prokaryotic H_2O_2-sensing protein (Belousov *et al.*, 2006). Upon exposure to H_2O_2, the regulatory domain of OxyR undergoes a dramatic conformational change leading to an increase in cpYFP fluorescence (Belousov *et al.*, 2006). HyPer demonstrates affinity to H_2O_2 but is insensitive to other oxidants including $O^{2-}\cdot$, reactive nitrogen species, NO, and $ONOO\cdot$ (Belousov *et al.*, 2006).

3.7. Transformation of Bacteria

3.7.1. Introduction of expression vectors

Ultracompetent GC10 bacterial cells (Sigma-Aldrich, St.Louis, MO) (transformation efficiency is ~1×10^9 colony-forming units/µg of plasmid DNA) were used for transformation. Vector (~10 ng) was added to GC10 cells (50 µl) and incubated at 4ºC for 30 minutes. Cells were then heat shocked in a water bath at 42ºC for 45 seconds. This heat shock step permeabilizes the membrane of the competent cells so that the expression vector can enter the cells. Following heat shock, GC10 cells were added to LB Broth (950 µl) and incubated for 60 minutes at 37ºC. Incubation allows the cell membranes to recover from heat shock and permits cell replication to begin. Transformed bacteria were then plated onto LB agar plates. Ampicillin (100 µg/ml)-resistant plates were used for pMITO-2mt8CG2 vector. Kanamycin (50 µg/ml)-resistant plates were used for pShuttle-CMV and pHyPer-Cyto vectors, respectively. Agar plates were then incubated at 37°C for 16 to 20 hours. Following incubation, bacterial colonies which have taken up the expression vector and therefore resistant to the antibiotic added to the agar plate, appear on agar plates.

3.7.2. DNA Maxiprep

LB Broth (3 ml) was supplemented with ampicillin (100 µg/ml) (for pMITO-2mt8CG2) or kanamycin (50 µg/ml) (for pShuttle-CMV and pHyPer-Cyto). LB Broth supplemented with antibodies was inoculated with a single bacterial colony and incubated at 37°C at 200 RPM for 6 to 8 hours. This "starter culture" was then added to a large volume of LB Broth (150 ml) supplemented with antibodies and incubated at 37°C for 16 to 20 hours or until the solution turns turbid. Incubation allows amplification of the bacteria which have taken up the expression vector. Plasmid cDNA was purified from the bacterial culture using Qiagen Maxiprep HiSpeed Plasmid Purification kit (Qiagen, Valencia, CA).

3.7.3. Quantification of DNA

Maxipreped DNA (1:80 dilution) was quantified by measuring the absorbance of UV light at 230 nm (A230), 260 nm (A260), and 280 nm (A280 nm) using a UV spectrophotometer. DNA concentration was calculated using the equation:

$$\text{DNA concentration (µg/ml)} = (A260 - A230) \times \text{dilution factor} \times 50\ \text{µg/ml}$$

Nucleic acid purity was estimated from A260/A280 and A260/A230 ratios. Ratios between 1.8 and 2.0 generally represent high-quality nucleic acid sample. Reduction of A260/A280 and A260/A230 ratios indicate contamination with protein and organic compounds, respectively.

3.8. Reverse Permeabilization

3.8.1. Composition of solutions used

To deliver expression vectors into smooth muscle cells of intact arteries, reverse permeabilization was used (Lesh *et al.*, 1995; Welsh *et al.*, 2002). Compositions of the solutions used for reverse permeabilization are as follows. Solution 1 (in mM): 10 EGTA, 120 KCl, 5 ATP, 2 $MgCl_2$, 20 TES (pH 6.8 at 4°C); solution 2 (in mM): 120 KCl, 5 ATP, 2 $MgCl_2$, 20 TES (pH 6.8 at 4°C); solution 3 (in mM): 120 KCl, 5 ATP, 10 $MgCl_2$, 20 TES (pH 6.8 at 4°C); solution 4 (in mM): 140 NaCl, 5 KCl, 10 $MgCl_2$, 5.6 glucose, 2 MOPS (pH 7.1 at 22°C).

3.8.2. Procedure

Freshly isolated and cleaned arteries were placed into the following solutions: solution 1 for 20 minutes at 4°C, solution 2 containing expression vector (10 μg/ml) for 90 minutes at 4°C, solution 3 containing expression vector (10 μg/ml) for 30 minutes at 4°C, and solution 4 containing expression vector (10 μg/ml) for 30 minutes at room temperature. Ca^{2+} concentration in solution 4 was then increased incrementally to (in mM): 0.01, 0.1 and 1.8 at 15-minute intervals. Arteries were then placed in DMEM/F-12 culture medium supplemented with penicillin/streptomycin (1%) and placed in a 74% N_2/21% O_2/5% CO_2 incubator at 37°C for 4 days prior to use. **Fig. 3-1** illustrates HyPer-CYTO expression in smooth muscle cells of intact arteries.

3.8.3. Principle

The mechanism of reversible permeabilization has been suggested to involve binding of ATP^{4-} to cell surface receptors and the removal of membrane-associated divalent cations when the arteries are in solutions 1, 2, and 3 (Lesh *et al.*, 1995). The resulting increase in membrane permeability is responsible for the delivery of the expression vectors into the smooth muscle cells. The increase in membrane permeability is reversed in solution 4 by removal of extracellular ATP and addition of high [Mg^{2+}] followed by graded restoration of the physiological concentrations of extracellular Ca^{2+}. Arteries are then placed in DMEM/F-12 culture medium supplemented with penicillin/streptomycin (1%) for 4 days to allow expression of the genes of interest. Culture of arteries in serum-supplemented DMEM has been suggested to change the phenotype of smooth muscle cell from a contractile to an invasive proliferative one (Absher *et al.*, 1989; Campbell *et al.*, 1989; Eguchi *et al.*, 1994). To prevent the phenotypic change of smooth muscle cells, the arteries are incubated in serum-free DMEM. Studies suggest that reverse permeabilization does not alter the ultrastructural features and contractile properties of smooth muscle cells (Lesh *et al.*, 1995).

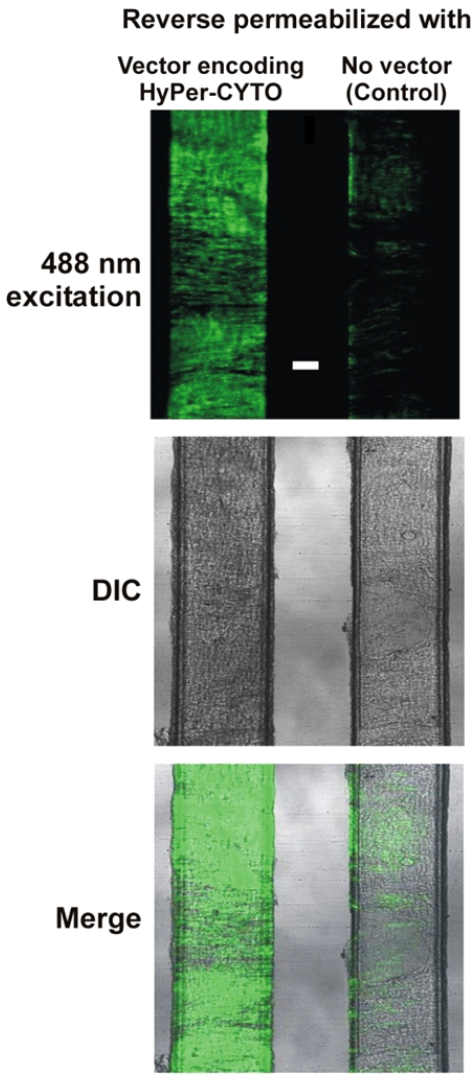

Figure 3-1. Reverse permeabilization of HyPer-CYTO in smooth muscle cells of intact arteries

Notes: Images comparing fluorescence in smooth muscle cells of intact arteries reverse permeabilized with either no vector or vectors encoding HyPer-CYTO. Rectangular glass cannula inserted intralumenally to provide a flat surface for imaging can be seen within each artery. Scale bar=20 μm.

3.9. Confocal Imaging of Genetically-Encoded Fluorescent Indicators

3.9.1. Introduction of indicators into arterial smooth muscle cells

pMITO-2mt8CG2, pShuttle-CMV, or pHyPer-Cyto vectors were inserted into smooth muscle cells of intact cerebral arteries using reverse permeabilization to express 2mt8CG2, mt-cpYFP, or HyPer-CYTO, respectively. Following incubation for 4 days in serum-free DMEM, cerebral artery segments were cannulated on borosilicate rectangular tubing for confocal imaging.

3.9.2. Imaging protocol

Cannulated artery segment was placed in a No. 0 glass coverslip bottom petri dish (MatTek Corporation, Ashland, MA). 2mt8CG2, mt-cpYFP, or HyPer-CYTO were excited with 488 nm light and emitted light >510 nm captured using a Zeiss LSM5 Pascal laser-scanning confocal microscope. In experiments where indicated, fluorescence was measured in smooth muscle cells of intact arteries. 2mt8CG2 fluorescence was measured using a z-resolution of ~4.5 μm, and mt-cpYFP and HyPer-CYTO fluorescence were measured using a z-resolution of ~2.5 μm. Adjusting the z-plane, the field for image acquisition was chosen in a region containing exclusively of smooth muscle cells. Laser intensity was kept at a minimum while choosing the field to prevent laser-induced bleaching of the indicator fluorescence. Once the imaging field was chosen, the laser intensity was restored to original values. At the end of each experiment, smooth muscle cell viability was confirmed by application of CCCP, which uncouples the ETC and disrupts ψ_m, leading to decrease in 2mt8CG2 and mt-cpYFP fluorescence. For experiments performed using HyPer-CYTO, cell viability at the end of each experiment was confirmed by an elevation in fluorescence to H_2O_2 application.

3.9.3. Analysis of confocal images

Mean intensity of smooth muscle cells in the imaging field was used as a measure of fluorescence. Cerebral arteries reverse permeabilized with no vector were used as controls. Background (autofluorescence) was measured from smooth muscle cells in these arteries with the same imaging parameters (laser intensity, detector gain, and z-resolution) used to image smooth muscle cells of intact arteries expressing 2mt8CG2, mt-cpYFP, or HyPer-CYTO. Autofluorescence was then subtracted from all fluorescence measurements obtained from arteries expressing the fluorescent indicators. Following autofluorescence subtraction, changes in indicator fluorescence induced by pharmacological agents were calculated as a % of the initial pre-exposure fluorescence. Time control measurements were also obtained in arteries expressing the fluorescent indicators. Percentage changes in 2mt8CG2, mt-cpYFP, or HyPer-CYTO were corrected for indicator bleaching using time control measurements.

3.10. Localization of Mitochondria-Targeted Indicators

3.10.1. Loading smooth muscle cells with MitoTracker

To confirm targeting of 2mt8CG2 and mt-cpYFP to the mitochondria, colocalization experiments were performed with MitoTracker Orange CMTMRos (Molecular Probes, Invitrogen, Eugene, OR), an organic mitochondria-selective dye. MitoTracker Orange CMTMRos is a cell permeant dye which upon entering the cells is sequestered to the mitochondria because of its mildly thiol-reactive chloromethyl moiety (Poot *et al.*, 1996) (Molecular Probes, Invitrogen, Eugene, OR). Smooth muscle cells expressing 2mt8CG2 or mt-cpYFP were isolated from intact arteries. Dissociated smooth muscle cells were allowed to adhere to glass coverslips for 15 minutes and then incubated with prewarmed (37°C) DMEM/F-12 culture medium supplemented with penicillin/streptomycin (1%) containing MitoTracker Orange CMTMRos (100 nM) for 30 minutes at 37°C in a 74% N_2/21% O_2/5% CO_2 incubator. Following wash with DMEM/F-12 culture medium for 10 minutes at 37°C, cells were fixed with 4% paraformaldehyde in phosphate-buffered saline (PBS) for 15 minutes at room temperature and imaged using a Zeiss LSM5 Pascal laser-scanning confocal microscope.

3.10.2. Imaging protocol

MitoTracker and 2mt8CG2 or mt-cpYFP were imaged using an interleaved image acquisition protocol. Interleaved image acquisition requires sequential collection of fluorescence images from the same field for one channel followed immediately for another channel. MitoTracker was excited with 545 nm light and emitted light >560 nm was captured. 2mt8CG2 or mt-cpYFP was excited with 488 nm light and emitted light 505-530 nm captured. Bandpass emission filter of 505-530 nm collects fluorescence emitted within that range, and a long pass emission filter of >510 nm collects all fluorescence emitted above 510 nm. Bandpass emission filter of 505-530 nm was used to collect 2mt8CG2 or mt-cpYFP fluorescence to prevent bleedthrough of MitoTracker fluorescence (which emits at wavelength >560 nm) into 2mt8CG2 or mt-cpYFP emission. Isolated smooth muscle cells were imaged using a z-resolution of ~1 μm to visualize organelle distribution in the cytosol.

3.10.3. Analysis of confocal images

Data was analyzed using the Zeiss LSM5 Pascal colocalization module, which permits interactive analysis of fluorescence from two channels of an image. In a smooth muscle cell, colocalization would occur when fluorescence of 2mt8CG2 or mt-cpYFP, and MitoTracker, a mitochondria-selective indicator are present in the same pixel. Therefore, weighted colocalization between 2mt8CG2 or mt-cpYFP and MitoTracker was used to quantify mitochondrial targeting of the fluorescent indicator. Weighted colocalization is determined as the sum of intensities of colocalizing pixels in 2mt8CG2

or mt-cpYFP channel compared to sum of intensities of all 2mt8CG2 or mt-cpYFP pixels above threshold (background). The values for weighted colocalization range from 0 to 100%, where 0 indicates no colocalization, and 100 indicates colocalization of all pixels. Threshold value was taken from a region in the imaging field where no cells are present.

3.11. Imaging 2mt8CG2 in HEK293 Cells

3.11.1. Transfection of HEK293 cells with 2mt8CG2

Human Embryonic Kidney 293 (HEK293) cells (ATCC, Manassas, VA) were maintained in DMEM culture medium supplemented with 10% fetal bovine serum (FBS) (Cellgro, Manassas, VA) and penicillin-streptomycin (1%) under standard tissue culture conditions (74% N_2/21% O_2/5% CO_2; 37°C). HEK293 cells were grown on sterile glass coverslips placed in 35 mm petri dishes to achieve 20-50% confluency and transfected using the Ca^{2+} phosphate method. Briefly, a reaction mixture containing 0.5 µg of pMITO-2mt8CG2 and 0.125 M $CaCl_2$ in N,N-bis(2-hydroxyethyl)-2-aminoethanesulfonic acid (BES)-buffered solution was added dropwise to HEK293 cells and placed at 37°C for 16 to 18 hours in a 74% N_2/21% O_2/5% CO_2 incubator. Following aspiration of media, cells were washed with sterile PBS and incubated in DMEM for 24 hours at 37°C in a 74% N_2/21% O_2/5% CO_2 incubator.

3.11.2. Imaging protocol

2mt8CG2 was excited with 488 nm light and emitted light >510 nm captured using a Zeiss LSM5 Pascal laser-scanning confocal microscope using a z-resolution of ~1 µm.

3.12. Tetramethylrhodamine, Methyl Ester Imaging for ψ_m Measurements

3.12.1. Principle

ψ_m was studied using tetramethylrhodamine, methyl ester (TMRM) (Molecular Probes, Invitrogen, Eugene, OR), a membrane-permeant fluorescent potentiometric indicator (Scaduto, Jr. & Grotyohann, 1999; Cheranov & Jaggar, 2004; Xi *et al.*, 2005). Following cell permeation, TMRM is cleaved by intracellular esterases to yield a cationic fluorescent probe. The mitochondrial matrix is negatively charged compared to the cytosol, thus enabling the uptake of the cationic TMRM into the mitochondrial matrix (Scaduto, Jr. & Grotyohann, 1999). Mitochondrial depolarization makes the mitochondria more positively charged, thereby leading to extrusion of TMRM from the mitochondria into the cytosol, and eventually from the cell, leading to a decrease in TMRM fluorescence.

3.12.2. Procedure

A small volume (100 µl) of Ca^{2+}-free solution containing freshly isolated arterial smooth muscle cells was placed on a No. 0 glass coverslip bottom petri dish. Cells were allowed to adhere to the coverslip for 15 minutes. Cells were subsequently incubated in HEPES-buffered PSS containing TMRM (100 nM) for 20 minutes, followed by a 15-minute wash in HEPES-buffered PSS. Solutions were perfused through the petri dish at room temperature. Perfusing solutions containing TMRM (1 nM) in addition to the stimulus were used to maintain a steady extracellular TMRM concentration. This was found to facilitate TMRM reuptake into the mitochondria when the depolarizing stimulus was washed off and when ψ_m returned to its resting negative value. At the end of each experiment, cell viability was confirmed by application of CCCP, which uncouples the ETC and disrupts ψ_m, leading to a decrease in TMRM fluorescence.

3.12.3. Imaging

In a region, every TMRM-loaded smooth muscle cell was chosen as a separate zone and fluorescence from every zone was collected. To measure temporal changes in TMRM intensity, smooth muscle cells were excited with 535 nm light, and background corrected fluorescence collected every 1 second at 610 nm using a Dage MTI iCCD camera and Ionwizard software (Ionoptix, Milton, MA). Background fluorescence was collected from a zone where no smooth muscle cells were present.

3.12.4. Analysis

Background-corrected TMRM fluorescence measurements for 2 minutes prior to addition of a stimulus were averaged to obtain the control fluorescence. TMRM fluorescence changes in response to stimuli were normalized to the pre-exposure control fluorescence.

3.13. Dichlorofluorescein Imaging for ROS Measurements

3.13.1. Principle

ROS measurements in isolated intact cerebral artery segments (1–2 mm) were performed using CM-H_2DCFDA (Molecular Probes, Invitrogen, Eugene, OR), a cell-permeant ROS indicator. CM-H_2DCFDA , which is an acetylated form of 2′,7′-dichlorofluorescein (DCF) is hydrolyzed by intracellular esterases to remove the acetate groups yielding the nonfluorescent derivative dichlorodihydrofluorescein (H_2DCF) (Jakubowski & Bartosz, 2000). ROS oxidize the nonfluorescent H_2DCF to fluorescent DCF (Jakubowski & Bartosz, 2000; Cheranov & Jaggar, 2006). Amount of DCF fluorescence is proportional to the amount of ROS present. DCF fluorescence changes

can therefore be used to measure changes in ROS levels in arterial smooth muscle cells. The thiol-reactive chloromethyl group forms covalent bonds with intracellular components, permitting retention within the cell (Jakubowski & Bartosz, 2000).

3.13.2. Procedure

Cerebral artery segments were cannulated on borosilicate rectangular tubing and incubated for 60 minutes at room temperature in HEPES-buffered PSS containing CM-H_2DCFDA (10 μM). The DCF-loaded arteries were washed with HEPES-buffered PSS for 15 minutes at room temperature. Following wash, the cannulated arteries were placed on a No. 0 glass coverslip bottom petri dish and imaged using a confocal microscope.

3.13.3. Imaging

DCF was excited with 488 nm light, and emitted light >510 nm was collected using a Zeiss LSM5 Pascal laser-scanning confocal microscope using a z-resolution of ~4.5 μm. Because the dye is susceptible to photo-oxidation, DCF fluorescence can increase spontaneously upon exposure to excitation light (Afzal *et al.*, 2003; Cheranov & Jaggar, 2006). To reduce the laser-induced photo-oxidation, each arterial region was scanned only once, and the laser intensity was set to minimize excitation.

3.13.4. Analysis

Mean intensity of DCF fluorescence from smooth muscle cells in the imaging field was subtracted from background (autofluorescence) to obtain the corrected fluorescence in a field. Autofluorescence was measured in control arteries that were not loaded with DCF but underwent the same imaging protocol (laser intensity, detector gain, and z-resolution). Following autofluorescence subtraction, changes in DCF fluorescence induced by pharmacological agents were calculated as a % of the initial pre-exposure fluorescence. % changes in DCF fluorescence were then corrected for time-dependent photo-oxidation-induced elevation in DCF fluorescence. Time control measurements were obtained in smooth muscle cells of intact DCF-loaded arteries that underwent the same imaging protocol, but were not exposed to stimuli.

3.14. NAD(P)H Oxidase Inhibitors

$gp91^{phox}$ docking sequence represents the binding site of $p47^{phox}$ subunit of NAD(P)H oxidase (Rey *et al.*, 2001). $p47^{phox}$ translocation to the smooth muscle cell membrane and anchoring with $gp91^{phox}$ is required for NAD(P)H oxidase activation (Rey *et al.*, 2001). Therefore, to prevent association of NAD(P)H oxidase subunits and activation of NAD(P)H oxidase, peptides were used.

gp91ds-tat peptide contains the $gp91^{phox}$ docking sequence (NH_2-LQRRIRTSC-COOH) (Rey *et al.*, 2001) conjugated to the N-terminus of a specific amino acid peptide (NH_2-RRRQRRKKR-COOH) of HIV viral coats (HIV-tat), which is known to be internalized by all cells (Fawell *et al.*, 1994). gp91scrm-tat contains a scrambled gp91 peptide (NH_2-RSQRTIRLC-COOH) conjugated to N-terminus of HIV-tat (Rey *et al.*, 2001). gp91ds-tat and gp91scrm-tat peptides were synthesized by Tufts University Core Facility (Boston, MA).

3.15. NF-κB Immunofluorescence

3.15.1. Principle

NF-κB immunofluorescence was performed to study NF-κB p50 localization in the smooth muscle cells of intact arteries. Following treatment, arteries were incubated with anti-p50 antibody and the corresponding fluorophore-conjugated secondary antibody. Nucleus was labeled using a dimeric cyanine nucleic acid stain. Upon nuclear translocation of p50, colocalization of fluorophore (attached to the secondary antibody) and nucleic acid stain was anticipated.

3.15.2. Procedure

Intact arteries were exposed to pharmacological agents in DMEM/F-12 culture medium supplemented with penicillin/streptomycin (1%) and incubated in a 74% N_2/21% O_2/5% CO_2 incubator at 37ºC. Following treatment, arteries were fixed with 4% paraformaldehyde in PBS for 1 hour at room temperature, and washed three times for 5 minutes each with PBS. Permeabilization of cell membrane to facilitate passage of antibodies into cells to bind the protein(s) of interest was done using 0.5% TritonX-100 dissolved in PBS for 15 minutes at room temperature. After three washes with PBS, arteries were incubated in 5% BSA in PBS for 1 hour at room temperature. Arteries were then incubated with mouse monoclonal anti-NF-κB p50 antibody (1:100 dilution; Santa Cruz Biotechnology Inc., Santa Cruz, CA) overnight at 4°C. The epitope recognized by the anti-NF-κB p50 antibody is located in the N-terminus (amino acids 120-239) of NF-κB p50 of human origin. After five washes with PBS at room temperature, arteries were incubated with Cy3-conjugated goat anti-mouse IgG (1:100 dilution; Jackson ImmunoResearch, West Grove, PA) for 1 hour at 37°C. After ten washes with PBS at room temperature, YOYO-1 iodide (1:10,000 dilution; Molecular Probes, Invitrogen, Eugene, OR), a fluorescent nucleic acid indicator and Ribonuclease A (RNase A) (250 µg/ml; Sigma-Aldrich, St.Louis, MO) were added for 30 minutes at 37ºC to counterstain smooth muscle cell nuclei. RNase A was added to destroy cellular RNA and thereby prevent YOYO-1 binding to RNA. A borosilicate rectangular tubing was then placed in the lumen of each fixed artery to provide a flat surface for imaging. The artery was then mounted on a glass slide and used for imaging.

3.15.3. Imaging

NF-κB localization in smooth muscle cells of intact arteries was examined using a Zeiss LSM 5 Pascal laser-scanning confocal microscope using a z-resolution of ~0.8 μm. Cy3 was excited with 545 nm light, and emitted light >560 nm was collected. YOYO-1 was excited with 488 nm light, and emitted light 505-530 nm was collected. YOYO-1 fluorescence was collected using bandpass emission filter (505-530 nm) instead of long pass emission filter (>510 nm) to prevent collection of Cy3 fluorescence into the YOYO-1 channel.

3.15.4. Analysis

Data was analyzed using the Zeiss LSM5 Pascal colocalization module. Colocalization of p50 and YOYO-1 was determined using weighted colocalization, as previously described in section 3.10.3. Weighted colocalization of p50 pixels with YOYO-1 pixels in the field was used to quantify p50 nuclear translocation. Threshold value for each channel was taken from a region in the imaging field outside the artery.

3.16. NF-κB-Dependent Luciferase Reporter Gene Activity

3.16.1. Vectors encoding luciferase

NF-κB-p-Luc vector contains a luciferase reporter gene under the control of an NF-κB promoter (κB sites in the promoter region of the immunoglobulin gene). Three κB sites in the promoter regions are as follows: GGAAATTCCCC (-63 to -53), AGGACTTTCC (-225 to -216), and GGGAAACCCC (-319 to -310) (Le Bail *et al.*, 1993; Arsura *et al.*, 2003; Kaur *et al.*, 2005). pGL3 Basic control vector (Promega Corporation, Madison, WI) which contains the luciferase reporter gene but no promoter was used as a control.

3.16.2. Principle

NF-κB-dependent transcriptional activity was studied using NF-κB-dependent luciferase reporter gene assay. NF-κB binds to promoter of NF-κB-p-Luc, leading to transcription of luciferase reporter gene, resulting in luciferase protein expression and fluorescence. Stimuli which activate NF-κB increase the number of NF-κB proteins binding to the κB sites in the promoter. Transcription of luciferase reporter gene is elevated, leading to an increase in luciferase protein expression and fluorescence. Therefore, fluorescence obtained from NF-κB-p-Luc is proportional to NF-κB activity.

pGL3 Basic vector contains a luciferase reporter gene but no promoter. Changes in NF-κB activity would therefore not alter the luciferase expression and fluorescence.

3.16.3. Procedure

NF-κB-p-Luc or pGL3 Basic vectors were inserted into smooth muscle cells of intact arteries using reverse permeabilization. The arteries were then placed for 3 days at 37ºC in DMEM/F-12 culture medium supplemented with penicillin/streptomycin (1%) in a 74% N_2/21% O_2/5% CO_2 incubator. After 3 days, the arteries were exposed to stimuli for an additional 24 hours at 37ºC. Arterial protein lysates were then isolated and quantified (described in detail in section 3.19). Luciferase activity was determined using the Luciferase Assay System (Promega Corporation, Madison, WI).

3.16.4. Measuring luciferase activity

Protein lysate (50 μg) was added to Luciferase Assay Reagent (100 μl) and luciferase luminescence was measured using a TD-20/20 luminometer (Turner Designs, Sunnyvale, CA). As suggested by the vendor (Promega), the luminometer was programmed to perform a 2-second measurement delay followed by a 10-second measurement read for luciferase activity. Luminescence measurements were corrected for background luciferase luminescence, which was recorded from lysates of arteries that underwent the same reverse permeabilization, culture, and luminescence measurement protocol, but were not exposed to NF-κB-p-Luc or pGL3 Basic vectors during the reverse permeabilization procedure.

3.17. Real-Time PCR

3.17.1. RNA isolation

Intact cerebral arteries were either untreated or treated with ET-1 (10 nM) in DMEM/F-12 culture medium supplemented with penicillin/streptomycin (1%) in a 74% N_2/21% O_2/5% CO_2 incubator for 6 hours at 37ºC. Following treatment, Trizol (Invitrogen, Eugene, OR) was added to arteries, homogenized, and incubated for 5 minutes at room temperature to completely dissociate cellular nucleoprotein complexes. Chloroform was added and centrifuged at 12000 × g for 15 minutes at 4°C to separate the samples into a DNA-containing phenol, a DNA/protein-containing interphase, and an RNA-containing aqueous phase. RNA in the aqueous phase was precipitated by adding isopropyl alcohol and centrifuged at 12000 × g for 10 minutes at 4°C. RNA precipitate which forms a gel-like pellet at the bottom of the tube was washed with 75% ethanol and reconstituted in RNase-free water.

3.17.2. Quantification of RNA

RNA concentration was quantified measuring the absorbance of UV light at 230 nm (A230), 260 nm (A260), and 280 nm (A280 nm) using a UV spectrophotometer.

RNA concentration was calculated from the equation:

$$\text{RNA concentration } (\mu g/ml) = (A260 - A230) \times \text{dilution factor} \times 40\ \mu g/ml$$

Nucleic acid purity was estimated from A260/A280 and A260/A230 ratios. Ratios between 1.8 and 2.0 generally represent high-quality nucleic acid sample.

3.17.3. Reverse transcription

RNA (~250 ng) from arteries for each condition was used in reverse transcription to obtain cDNA. The remaining RNA from each condition was used as template in negative control reactions for RT-PCR. cDNA was reverse transcribed from RNA using AffinityScript Multiple Temperature Reverse Transcriptase (Stratagene, Cedar Creek, TX). Briefly, RNA, random primers, and RNase-free water were added to a nuclease-free centrifuge tube and incubated at 65°C for 5 minutes. The mixture was slowly cooled to room temperature for 10 minutes, to allow annealing of primers to RNA. DTT (100 mM), dNTP (100 mM), buffer, and reverse transcriptase were added and the reaction incubated at 50°C for 1 hour. The reaction was stopped by heat inactivating the enzymes at 70°C for 15 minutes. Following reverse transcription, cDNA was used as template for RT-PCR.

3.17.4. Principle

TaqMan probes are designed to anneal to the DNA region which is amplified by a pair of primers. Probes consist of a fluorophore which is in close proximity to a quencher, which inhibits fluorescence from the fluorophore (Holland *et al.*, 1991). Using the DNA template, Taq DNA polymerase synthesizes the nascent strand from the 3' end of the primer. TaqMan probe that is annealed to the DNA is degraded by the 5' to 3' exonuclease activity of the polymerase. Degradation of the probe releases the fluorophore from it, thereby preventing it from being in close proximity to the quencher, resulting in elevation of fluorescence. Presence of more DNA templates causes probe binding to more DNA, leading to elevated fluorescence. Therefore, fluorescence detected is directly proportional to the amount of DNA template present in the PCR. Since the DNA template used is reverse-transcribed from mRNA, the fluorescence detected is an indication of the cellular mRNA levels and hence, is used to quantify changes in gene expression.

3.17.5. Primers and probes

RT-PCR assays, hydrolysis probes, and gene specific primers that span long introns were designed to distinguish cDNA from genomic DNA using primer design online software Universal Probe Library available at http://www.roche-applied-science.com/sis/rtpcr/upl/index.jsp. Primers were ordered

from Integrated DNA Techonologies (Coralville, IA). Hydrolysis probes were ordered from Molecular Resource Center, University of Tennessee Health Science Center (Memphis, TN). Primers and probes used for RT-PCR are listed in **Table 3-1**. Melting temperature of all the primers was between 59 and 60°C.

3.17.6. PCR conditions

Quantitative TaqMan PCR reactions were performed using an LC480 light cycler (Roche Applied Science, Indianapolis, IN). Each PCR mixture (10 µl) contained 5 µl of Taqman LC480 Master Mix, 0.1 µl of forward primer, 0.1 µl of reverse primer, 0.1 µl of hydrolysis probe, 2.7 µl of RNase-free water, and 2 µl of cDNA or mRNA template. Reaction was activated at 95ºC for 5 minutes. Following activation, amplification was performed with 40 cycles of denaturation for 10 seconds at 95ºC, and annealing of primers for 30 seconds at 60ºC, and 1 cycle of extension for 10 seconds at 72ºC. Reaction was cooled to 40°C for 5 minutes. A negative control using RNA instead of cDNA was carried out in each experiment. Standard curves using four 10-fold dilution steps of cDNA samples were run for all probe and primer pairs to determine PCR efficiency. PCR efficiency, determined by the slope of standard curves for all primer and probe pairs were between ~1.7 and 2.3.

3.17.7. Analysis

$Ca_V1.2$ mRNA expression under each condition was calculated from the difference between CT values (ΔCT) of $Ca_V1.2$ and ribosomal protein subunit 5 (Rps5), reference gene. ΔΔCT was calculated from the difference between the ΔCT values for control and ET-1 treatment. ET-1-induced elevation in $Ca_V1.2$ mRNA levels was calculated using the formula $100 \times (2^{-\Delta\Delta CT})$ (Livak & Schmittgen, 2001). All PCR reactions including standard curves were performed in triplicate.

3.18. Agarose Gel Electrophoresis

Products of RT-PCR were mixed with Green GoTaq Flexi Buffer (Promega Corporation, Madison, WI) and separated by electrophoresis using 2% agarose gel containing 0.01% ethidium bromide. Images of fluorescence from ethidium bromide bound to DNA within the gel were collected using the Kodak In-Vivo Imaging System (Carestream Health Inc., Woodbridge, CT) and the Kodak Molecular Imaging Software v4.5.1 (Carestream Health Inc., Woodbridge, CT).

3.19. Protein Quantification and Estimation

Cerebral arteries were homogenized in Laemmli sample buffer (2.5% SDS, 10% glycerol, 0.01% bromophenol blue, 5% β-mercaptoethanol, and 100 mM Tris-HCl, pH

Table 3-1. Primers and probes used in RT-PCR

Gene (Accession number)	**Forward primer (5'sequence3') (Position)**	**Reverse primer (5'sequence3') (Position)**	**Hydrolysis probe (Position)**
$Ca_V1.2$ (DQ538522.1)	GAGAGCTTTCCGTGTGCTTC (727-746)	GTTCAGGACCACCTGGAGAC (777-796)	CTGGAGTC (765-772)
Rps5 (NM_001105722.1)	GACTGAGAAGCCCGGTTTG (70-88)	CTTGATGTCCGGGGTCTCT (134-152)	CAGCCACA (115-122)
HGPRT (ENSRNOT00000045153.2)	TCAACGGGGGACATAAAAGT (394-413)	AGTGTCAATTATATCCAAACCCAAT (462-486)	TGGTGGAG (417-424)
Cyclophilin B (ENSRNOT00000022828.4)	ACGTGGTTTTCGGCAAAGT (524-542)	CTTGGTGTTCTCCACCTTCC (566-585)	TGGAAGGC (545-552)
β tubulin (ENSRNOT00000023452.4)	CAGAGCCATTCTGGTGGAC (239-257)	GCCAGCACCACTCTGACC (333-350)	GAGCCTGG (261-268)
β actin (ENSRNOT00000042459.1)	CCCGCGAGTACAACCTTCT (17-35)	CGTCATCCATGGCGAACT (71-88)	CAGCTCCT (38-45)

6.8). Tissue debris and nuclear fragments were removed by centrifugation at 6000 × g for 10 minutes at 4°C. The whole cell lysate, obtained as a supernatant was transferred to a fresh tube and used for protein quantification and Western blotting. A 5 µl aliquot of supernatant was placed on a nitrocellulose membrane, and following amido black staining, protein concentration was measured by spectrophotometric quantification at 630 nm.

3.20. Western Blotting

Protein extracts were heated for 3 minutes at 100°C. Proteins (30 µg per lane) were separated by size on 7.5% SDS-PAGE Tris-glycine gels. Prestained molecular weight markers (Bio-Rad, Hercules, CA) were used to monitor progress on the gel. Gel was run in MOPS-SDS Running Buffer (containing SDS and Tris-Glycine) at 200 V until the 37 kDa marker reached the bottom of the gel. Following this, the gel was placed onto a PVDF membrane treated with methanol and placed between two sheets of filter paper between two sponges, all soaked in Transfer Buffer (Tris base, glycine, and methanol), into a binding cassette. Proteins were transferred for 2 hours at 100 V using a Mini Trans Blot Cell (Bio-Rad, Hercules, CA). The apparatus was placed on ice to manage heat exchange during the transfer.

Membranes were blocked in 5% nonfat dry milk in Tris-buffered solution (TBS) with 0.1% Tween-20 (TBS-T) for 1 hour at room temperature. Membranes were then incubated with rabbit monoclonal anti-p105/p50 antibody (1:1000 dilution; Abcam Inc., Cambridge, MA), mouse monoclonal anti-$Ca_V1.2$ antibody (1:200 dilution; UC Davis/NINDS/NIMH NeuroMab Facility), or mouse monoclonal anti-actin antibody (1:50,000 dilution; Millipore, Billerica, MA) overnight at 4ºC in TBS-T and 5% nonfat dry milk. Anti-$Ca_V1.2$ antibody was produced against intracellular C-terminus (amino acids 1507-1733) of rabbit $Ca_V1.2$. Epitope recognized by the anti-actin antibody is located in the N-terminus (amino acids 50-70) of actin. Following overnight incubation with primary antibodies, membranes were washed three times with TBS-T for 5 minutes each, and incubated for 1-2 hours at room temperature with HRP-conjugated secondary antibody in TBS-T and 5% nonfat dry milk. Membranes were then washed three times with TBS-T for 5 minutes each, and incubated with enhanced chemiluminiscence substrate (Amersham, Arlington heights, IL) for the HRP enzyme conjugated in the secondary antibody.

HRP-induced chemiluminescence from bound secondary antibodies was detected using a Kodak In-Vivo Imaging System and visualized using the Kodak Molecular Imaging Software v4.5.1. Membranes were developed multiple times using different exposure times, to optimize band intensity for densitometric analysis.

The PVDF membranes can be reprobed for other proteins after probing them for one. To achieve this, the membrane was stripped using a Stripping Buffer (Thermo Scientific, Rockford, IL) for 15 minutes at room temperature, washed with TBS-T, reblocked, and reprobed as explained above.

3.21. Densitometric Analysis of Western Blots

Band intensity was quantified using digital densitometry using Quantity One software v4.6.9 (Bio-Rad, Hercules, CA). Briefly, background-subtracted band density was calculated by placing rectangular boxes of the same size around bands in each lane. Average band density was calculated from all images of the same blot acquired using different exposure times. Averaged band density for a protein was then normalized to the band density of actin for the corresponding sample. Actin was used to normalize data because pharmacological treatments used in this study did not alter its expression.

3.22. NF-κB p105 Knockdown

3.22.1. Principle

siRNA are long double-stranded RNA molecules that have a characteristic two nucleotide 3' overhang that allows them to be recognized by the enzymatic machinery of RNA interference. siRNA are separated into single strands which homology-dependently bind to target mRNA. siRNA-mRNA complex is eventually destroyed by the RNA-induced silencing complex, leading to target mRNA degradation. siRNA-mediated reduction in mRNA levels translate to a decrease in target protein levels.

3.22.2. Procedure

Two siRNAs directed against NF-κB p105 subunit (p105siRNA1 and p105siRNA2) (10 µg/ml each) (Qiagen, Valencia, CA) were used to inhibit p105 expression. p105siRNA1 and p105siRNA2 were directed against target sequences in regions 458-478 and 939-959, respectively of p105 sequence (XM_001075876). Scrambled siRNA (p105scrm) (20 µg/ml) (Qiagen, Valencia, CA) was used as a control. siRNAs were introduced into smooth muscle cells of intact cerebral arteries using reverse permeabilization (Lesh *et al.*, 1995; Welsh *et al.*, 2002). After 3 days in DMEM/F-12 culture medium supplemented with penicillin/streptomycin (1%) in a 74% N_2/21% O_2/5% CO_2 incubator at 37ºC, arteries were exposed to stimuli for an additional 24 hours at 37°C. Artery segments were then either used for pressurized artery diameter measurements or protein lysates were isolated, quantified, and used for Western blotting.

3.23. Pressurized Artery Diameter Measurements

3.23.1. Procedure

Experiments were performed using PSS containing (in mM): 112 NaCl, 4.8 KCl, 26 $NaHCO_3$, 1.8 $CaCl_2$, 1.2 MgSO4, 1.2 KH_2PO4, and 10 glucose (with pH adjusted to

7.4 with NaOH). Prior to use, PSS was oxygenated by bubbling with 74% N_2/21% O_2/5% CO_2. Endothelium-denuded artery segments 1–2 mm in length were cannulated at each end in a temperature-controlled perfusion chamber (Living Systems Instrumentation, Burlington, VT) containing PSS. Care was taken to cannulate artery segments that did not have a branch or tear in their wall. The chamber containing the cannulated artery was placed on the stage of a Nikon TS100-F microscope. Intravascular pressure was altered using a water-filled reservoir and monitored using a pressure transducer. Arterial wall diameter was measured at 1 Hz using a CCD camera attached to the Nikon TS100-F microscope and diameter changes measured in real time using the automatic edge-detection function of IonWizard software. Luminal flow was absent during experiments. Vessels were constantly superfused with PSS alone or containing pharmacological agent(s).

At the beginning of each experiment, the artery was allowed to equilibrate for 10 minutes at an intravascular pressure of ~10 mm Hg. The artery dilated during this equilibration process because of its exposure to warm PSS. After the arterial diameter at 10 mm Hg became stable for a period of 5 minutes, the intravascular pressure was elevated to ~60 mm Hg. Elevation of intravascular pressure to 60 mm Hg resulted in arterial dilation. The artery was allowed to sense the elevated intravascular pressure and develop pressure-induced vasoconstriction (myogenic tone). Pharmacological stimuli were perfused only after myogenic tone remained steady for a period of 15 minutes. After perfusion of the stimulus in PSS, stable diameter achieved for a period of 5 minutes was considered as active diameter. After a stimulus was washed off, time was given for the arterial diameter to return to its myogenic tone before addition of the next stimulus. Arterial diameter after perfusion of Ca^{2+}-free solution containing EGTA (10 mM) and nimodipine (1 μM) was considered as passive diameter. Endothelial denudation was confirmed by the lack of response to carbachol (1 μM), an endothelial-dependent vasodilator.

3.23.2. Analysis

Experimental traces were analyzed using IonWizard software. Measurements were obtained when the diameter remained stable. Myogenic tone (%) was calculated as 100 × (1-active diameter/passive diameter).

3.24. Reagents and Chemicals

XeC and 17-octadecynoic acid (17-ODYA) were purchased from Cayman Chemical Company (Ann Arbor, MI). Manganese (III) tetrakis (1-methyl-4-pyridyl) porphyrin (MnTMPyP) was purchased from AG Scientific Inc.(San Diego, CA). Apocynin and Ru360 were purchased from EMD Chemicals (Gibbstown, NJ). Recombinant rat TNF-α was purchased from BD Pharmingen (BD Biosciences, San Jose, CA). All other reagents and chemicals were purchased either from Sigma-Aldrich Company (St.Louis, MO) or Fisher Scientific (Pittsburgh, PA), unless specified.

3.25. Statistical Analysis

OriginLab and GraphPad InStat software were used for statistical analyses. Values are expressed as mean±SEM. Student's *t*-test with two-tail p value was used for comparing paired and unpaired data from two populations. Ordinary one-way ANOVA followed by Student-Newman-Keuls post-hoc test were used for all multiple data comparisons. For ANOVA, the values were assumed to be sampled from a Gaussian distribution. Repeated measures ANOVA could not be performed since all the conditions to be compared were not paired and the sample numbers were not identical. Adjustments for multiple comparisons were made when necessary. $P<0.05$ was considered statistically significant.

Power analysis was carried out where $P>0.05$ to verify that sample size was sufficient to give a power value of >0.8. Power value, which is directly proportional to the sample size, is the probability of correctly rejecting the null hypothesis that there is no significant difference between the groups. The Type I error probability that the null hypothesis was falsely rejected was set to 0.05. Power analysis was performed using PS Power and Sample Size Calculations software (Dupont & Plummer, Jr., 1990).

CHAPTER 4. RESULTS*

4.1. ET-1 Modifies Local and Global Ca^{2+} Signals in Cerebral Artery Smooth Muscle Cells

The regulation of local and global Ca^{2+} signals by ET-1, a PLC-coupled receptor agonist and vasoconstrictor, was studied in smooth muscle cells of endothelium-denuded cerebral artery segments using Noran Oz high-speed laser-scanning confocal imaging and fluo-4 AM. ET-1 elevated mean Ca^{2+} wave frequency from ~0.34 to 1.42 Hz (~135% of control), reduced mean Ca^{2+} spark frequency from ~1.06 to 0.4 Hz (~32% of control), and increased mean global $[Ca^{2+}]_i$ from ~193 to 253 nM (~127% of control) (**Fig. 4-1**). Pretreatment with XeC, an IP_3R inhibitor (Gafni *et al.*, 1997) did not alter ET-1-induced Ca^{2+} spark inhibition but blocked ET-1-induced Ca^{2+} wave activation (**Fig. 4-1D**). In the presence of XeC, ET-1 elevated global $[Ca^{2+}]_i$ from ~193 to 225 nM (~113% of control) (**Fig. 4-1D**). Data indicate that ET-1-induced IP_3R activation increases Ca^{2+} wave frequency and contributes to global $[Ca^{2+}]_i$ elevation but does not regulate ET-1-induced Ca^{2+} spark inhibition.

4.2. ET-1-Induced IP_3R-Mediated SR Ca^{2+} Release Elevates $[Ca^{2+}]_{mito}$ in Cerebral Artery Smooth Muscle Cells

To study $[Ca^{2+}]_{mito}$ in arterial smooth muscle cells, complex loading procedures have previously been used to enhance mitochondrial loading of synthetic, inorganic Ca^{2+} indicators such as Rhod-2 (Monteith & Blaustein, 1999). Since inorganic Ca^{2+} indicators cannot be targeted to specific subcellular localizations, non-specific measurements of $[Ca^{2+}]_{mito}$ were inevitably obtained (Hajnoczky *et al.*, 1995; Monteith & Blaustein, 1999; Kaftan *et al.*, 2000; Trollinger *et al.*, 2000; Collins *et al.*, 2001; Gerasimenko & Tepikin, 2005). To specifically measure $[Ca^{2+}]_{mito}$, genetically-encoded, targetable Ca^{2+} indicators have been developed (Griesbeck *et al.*, 2001; Filippin *et al.*, 2005). Regulation of $[Ca^{2+}]_{mito}$ by ET-1-induced Ca^{2+} signals was measured in smooth muscle cells of intact arteries using 2mt8CG2, a genetically-encoded, mitochondria-targeted, fluorescent Ca^{2+} indicator (Griesbeck *et al.*, 2001; Filippin *et al.*, 2005).

* Portions of this chapter adapted with permission. Narayanan D, Xi Q, Pfeffer LM, & Jaggar JH (2010). Mitochondria control functional $Ca_V1.2$ expression in smooth muscle cells of cerebral arteries. *Circ Res* **107**, 631-641.

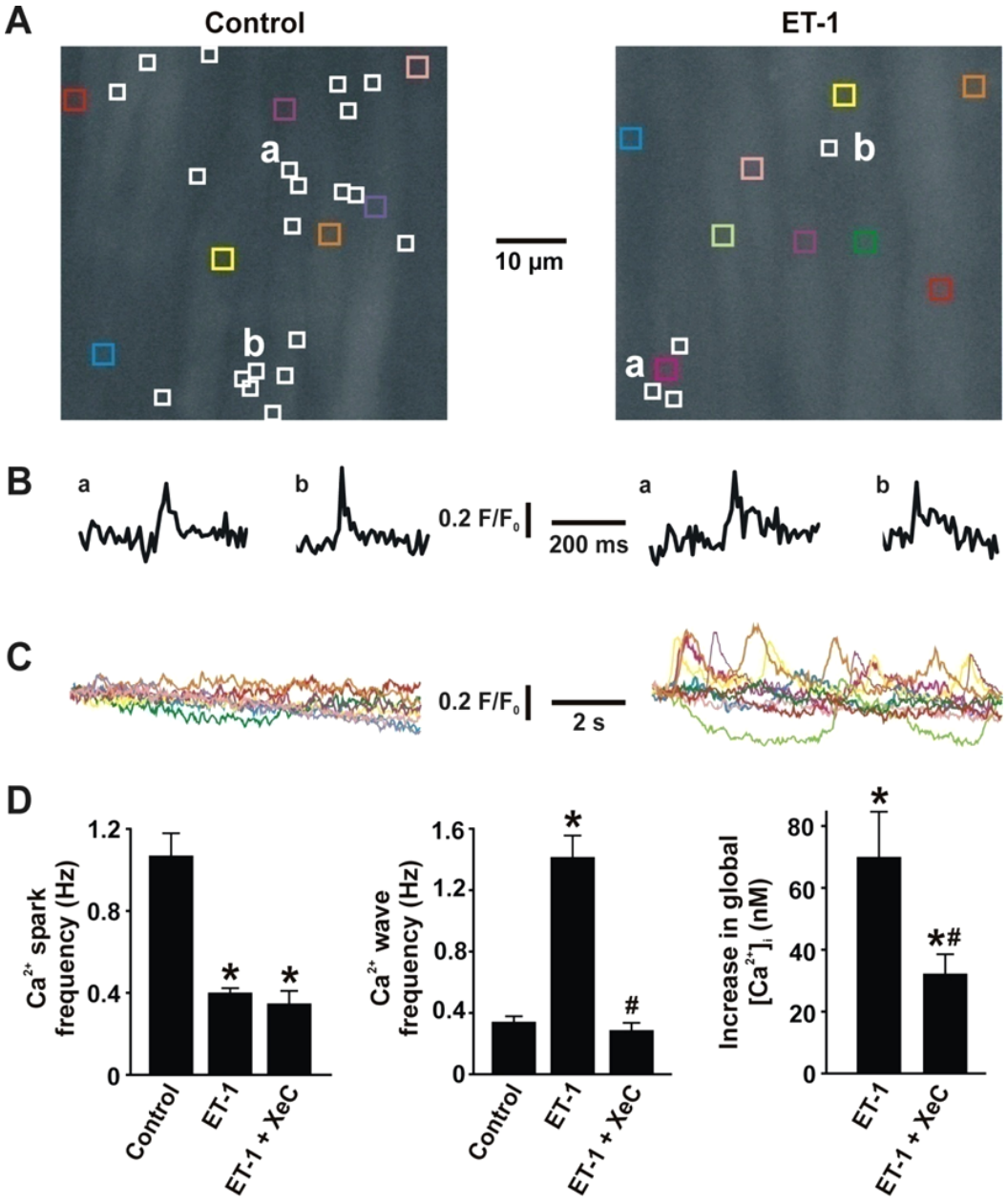

Figure 4-1. ET-1 regulates local and global Ca^{2+} signals in arterial smooth muscle cells

Notes: A, Confocal images illustrating average fluo-4 fluorescence in smooth muscle cells in the same artery in control and after ET-1 (10 nM). White boxes illustrate locations where Ca^{2+} sparks occurred during 10 seconds of imaging. Colored boxes illustrate locations from where normalized fluorescence (F/F_0) over time traces shown in C were obtained. B, Two representative Ca^{2+} sparks that occurred at locations labeled in A for each condition. C, F/F_0 over time traces illustrate that ET-1 elevates Ca^{2+} wave frequency. D, Mean data (n=7 for each condition). Values are expressed as mean±SEM. * indicates $P<0.05$ compared to control. # indicates $P<0.05$ compared to ET-1.

4.2.1. Mitochondrial localization of 2mt8CG2

4.2.1.1. HEK293 cells

2mt8CG2 expression in HeLa cells produces punctuate fluorescence when localized to mitochondria (Filippin *et al.*, 2005). Here, transfection of HEK293 cells with the pMITO-2mt8CG2 vector by using Ca^{2+} phosphate, reproduced the punctuate fluorescence pattern when visualized using a Zeiss LSM 5 Pascal laser-scanning confocal microscope, suggesting mitochondrial localization of 2mt8CG2 (**Fig. 4-2A**).

4.2.1.2. Cerebral artery smooth muscle cells

pMITO-2mt8CG2 vector was inserted into smooth muscle cells of intact cerebral arteries using reverse permeabilization (Lesh *et al.*, 1995; Welsh *et al.*, 2002). Confocal imaging revealed punctate staining in smooth muscle cells, indicating mitochondrial localization of 2mt8CG2 (**Fig. 4-2B**). To confirm mitochondrial targeting of 2mt8CG2, colocalization studies were performed using MitoTracker Orange. 2mt8CG2 fluorescence exhibited ~95% pixel colocalization with MitoTracker Orange, confirming mitochondrial localization (**Fig. 4-2C**).

4.2.2. $[Ca^{2+}]_{mito}$ measurements using 2mt8CG2

In smooth muscle cells of intact arteries, ET-1 increased mean 2mt8CG2 fluorescence to ~140% of control, and this elevation was blocked by thapsigargin and XeC (**Fig. 4-3A,B**), suggesting that ET-1 elevates $[Ca^{2+}]_{mito}$ due to IP_3R-mediated SR Ca^{2+} release. Thapsigargin was applied 15 minutes prior to ET-1, a time course sufficient to deplete SR Ca^{2+} load (Xi *et al.*, 2008). Ionomycin, a Ca^{2+} ionophore (Liu & Hermann, 1978), elevated mean 2mt8CG2 fluorescence to ~137% of control in smooth muscle cells of intact arteries (**Fig. 4-3B**), consistent with the fluorescence range of this indicator (Filippin *et al.*, 2003; Filippin *et al.*, 2005). Ru360, a MCU blocker (Matlib *et al.*, 1998), also blocked the ET-1-induced elevation in 2mt8CG2 fluorescence (**Fig. 4-3B**), indicating that ET-1-induced mitochondrial Ca^{2+} uptake occurs through the MCU. Thapsigargin, XeC, or Ru360 alone did not alter 2mt8CG2 fluorescence (**Fig. 4-3B**). Membrane depolarization (60 mM K^+), which elevates global $[Ca^{2+}]_i$, did not alter 2mt8CG2 fluorescence (**Fig. 4-3B**), suggesting that $[Ca^{2+}]_{mito}$ elevation occurs due to local Ca^{2+} signals and not due to global $[Ca^{2+}]_i$ elevation. CCCP, a protonophore that disrupts ψ_m by permeabilizing the inner mitochondrial membrane to H^+ (Goldsby & Heytler, 1963; Heytler, 1963) and abolishes the driving force for mitochondrial Ca^{2+} uptake (McCarron & Muir, 1999), reduced 2mt8CG2 fluorescence to ~63% of control (**Fig. 4-3B**). Results with Ru360 and CCCP confirm the mitochondrial localization of 2mt8CG2. These data indicate that ET-1-induced IP_3R-mediated SR Ca^{2+} release elevates $[Ca^{2+}]_{mito}$ in arterial smooth muscle cells.

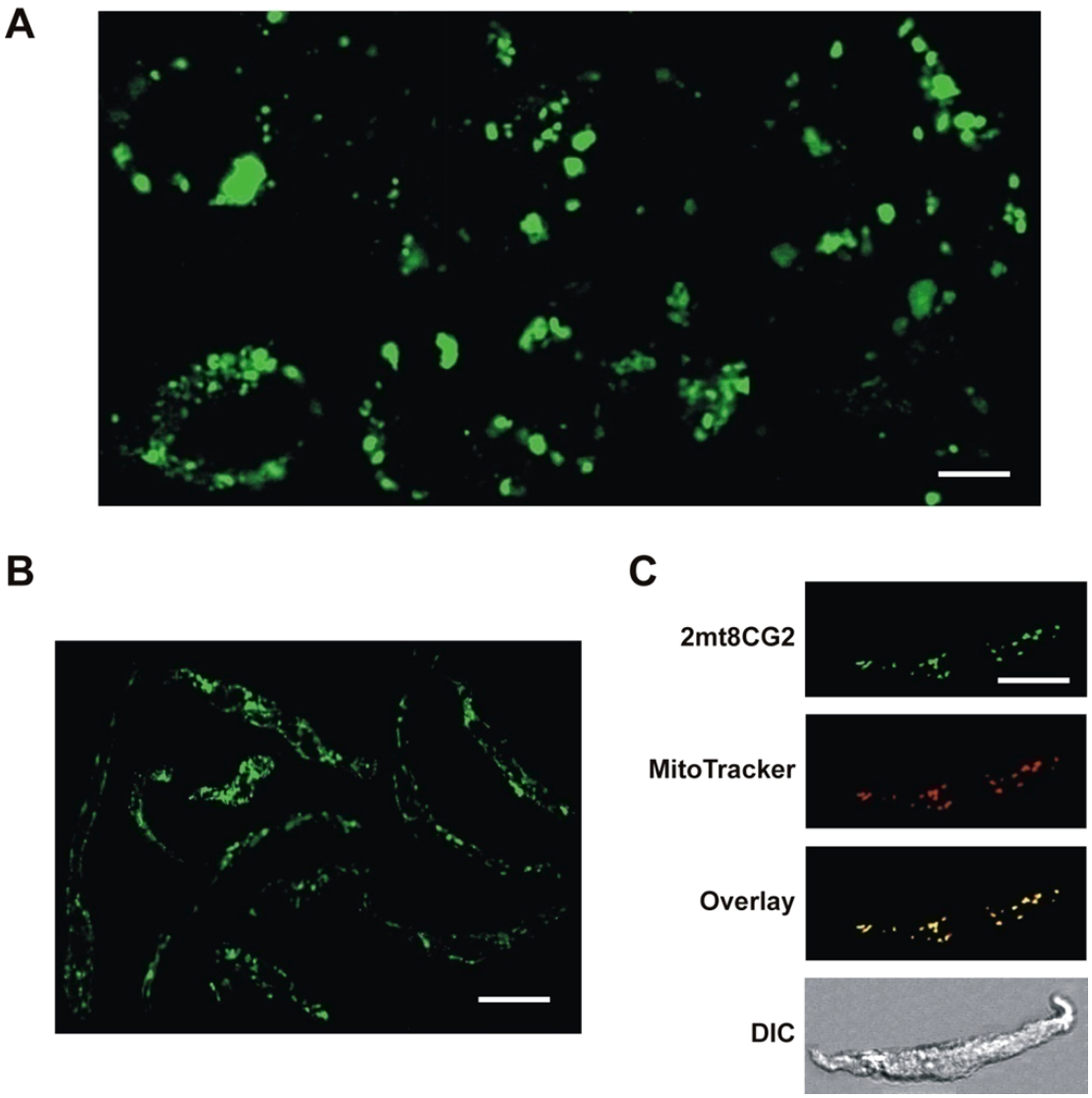

Figure 4-2. Mitochondrial localization of 2mt8CG2 in HEK293 cells and cerebral artery smooth muscle cells

Notes: A, Confocal image illustrates punctate fluorescence of 2mt8CG2 in HEK293 cells. B, Confocal image of smooth muscle cells dissociated from arteries reverse permeabilized with pMITO-2mt8CG2. Punctate pattern of fluorescence suggests mitochondrial targeting of 2mt8CG2. C, Colocalization of punctate 2mt8CG2 fluorescence with MitoTracker Orange in a smooth muscle cell. Colocalization quantified using weighted colocalization was 94.8±0.8% (n=10, $p<0.001$). Scale bar=10 μm.

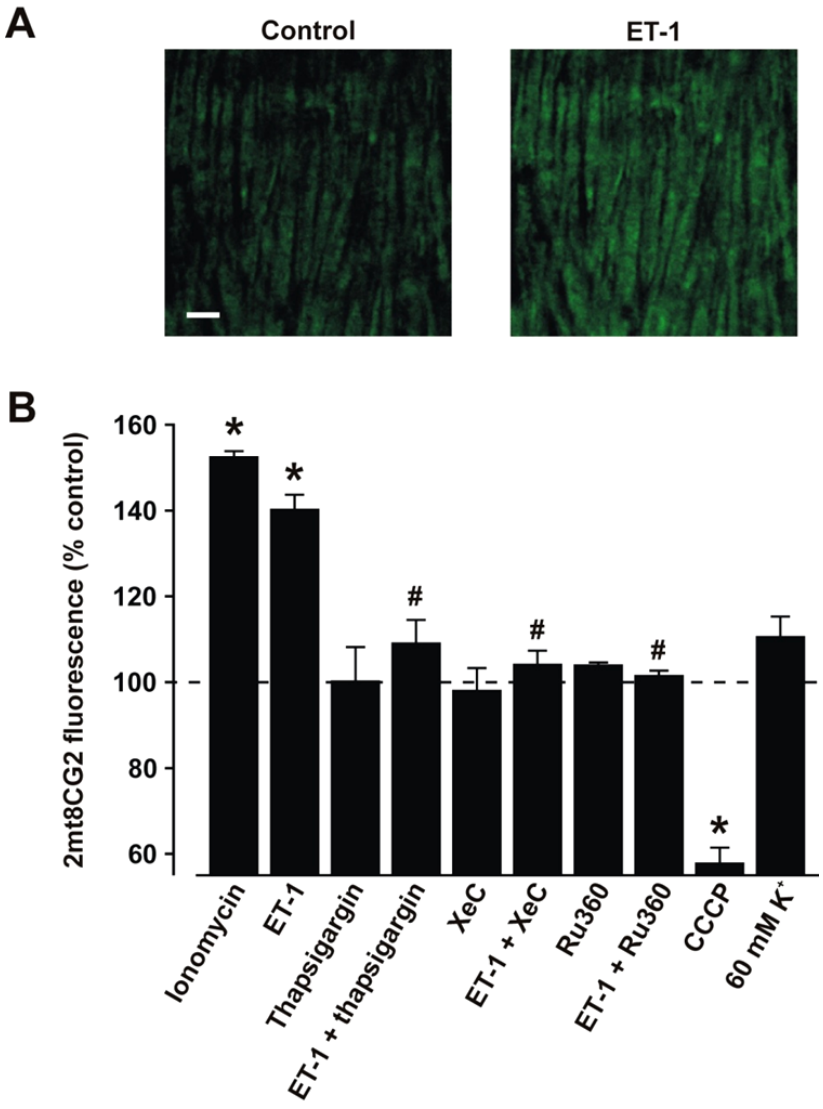

Figure 4-3. ET-1-induced IP_3R-mediated SR Ca^{2+} release elevates $[Ca^{2+}]_{mito}$ in arterial smooth muscle cells

Notes: A, Confocal images of 2mt8CG2 fluorescence in smooth muscle cells in the same area of a cerebral artery in control and ET-1. Scale bar=10 μm. B, Average changes in 2mt8CG2 fluorescence for ionomycin (10 μM, n=7), ET-1 (n=8), thapsigargin (100 nM, n=5), ET-1+thapsigargin (n=6), XeC (20 μM, n=5), ET-1+XeC (n=6), Ru360 (10 μM, n=4), ET-1+Ru360 (n=4), CCCP (10 μM, n=4), and 60 mM K^+ (n=6). ET-1 concentration was 100 nM in all experiments. Values are expressed as mean±SEM. * indicates $P<0.05$ compared to control. # indicates $P<0.05$ compared to ET-1.

4.3. ET-1-Induced IP_3R-Mediated SR Ca^{2+} Release Depolarizes Mitochondria in Cerebral Artery Smooth Muscle Cells

Regulation of mitochondria potential ET-1 was studied in isolated smooth muscle cells using TMRM. ET-1 (30 nM) reversibly reduced TMRM fluorescence intensity to ~67% of control (**Fig. 4-4A-C**). A second application of ET-1 (30 nM) produced a similar amplitude change in TMRM fluorescence (~69% of control), indicating that the first ET-1 application did not desensitize the ET-1 receptors (**Fig. 4-4A,B**). ET-1 caused concentration-dependent reduction in TMRM fluorescence with an EC_{50} of 29 nM (**Fig. 4-4B**). Thapsigargin and XeC abolished the ET-1-induced reduction in TMRM fluorescence, but did not alter TMRM fluorescence when applied alone (**Fig. 4-4C**). CCCP reduced TMRM fluorescence intensity to ~34% of control, whereas 60 mM K^+ did not alter TMRM fluorescence (**Fig. 4-4C**). These data indicate that ET-1-induced IP_3R-mediated SR Ca^{2+} release depolarizes mitochondria in arterial smooth muscle cells. In contrast, a global $[Ca^{2+}]_i$ elevation does not alter ψ_m.

4.4. ET-1-Induced IP_3R-Mediated SR Ca^{2+} Release and $[Ca^{2+}]_{mito}$ Elevation Stimulates MitoROS Generation

4.4.1. MitoROS measurements using mt-cpYFP

To examine physiological functions of $[Ca^{2+}]_{mito}$, we tested the hypothesis that an elevation in $[Ca^{2+}]_{mito}$ may alter mitoROS generation. MitoROS was measured using mt-cpYFP, a genetically-encoded mitochondria-targeted fluorescent $O_2^{-\cdot}$ indicator (Wang *et al.*, 2008a).

4.4.1.1. Mitochondrial localization of mt-cpYFP

Mitochondrial targeting of mt-cpYFP was studied by performing colocalization studies using MitoTracker Orange. mt-cpYFP fluorescence exhibited ~95% pixel colocalization with MitoTracker Orange, indicating mitochondrial localization (**Fig. 4-5**).

4.4.1.2. ET-1 elevates mitoROS production

In smooth muscle cells of intact arteries, ET-1 elevated mt-cpYFP fluorescence to ~199% of control, and this was blocked by XeC, Ru360, rotenone, a mitochondrial ETC complex I inhibitor (Fukami *et al.*, 1967), and micromolar CCCP (**Fig. 4-6A,B**). When applied alone, rotenone and micromolar CCCP reduced mt-cpYFP fluorescence to ~54 and 64% of control, respectively (**Fig. 4-6B**). In contrast, Ru360, XeC, and 60 mM K^+ did not alter mt-cpYFP fluorescence (**Fig. 4-6B**). In cerebral artery smooth muscle cells, 1 nM CCCP reduced TMRM fluorescence to ~87% of control, and elevated DCF fluorescence to ~140% of control, suggesting that a low concentration of CCCP induces a

Figure 4-4. ET-1-induced IP_3R-mediated SR Ca^{2+} release depolarizes mitochondria in arterial smooth muscle cells

Notes: A, ET-1 caused reproducible mitochondrial depolarization in cerebral artery smooth muscle cells. ET-1-induced mitochondrial depolarization was blocked by pretreatment with XeC (20 μM). B, Concentration-dependent mitochondrial depolarization by ET-1 (n=4-7). C, Average changes in TMRM fluorescence for ET-1 (n=37), second ET-1 application (n=12), thapsigargin (100 nM, n=18), ET-1+thapsigargin (n=18), XeC (20 μM, n=12), ET-1+XeC (n=12), 60 mM K^+ (n=10), and CCCP (10 μM, n=65). ET-1 concentration was 30 nM in all experiments. Values are expressed as mean±SEM. * indicates $P<0.05$ compared to control. # indicates $P<0.05$ compared to ET-1.

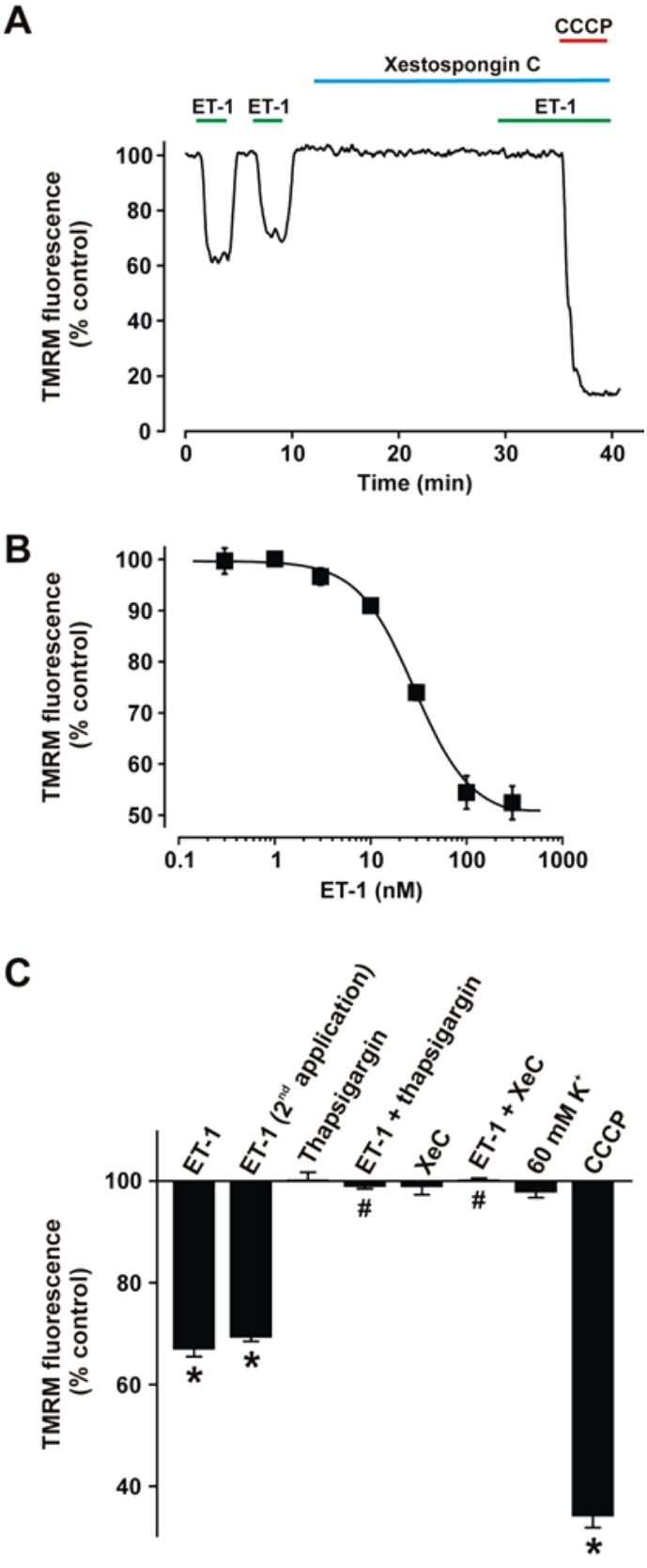
A
CCCP
Xestospongin C
ET-1
ET-1
ET-1
TMRM fluorescence (% control)
100
80
60
40
20
0
0
10
20
30
40
Time (min)
B
TMRM fluorescence (% control)
100
90
80
70
60
50
0.1
1
10
100
1000
ET-1 (nM)
C
TMRM fluorescence (% control)
100
80
60
40
ET-1
ET-1 (2nd application)
Thapsigargin
ET-1 + thapsigargin
XeC
ET-1 + XeC
60 mM K+
CCCP
*
*
#
#
*

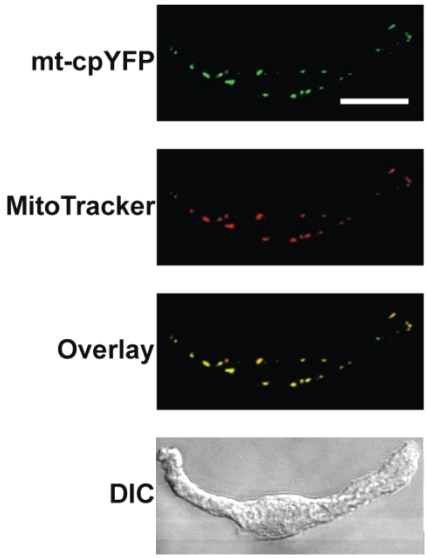

Figure 4-5. Mitochondrial localization of mt-cpYFP in cerebral artery smooth muscle cells

Notes: Confocal images illustrate colocalization of punctate mt-cpYFP fluorescence with MitoTracker Orange in a smooth muscle cell. Colocalization quantified using weighted colocalization was 94.7±1.2% (n=10, $p<0.001$). Scale bar=10 μm.

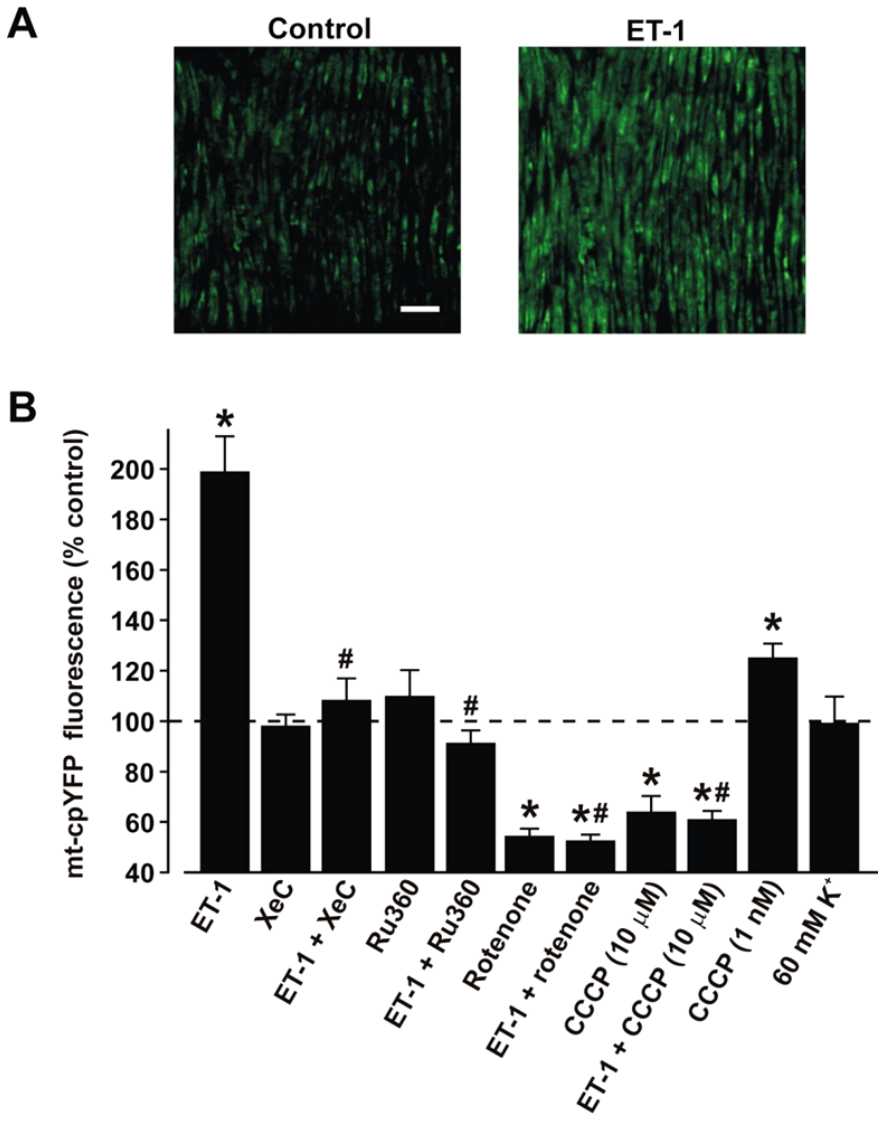

Figure 4-6. ET-1-induced IP_3R-mediated SR Ca^{2+} release and mitochondrial Ca^{2+} uptake elevates mitoROS generation in arterial smooth muscle cells

Notes: A, Original images illustrating ET-1-induced elevation in mt-cpYFP fluorescence in smooth muscle cells of an intact artery. Scale bar=20 μm. B, Average mt-cpYFP fluorescence changes in smooth muscle cells of intact arteries. ET-1, XeC (20 μM), ET-1+XeC, Ru360 (10 μM), ET-1+Ru360, rotenone (10 μM), ET-1+rotenone, CCCP (10 μM), ET-1+CCCP, CCCP (1 nM), and 60 mM K^+. ET-1 concentration was 100 nM in all experiments. n=5 for each condition. Values are expressed as mean±SEM.
* indicates $P<0.05$ compared to control. # indicates $P<0.05$ compared to ET-1.

small mitochondrial depolarization and increases mitoROS generation (Xi *et al.*, 2005). Similarly, here 1 nM CCCP elevated mt-cpYFP fluorescence to ~124% of control (**Fig. 4-6B**). These data indicate that mitochondria generate ROS in the absence of ET-1, and that ET-1-induced IP_3R-mediated SR Ca^{2+} release and $[Ca^{2+}]_{mito}$ elevation stimulate mitoROS generation. Results with Ru360, rotenone, and micromolar CCCP confirm the mitochondrial localization of mt-cpYFP.

4.4.2. ET-1-induced mitoROS generation elevates cytosolic ROS levels

Cytosolic ROS was measured using HyPer-CYTO, a genetically-encoded fluorescent cytosolic H_2O_2 indicator (**Fig. 3-1**) (Belousov *et al.*, 2006). Exogenous H_2O_2 elevated HyPer-CYTO fluorescence to ~234% of control (**Fig. 4-7A**). ET-1 similarly increased HyPer-CYTO fluorescence in smooth muscle cells of endothelium-intact and -denuded arteries to ~158 and 168% of control, respectively (**Fig. 4-7B,C**). When applied alone, rotenone and MnTMPyP, a SOD and catalase mimetic (Faulkner *et al.*, 1994), reduced HyPer-CYTO fluorescence ~75 and 80% of control, respectively (**Fig. 4-7C**). Rotenone and MnTMPyP blocked the ET-1-induced elevations in HyPer-CYTO fluorescence (**Fig. 4-7C**). These data indicate that mitoROS production contributes to cytosolic ROS levels in the absence of ET-1 and that ET-1-induced mitoROS elevation leads to an increase in cytosolic ROS in cerebral artery smooth muscle cells.

4.4.3. ROS measurements using DCF

4.4.3.1. ET-1 stimulates ROS generation

To confirm measurements obtained using mt-cpYFP and HyPer-CYTO, ROS levels were studied in smooth muscle cells of cerebral arteries using CM-H_2DCFDA, an inorganic fluorescent ROS indicator. ET-1 increased mean DCF fluorescence in smooth muscle cells of endothelium-intact and -denuded arteries to ~154 and 151% of control, respectively (**Fig. 4-8A,B**). Exogenous H_2O_2 application elevated mean DCF fluorescence intensity to ~219% of control (**Fig. 4-8B**). ET-1-induced DCF fluorescence elevations were blocked by thapsigargin, XeC, and MnTMPyP (**Fig. 4-8B**). When applied alone, thapsigargin and XeC did not alter, but MnTMPyP reduced DCF fluorescence to ~74% of control (**Fig. 4-8B**). 60 mM K^+, which leads to global $[Ca^{2+}]_i$ elevation did not alter DCF fluorescence (**Fig. 4-8B**). These data confirm the finding that ET-1-induced IP_3R-mediated SR Ca^{2+} release stimulates ROS generation.

4.4.3.2. Source of ET-1-induced ROS elevation is mitochondria

ET-1-induced DCF fluorescence elevations were blocked by CCCP and rotenone (**Fig. 4-9A**). In the presence of oxypurinol, a xanthine oxidase inhibitor (Elion *et al.*, 1968) and 17-ODYA, a cytochrome P450 blocker (Zou *et al.*, 1994), ET-1 elevated DCF

Figure 4-7. ET-1-induced IP_3R-mediated SR Ca^{2+} release elevates cytosolic ROS in arterial smooth muscle cells

Notes: A,B, Confocal images illustrating that exogenous H_2O_2 (A) and ET-1 (B) elevates HyPer-CYTO fluorescence in arterial smooth muscle cells. C, Average changes in HyPer-CYTO fluorescence for H_2O_2 (100 μM), ET-1 (endothelium-intact), ET-1 (endothelium-denuded), rotenone (10 μM), ET-1+rotenone, MnTMPyP (10 μM), and ET-1+MnTMPyP. ET-1 concentration was 100 nM in all experiments. n=5 for each condition. Values are expressed as mean±SEM. * indicates $P<0.05$ compared to control. # indicates $P<0.05$ compared to ET-1.

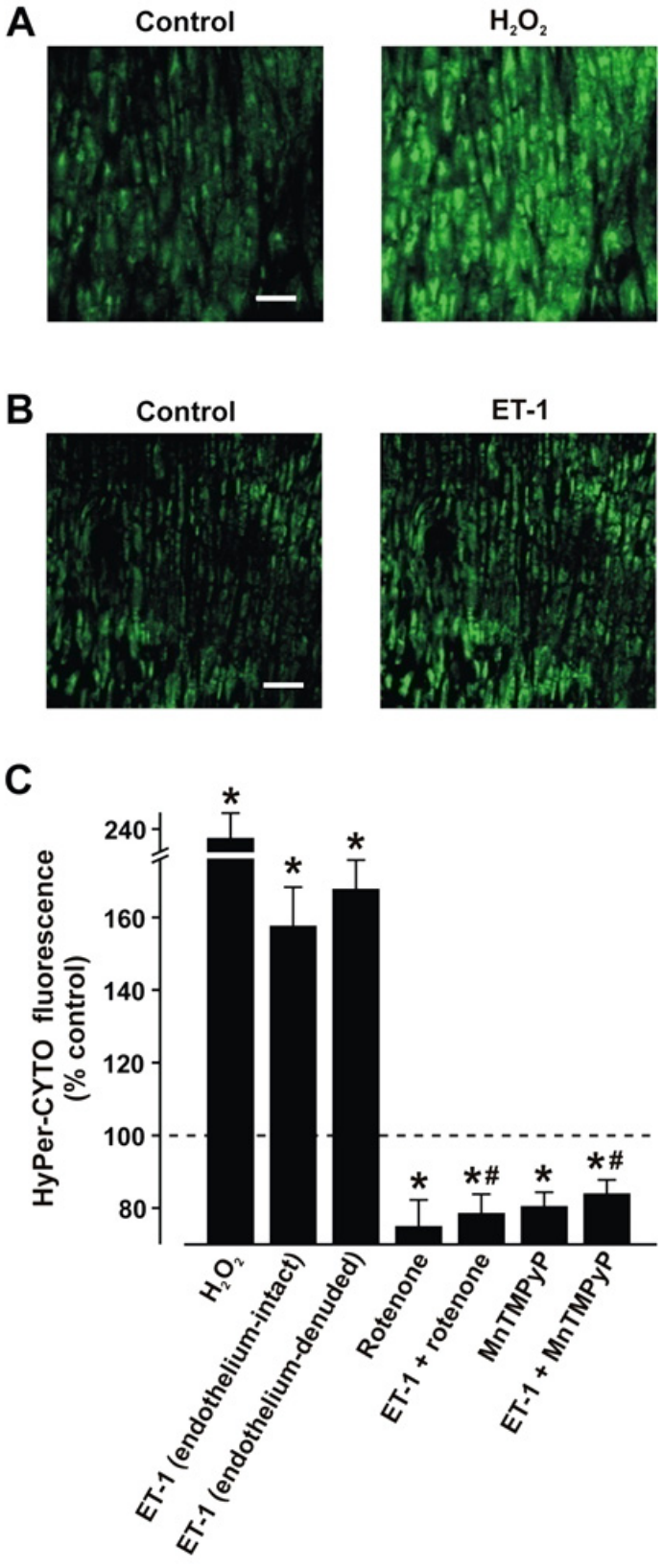
A
Control
H2O2
B
Control
ET-1
C
HyPer-CYTO fluorescence (% control)
240
160
140
120
100
80
*
*
*
*
*#
*
*#
H2O2
ET-1 (endothelium-intact)
ET-1 (endothelium-denuded)
Rotenone
ET-1 + rotenone
MnTMPyP
ET-1 + MnTMPyP

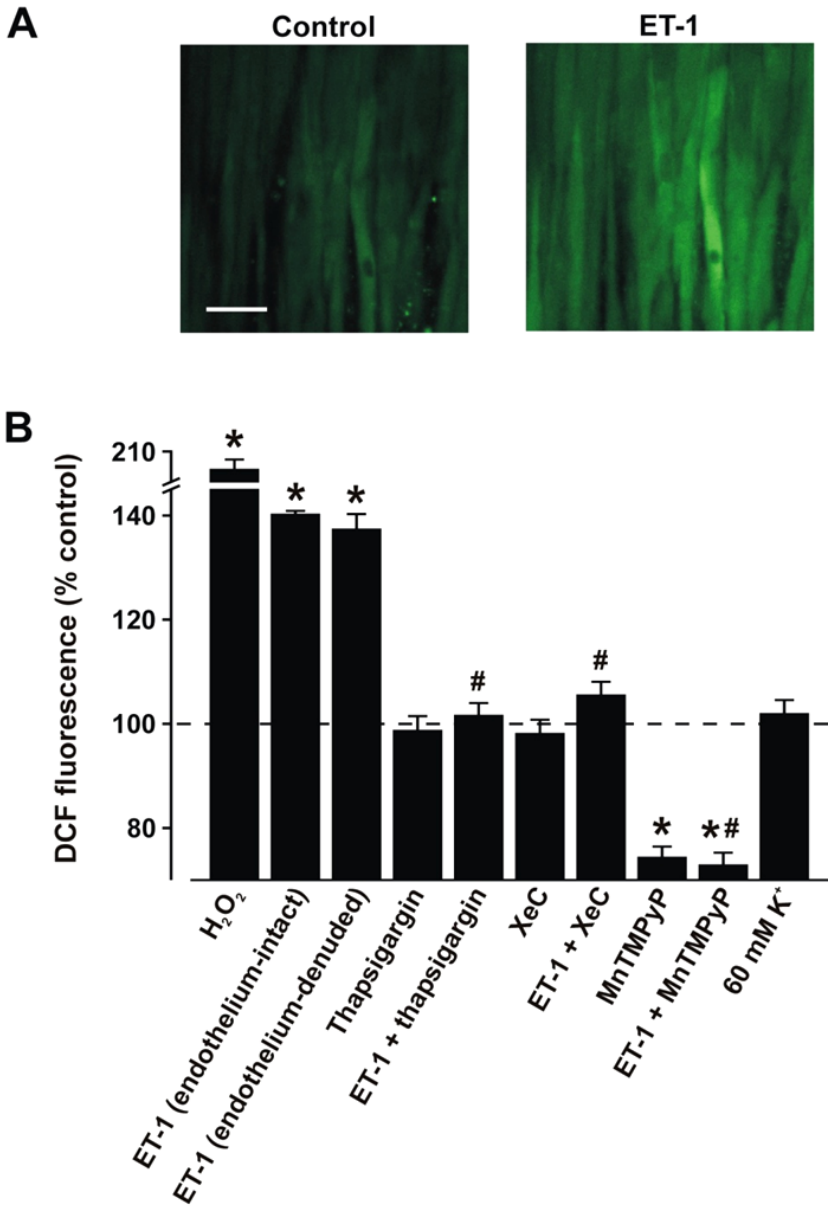

Figure 4-8. ET-1-induced IP_3R-mediated SR Ca^{2+} release elevates DCF fluorescence in arterial smooth muscle cells

Notes: A, Confocal images of DCF fluorescence in smooth muscle cells of the same cerebral artery in control and ET-1. Scale bar=20 μm. B, Mean DCF fluorescence changes in arterial smooth muscle cells. H_2O_2 (100 μM, n=6), ET-1 (endothelium-intact, n=10), ET-1 (endothelium-denuded, n=6), thapsigargin (100 nM, n=5), ET-1+thapsigargin (n=10), XeC (20 μM, n=5), ET-1+XeC (n=6), MnTMPyP (10 μM, n=5), ET-1+MnTMPyP (n=6), and 60 mM K^+ (n=6). Values are expressed as mean±SEM. * indicates $P<0.05$ compared to control. # indicates $P<0.05$ compared to ET-1.

Figure 4-9. ET-1-induced mitoROS generation elevates DCF fluorescence in arterial smooth muscle cells

Notes: A, Mean DCF fluorescence change for ET-1 (endothelium-intact, n=10), rotenone (10 μM, n=5), ET-1+rotenone (n=10), CCCP (10 μM, n=5), ET-1+CCCP (n=10), gp91ds-tat (50 μM, n=5), ET-1+gp91ds-tat (n=5), oxypurinol (10 μM, n=5), ET-1+oxypurinol (n=6), 17-octadecynoic acid (10 μM, n=5), and ET-1+17-octadecynoic acid (n=6). B, Mean DCF fluorescence change for TNF-α (100 ng/ml, n=5), ET-1 (endothelium-intact, n=10), gp91scrm-tat (50 μM, n=5), TNF-α+gp91scrm-tat (n=5), ET-1+gp91scrm-tat (n=5), gp91ds-tat (50 μM, n=5), TNF-α+gp91ds-tat (n=5), and ET-1+gp91ds-tat (n=5). ET-1 concentration was 100 nM in all experiments. * indicates $P<0.05$ compared to control. Values are expressed as mean±SEM. # indicates $P<0.05$ compared to ET-1. § indicates $P<0.05$ compared to TNF-α.

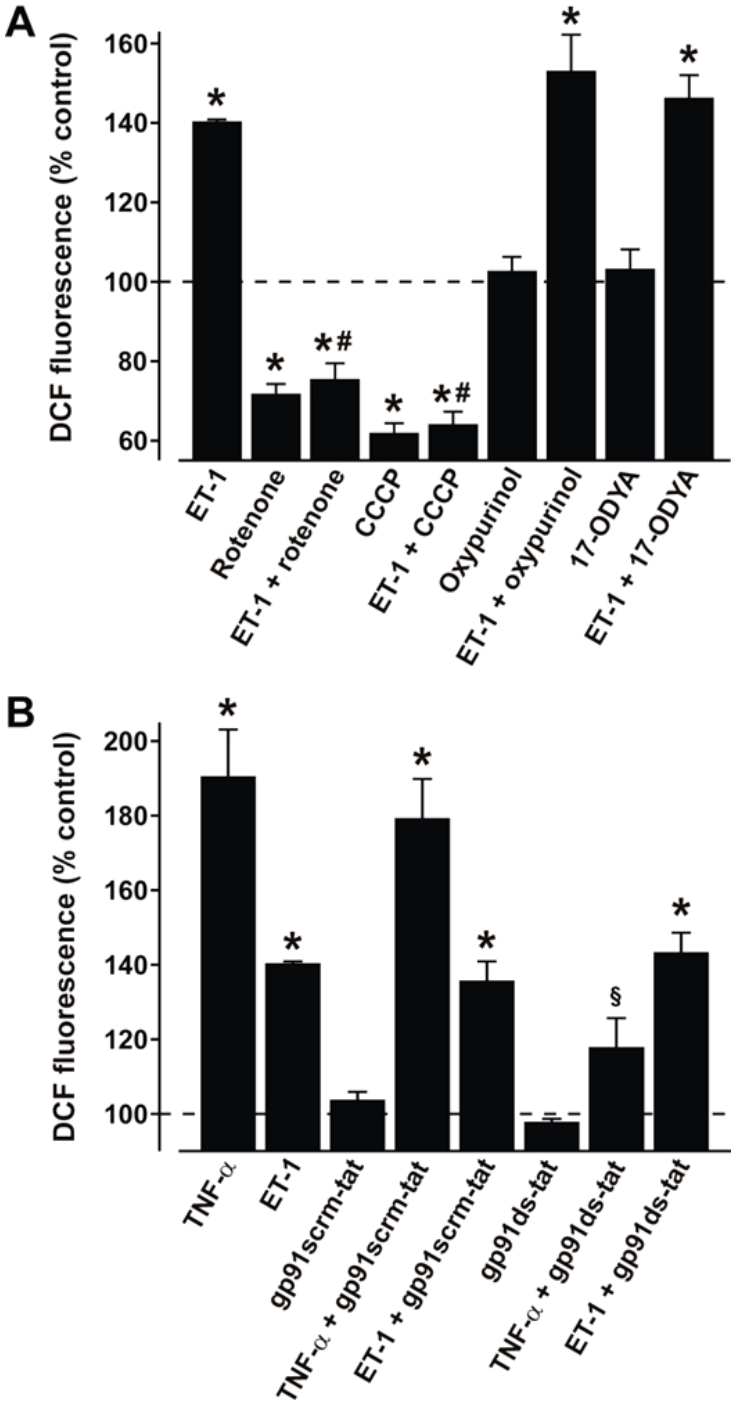
A
DCF fluorescence (% control)
160
140
120
100
80
60
*
*
*#
*
*#
*
*
ET-1
Rotenone
ET-1 + rotenone
CCCP
ET-1 + CCCP
Oxypurinol
ET-1 + oxypurinol
17-ODYA
ET-1 + 17-ODYA
B
DCF fluorescence (% control)
200
180
160
140
120
100
*
*
*
*
§
*
TNF-α
ET-1
gp91scrm-tat
TNF-α + gp91scrm-tat
ET-1 + gp91scrm-tat
gp91ds-tat
TNF-α + gp91ds-tat
ET-1 + gp91ds-tat

fluorescence to ~153 and 146% of control, respectively (**Fig. 4-9A**). Oxypurinol and 17-ODYA did not alter baseline DCF fluorescence, whereas CCCP and rotenone alone decreased baseline DCF fluorescence to ~62 and 72% of control, respectively (**Fig. 4-9A**).

TNF-α, which stimulates NAD(P)H oxidase-derived ROS in cerebral artery smooth muscle cells (Cheranov & Jaggar, 2006), elevated DCF fluorescence to ~190% of control (**Fig. 4-9B**). gp91ds-tat did not alter baseline DCF fluorescence, whereas blocked DCF fluorescence elevations induced by TNF-α, suggesting that gp91ds-tat inhibits NAD(P)H oxidase (**Fig. 4-9B**). In the presence of gp91ds-tat, ET-1 increased DCF fluorescence to ~143% of control (**Fig. 4-9B**). Scrambled gp91-tat did not alter baseline DCF fluorescence, or ET-1- or TNF-α-induced DCF fluorescence elevations (**Fig. 4-9B**).

Data obtained using DCF confirm ROS measurements obtained using mt-cpYFP and HyPer-CYTO, that mitochondria generate ROS in the absence of ET-1, and that ET-1-induced IP_3R-mediated SR Ca^{2+} release and $[Ca^{2+}]_{mito}$ elevation stimulate mitoROS generation, leading to an increase in cytosolic ROS in cerebral artery smooth muscle cells.

4.5. ET-1-Induced IP_3R-Mediated MitoROS Elevation Stimulates NF-κB

4.5.1. ET-1 stimulates nuclear translocation of NF-κB p50

To examine physiological functions of an IP_3R-mediated mitoROS elevation, we tested the hypothesis that mitochondria regulate the expression of genes that modulate smooth muscle cell contractility. Therefore, immunofluorescence was performed to study cellular localization of the p50 subunit of NF-κB, a ROS-sensitive transcription factor (Lee *et al.*, 2008), in arterial smooth muscle cells. ET-1 increased mean pixel colocalization of p50 with YOYO-1 from ~12 to 22% (**Fig. 4-10A-C**), suggesting that ET-1 stimulates nuclear translocation of p50.

4.5.2. ET-1 elevates NF-κB-dependent transcriptional activity

To investigate the regulation of NF-κB-dependent transcriptional activity, assays were performed using vectors that express firefly luciferase under the control of an NF-κB promoter. As a control, regulation of luciferase activity by TNF-α, which activates NF-κB (Li *et al.*, 1999) was measured. TNF-α increased mean luciferase activity to ~547% of control (**Fig. 4-11**). ET-1 increased luciferase activity to ~372% of control, and this was blocked by thapsigargin and XeC (**Fig. 4-11**). Rotenone and MnTMPyP reduced the ET-1-induced elevation in luciferase activity to ~152 and 109% of control, respectively (**Fig. 4-11**). Exogenous H_2O_2 elevated luciferase activity to ~252% of control, and this effect was not altered by rotenone, indicating that rotenone did not cause general inhibition of luciferase expression (**Fig. 4-11**). When applied alone, thapsigargin,

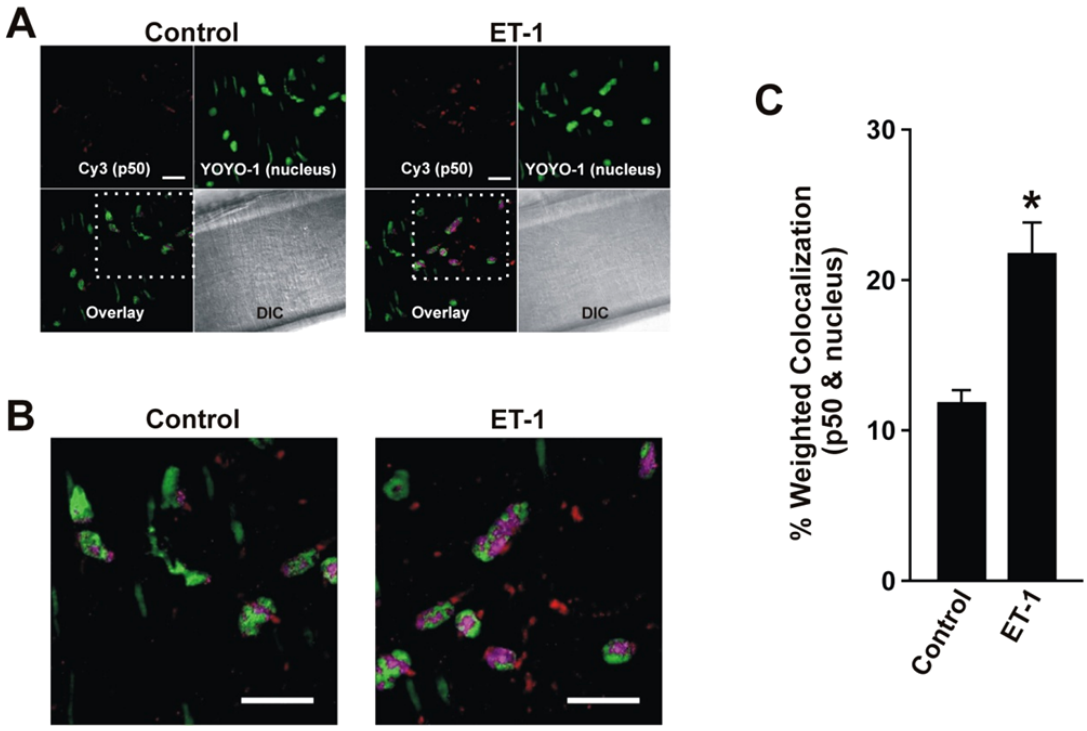

Figure 4-10. ET-1 stimulates p50 nuclear translocation in arterial smooth muscle cells

Notes: A, Immunofluorescence images of smooth muscle cells in arteries illustrating YOYO-1 (nuclear stain, green), p50 (red), overlay, and DIC (lumenally-inserted rectangular glass cannula can be seen). B, Enlarged images indicated by boxes in A illustrate ET-1-induced elevation in p50 and YOYO-1 pixel colocalization (purple). Scale bars=20 μm. C, Mean data for weighted pixel colocalization (n=10 for each). Values are expressed as mean±SEM. * indicates $P<0.05$ compared to control.

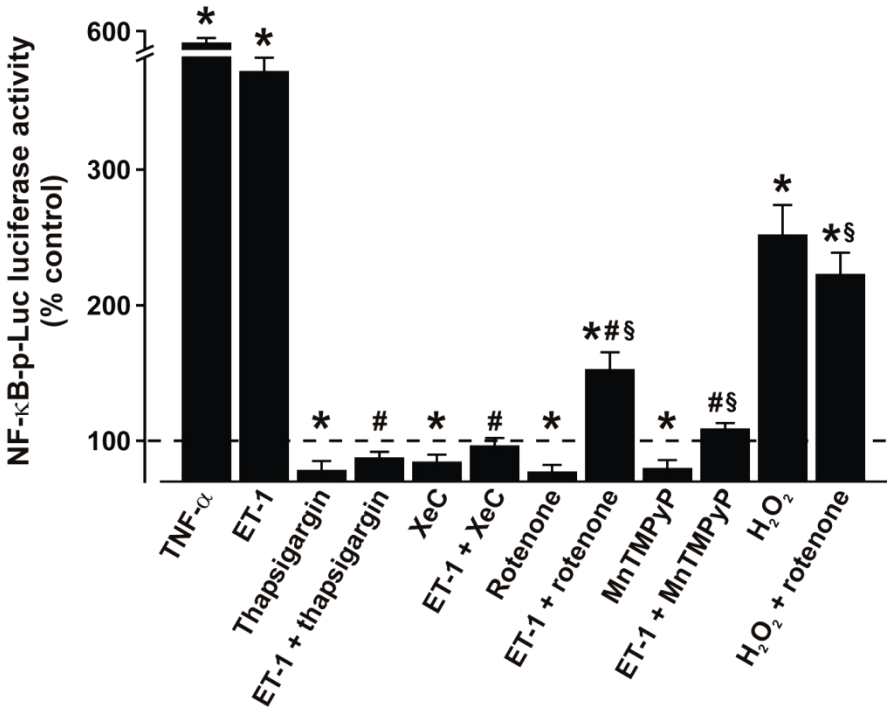

Figure 4-11. ET-1 stimulates NF-κB-dependent transcription through IP_3R-mediated SR Ca^{2+} release and mitoROS elevation in arterial smooth muscle cells

Notes: Average NF-κB-p-Luc luciferase activity with TNF-α (100 ng/ml, n=4), ET-1 (n=5), thapsigargin (100 nM, n=5), ET-1+thapsigargin (n=5), XeC (20 μM, n=5), ET-1+XeC (n=5), rotenone (1 μM, n=5), ET-1+rotenone (n=5), MnTMPyP (10 μM, n=4), ET-1+MnTMPyP (n=4), H_2O_2 (100 μM, n=4), and H_2O_2+rotenone (n=4). ET-1 concentration was 100 nM in all experiments. Values are expressed as mean±SEM. * indicates $P<0.05$ compared to control. # indicates $P<0.05$ compared to ET-1. § indicates $P<0.05$ compared to rotenone or MnTMPyP.

XeC, rotenone, and MnTMPyP reduced luciferase activity to ~84, 78, 77, and 80% of control, respectively (**Fig. 4-11**). TNF-α, ET-1, thapsigargin, XeC, rotenone, MnTMPyP, and H_2O_2 did not alter luciferase activity in arteries in which a promoter-deficient control vector was inserted (**Fig. 4-12**). These data indicate that IP_3R-mediated SR Ca^{2+} release stimulates NF-κB primarily by elevating mitoROS generation, but also via a secondary mitochondria- and ROS-independent pathway in arterial smooth muscle cells.

4.5.3. ROS measurements corresponding to transcriptional studies

For transcriptional studies performed using luciferase reporter assays, arteries were exposed to stimuli for 24 hours. To determine if the inhibitors used, blocked the ET-1-induced ROS elevations which corresponded to the time points used in the above transcriptional studies, ROS levels were measured using DCF. After a 24-hour incubation in control, ET-1 elevated DCF fluorescence to ~145% of control (**Fig. 4-13**). ET-1-induced DCF fluorescence elevations were blocked by 24-hour incubation in thapsigargin, XeC, or rotenone (**Fig. 4-13**). These data indicate that the inhibitors used for a period of time in transcriptional studies blocked the ET-1-induced ROS elevations.

4.6. ET-1-Induced IP_3R-Mediated SR Ca^{2+} Release Stimulates $Ca_V1.2$ Expression by MitoROS Elevation and NF-κB Activation

We sought to examine the functional significance of IP_3R-mediated, mitochondrial-dependent NF-κB activation. $Ca_V1.2$ channels are the principal Ca^{2+} influx pathway in smooth muscle cells of resistance-size arteries and are essential for contractility regulation by a wide variety of stimuli, including intravascular pressure and membrane potential (Cheng *et al.*, 2007). However, mechanisms that regulate CACNA1C transcription in arterial smooth muscle cells are unclear. Three NF-κB binding motifs are located immediately upstream of the human Cav1.2 promoter (Shi *et al.*, 2005). Therefore, we tested the hypothesis that ET-1-induced IP_3R-mediated, mitoROS-dependent NF-κB activation regulates $Ca_V1.2$ expression in cerebral arteries.

4.6.1. ET-1 stimulates $Ca_V1.2$ gene transcription

To study ET-1 regulation of gene expression we performed RT-PCR. We sought to identify a reference gene whose transcription is not affected by ET-1 (6 hours). RT-PCR reactions were performed for five genes, namely beta (β) actin, beta (β) tubulin, cyclophilin B, hypoxanthine-guanine phosphoribosyltransferase (HGPRT), and Rps5. CT values for the reference genes in control and ET-1 are shown in **Table 4-1**. Rps5 which had the least difference in average CT values between control and ET-1 treatment groups was chosen as the reference gene.

RT-PCR data indicated that in cerebral arteries, ET-1 increased $Ca_V1.2$ channel mRNA expression to ~244% of control, after normalization to Rps5 (**Fig. 4-14D**).

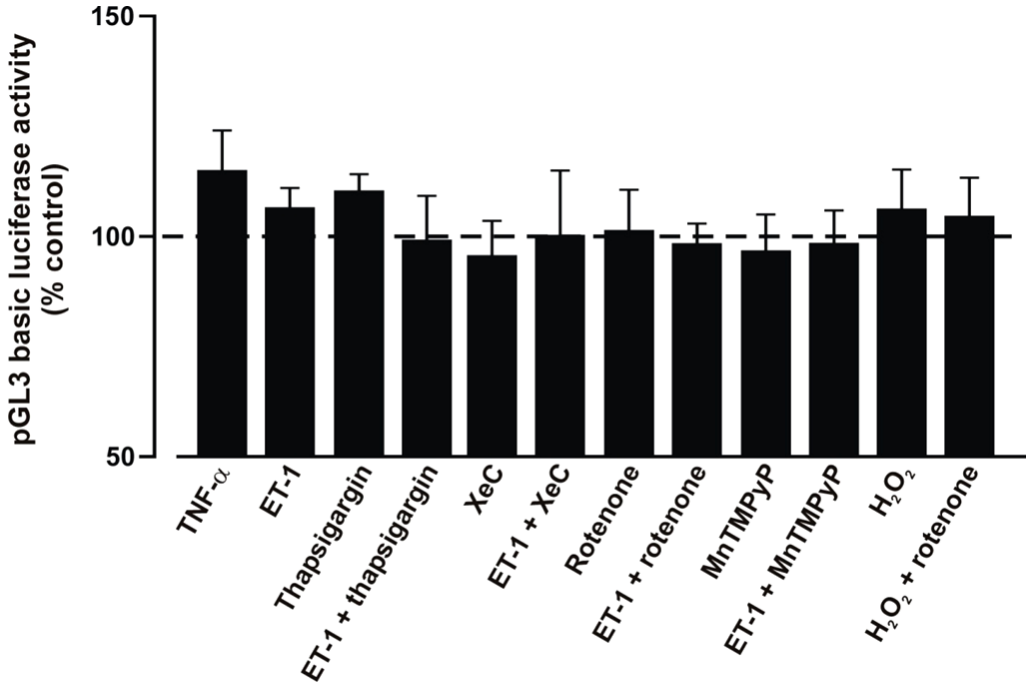

Figure 4-12. Mean changes in promoter-deficient (pGL3 Basic) luciferase activity

Notes: Mean data. TNF-α (100 ng/ml, n=4), ET-1 (n=5), thapsigargin (100 nM, n=4), ET-1+thapsigargin (n=4), XeC (20 μM, n=3), ET-1+XeC (n=3), rotenone (1 μM, n=4), ET-1+rotenone (n=4), MnTMPyP (10 μM, n=3), ET-1+MnTMPyP (n=3), H_2O_2 (100 μM, n=3), and H_2O_2+rotenone (n=3). ET-1 concentration was 100 nM in all experiments. Values are expressed as mean±SEM.

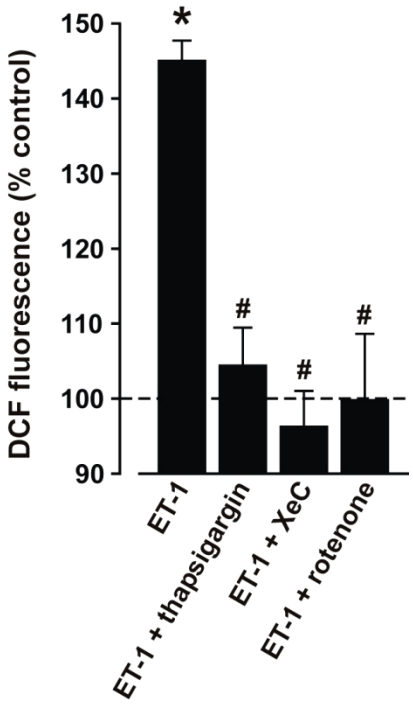

Figure 4-13. ROS measurements at time points used for transcriptional studies

Notes: Average change in DCF fluorescence with ET-1 (100 nM, n=5) after a 24 hour incubation in control, in the presence of thapsigargin (100 nM, n=3), XeC (20 μM, n=3), or rotenone (1 μM, n=5). Values are expressed as mean±SEM. * indicates $P<0.05$ compared to control. # indicates $P<0.05$ compared to ET-1.

Table 4-1. Identification of reference gene for RT-PCR

Gene	$CT_{control}$	CT_{ET-1}	$CT_{control} - CT_{ET-1}$
Rps5	25.43	24.83	0.60
HGPRT	31.90	31.21	0.69
Cyclophilin B	27.39	26.71	0.68
β tubulin	32.81	32.12	0.69
β actin	22.5	21.53	0.97

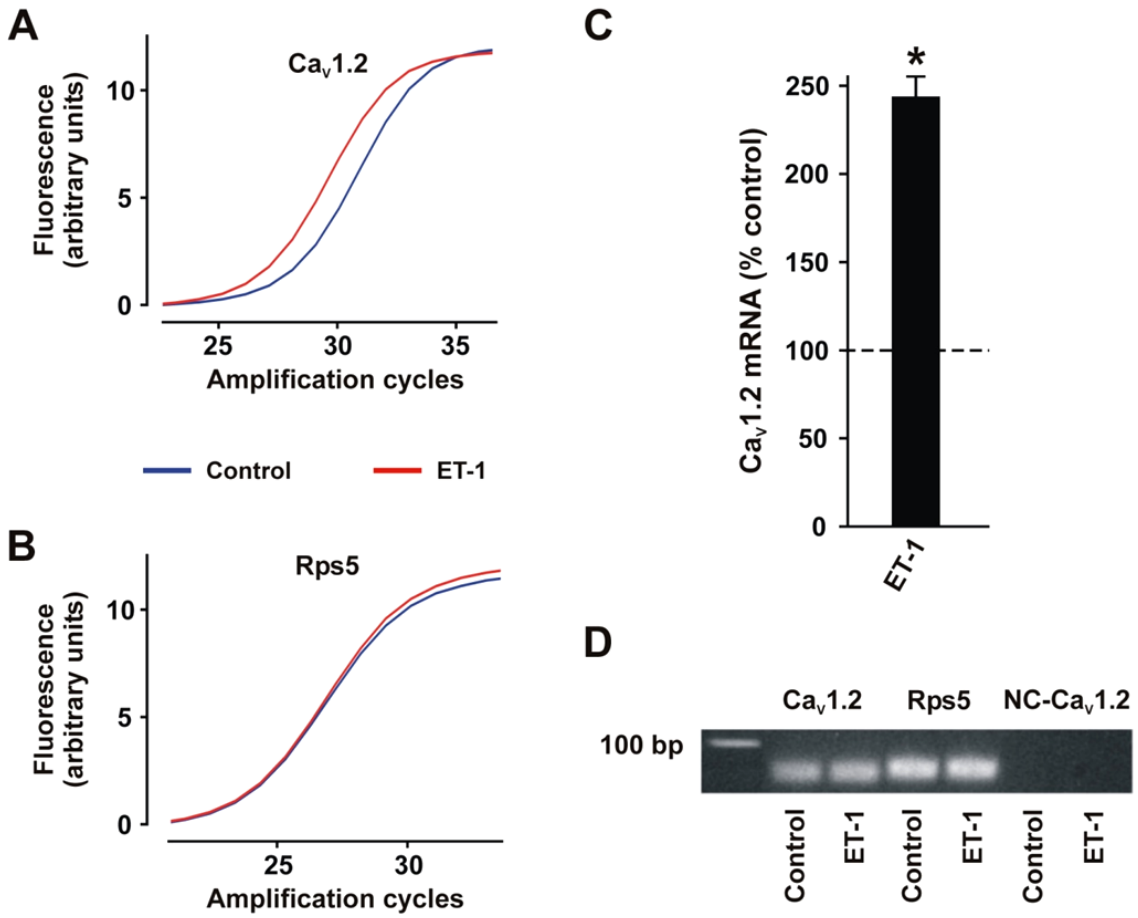

Figure 4-14. ET-1 stimulates $Ca_V1.2$ gene transcription in cerebral arteries

Notes: A,B, Representative amplification curves generated with probes and RT-PCR primers specific for $Ca_V1.2$ (A) and Rps5 (B) genes in control (blue) and ET-1(10 nM)-treated (red) arteries. The data points for the amplification curves shown were obtained by calculating the average of data points from triplicates for each condition. C, Application of ET-1 (10 nM) for 6 hours elevated mean $Ca_V1.2$ mRNA in cerebral arteries compared to control arteries (n=7 for each condition). Values are expressed as mean±SEM. * indicates $P<0.05$ compared to control. D, Agarose gel illustrating transcripts amplified using RT-PCR primers for $Ca_V1.2$ (70 bp) and Rps5 (83 bp) from cerebral arteries in control and ET-1 (10 nM). NC, negative control using cerebral artery mRNA.

4.6.2. ET-1-induced IP_3R activation and mitoROS elevation stimulate $Ca_V1.2$ expression

Western blotting indicated that ET-1 (24 hrs) increased $Ca_V1.2$ channel (190 and 240 kD bands) protein to ~141% of control (**Fig. 4-15A,B**). XeC, rotenone, and MnTMPyP alone reduced basal $Ca_V1.2$ expression to ~87, 89, and 80% of control, respectively (**Fig. 4-15A,B**). XeC blocked the ET-1-induced elevation in $Ca_V1.2$ expression (**Fig. 4-15A,B**). Rotenone and MnTMPyP reduced the ET-1-induced elevation in $Ca_V1.2$ expression to ~113 and 90% of control, respectively (**Fig. 4-15B**). Exogenous H_2O_2 increased $Ca_V1.2$ expression to ~128% of control, and this elevation was not altered by rotenone, indicating that rotenone did not induce non-specific inhibition of $Ca_V1.2$ expression (**Fig. 4-15B**). These data indicate that ET-1-induced IP_3R-mediated SR Ca^{2+} release and mitoROS elevation stimulate $Ca_V1.2$ expression in cerebral arteries.

4.6.3. ET-1-induced NF-κB activation elevates $Ca_V1.2$ expression

Two different siRNAs were used to knockdown expression of p105, the p50 precursor (Baeuerle & Baltimore, 1996). p105siRNA1, p105siRNA2, and a combination of both siRNAs (p105siRNAs) reduced mean p105 protein to ~73, 80, and 57%, respectively, of that in arteries treated with scrambled siRNA (p105scrm) (**Fig. 4-16A,B**).

p105siRNAs reduced $Ca_V1.2$ expression to ~64% of p105scrm (**Fig. 4-17A,B**), indicating that NF-κB controls basal $Ca_V1.2$ expression. In p105scrm-treated arteries, ET-1 increased $Ca_V1.2$ protein to ~136% of p105scrm (**Fig. 4-17A,B**). In p105siRNAs-treated arteries, ET-1 increased $Ca_V1.2$ protein from ~64 to 74% of p105scrm (~117% of p105siRNAs) (**Fig. 4-17A,B**). These data indicate that IP_3R-mediated SR Ca^{2+} release stimulates $Ca_V1.2$ expression via mitochondria-dependent NF-κB activation.

4.7. ET-1-Induced IP_3R-Mediated SR Ca^{2+} Release Also Stimulates p105 Expression

The p105 gene promoter contains an NF-κB-binding sequence, and p50 activation can elevate p105 expression (Ten *et al.*, 1992). Therefore, mechanisms that regulate NF-κB subunit expression in cerebral arteries were investigated. Inhibiting IP_3R-mediated SR Ca^{2+} release using XeC reduced basal p105 and p50 expression to ~87 and 90% of control, respectively (**Fig. 4-18A,B**). Inhibiting mitoROS production using rotenone or dismutating cellular ROS using MnTMPyP, did not alter basal p105 or p50 expression (**Fig. 4-18B**). ET-1 elevated p105 and p50 expression to ~127 and 119% of control, respectively and XeC blocked this effect (**Fig. 4-18B**). In contrast, rotenone or MnTMPyP had no effect on the ET-1-induced elevation in p105 and p50 subunit expression (**Fig. 4-18B**). Exogenous H_2O_2 applied alone or in the presence of rotenone did not change p105 and p50 expression (**Fig. 4-18B**).

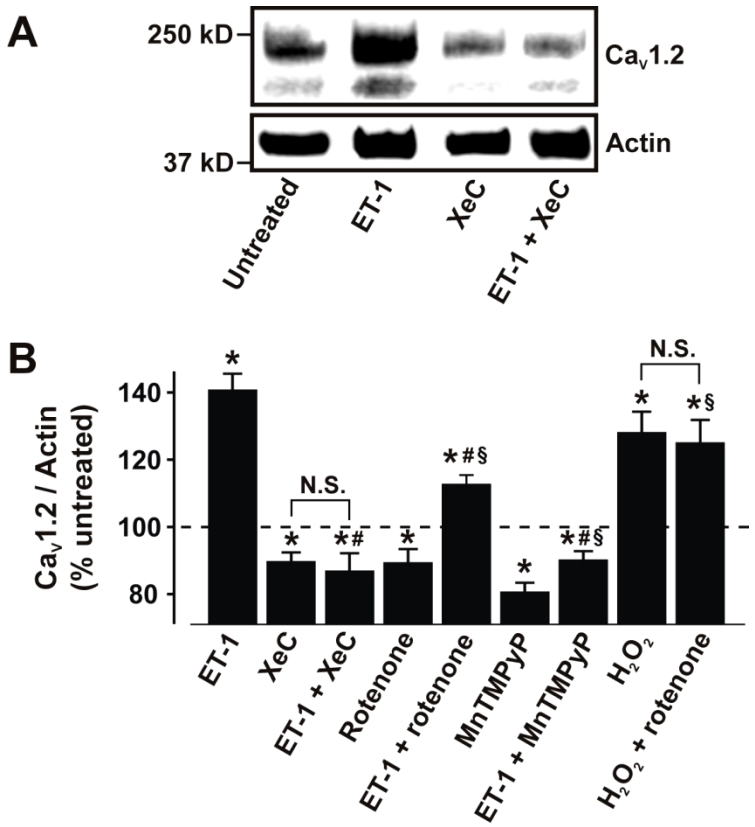

Figure 4-15. ET-1-induced IP_3R-mediated SR Ca^{2+} release and mitoROS elevation stimulate $Ca_V1.2$ protein expression in cerebral arteries

Notes: A, Western blot indicating that ET-1(10 nM) application for 24 hours elevated $Ca_V1.2$ protein expression and XeC (20 μM) blocked the ET-1-induced elevation in $Ca_V1.2$ expression. B, Mean data for ET-1 (n=12), XeC (20 μM, n=7), ET-1+XeC (n=7), rotenone (1 μM, n=6), ET-1+rotenone (n=6), MnTMPyP (10 μM, n=5), ET-1+MnTMPyP (n=5), H_2O_2 (100 μM, n=5), and H_2O_2+rotenone (n=5). ET-1 concentration was 10 nM in all experiments. Values are expressed as mean±SEM.
* indicates $P<0.05$ compared to control. # indicates $P<0.05$ compared to ET-1.
§ indicates $P<0.05$ compared to rotenone or MnTMPyP.

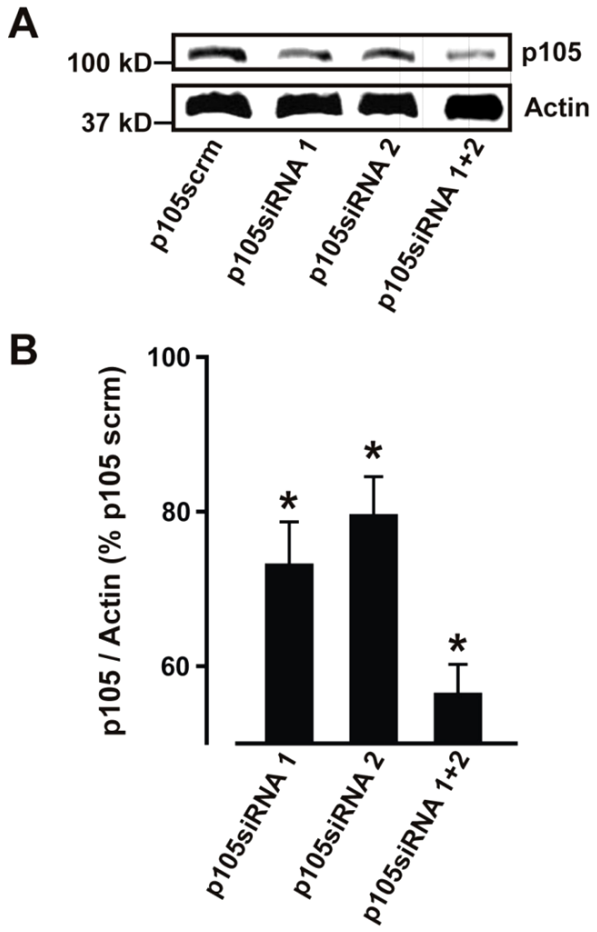

Figure 4-16. p105 knockdown in cerebral arteries

Notes: A, Western blot illustrating that p105siRNA1, p105siRNA2, and p105siRNA1+2 reduce p105 expression in cerebral arteries. B, Mean data. n=5 for each. Values are expressed as mean±SEM. * indicates $P<0.05$ compared to arteries reverse permeabilized with p105scrm.

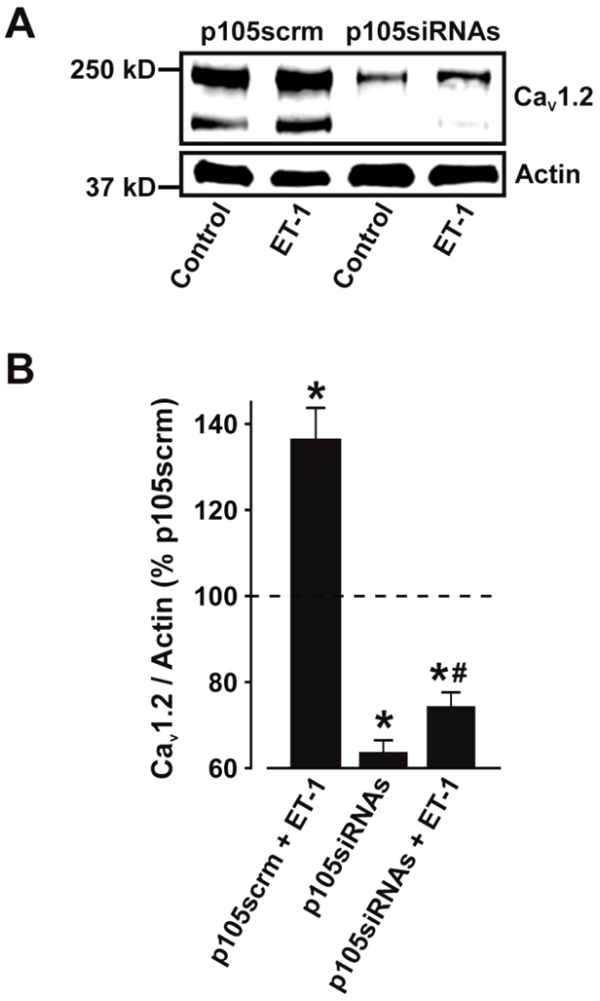

Figure 4-17. NF-κB controls basal and ET-1-induced elevation in functional $Ca_V1.2$ expression in cerebral arteries

Notes: A, Western blot illustrating effects of p105siRNAs (10 μg/ml each) on basal and ET-1-induced $Ca_V1.2$ expression. B, Mean data. n=5 for each. Values are expressed as mean±SEM. * indicates $P<0.05$ compared to arteries reverse permeabilized with p105scrm. # indicates $P<0.05$ compared to arteries reverse permeabilized with p105siRNAs.

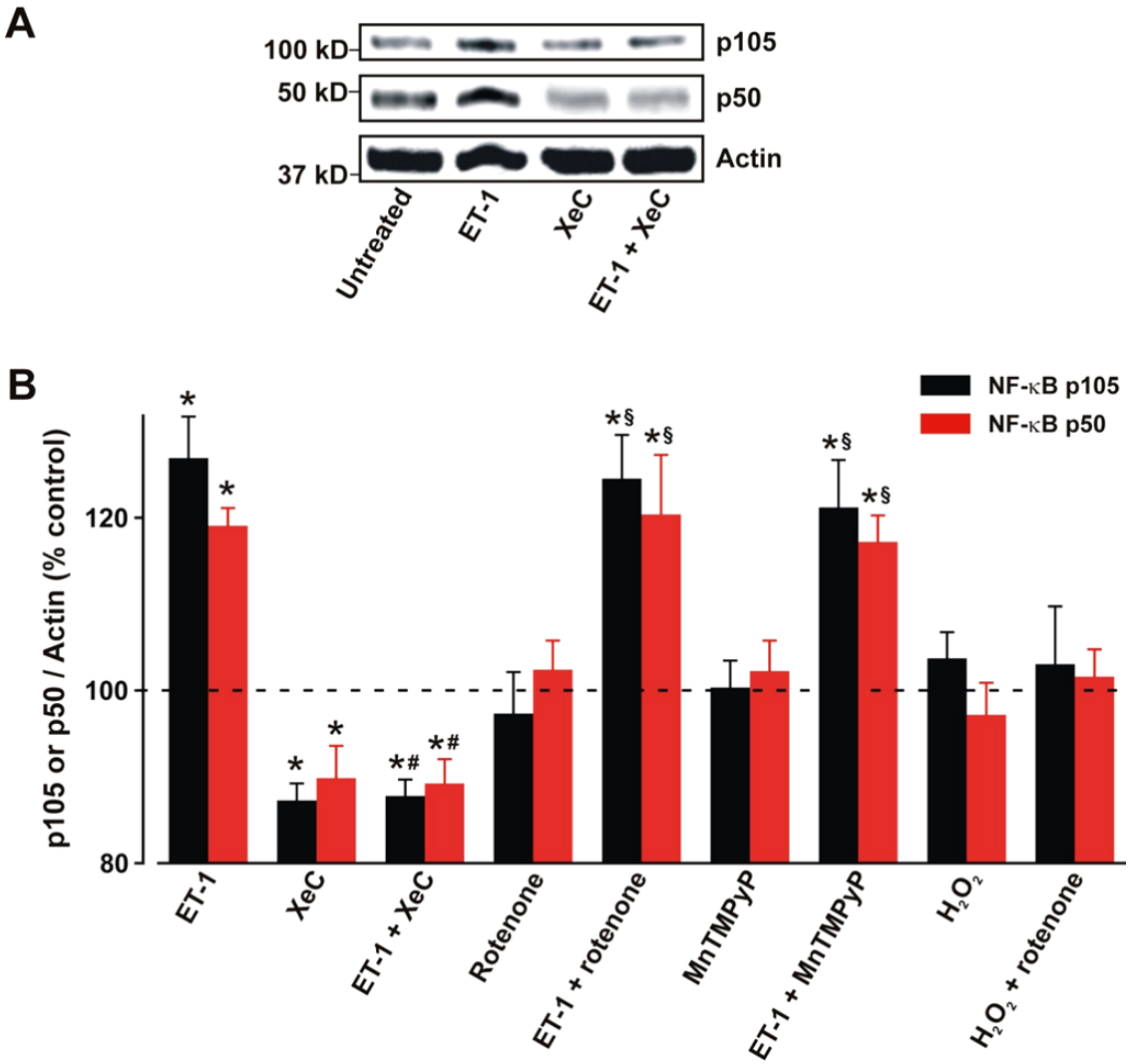

Figure 4-18. ET-1-induced IP_3R-mediated SR Ca^{2+} release elevates p105/p50 expression via a mitochondria-, and ROS-independent mechanism in cerebral arteries

Notes: A, Western blots indicating that XeC (20 μM) blocked an ET-1-induced elevation in p105 and p50 expression. B, Mean data for p105 (black) and p50 (red). p105 and p50 data were measured in the same blots, and thus experimental number is identical for each protein. ET-1 (n=8), XeC (20 μM, n=6), ET-1+XeC (n=6), rotenone (1 μM, n=5), ET-1+rotenone (n=5), MnTMPyP (10 μM, n=5), ET-1+MnTMPyP (n=5), H_2O_2 (100 μM, n=6), and H_2O_2+rotenone (n=6). Values are expressed as mean±SEM. * indicates $P<0.05$ compared to control. # indicates $P<0.05$ compared to ET-1. § indicates $P<0.05$ compared to rotenone or MnTMPyP.

4.8. ET-1-Induced NF-κB Activation Does Not Stimulate p105 Expression

p105siRNAs reduced p105 and p50 expression to ~57 and 53% of p105scrm (**Fig. 4-19A,B**). ET-1 increased p105 expression in p105scrm-treated arteries to ~123% of p105scrm, and in p105siRNAs-treated arteries from ~57 to 67% of p105scrm (~121% of p105siRNAs) (**Fig. 4-19A,B**). Similarly, ET-1 increased p50 expression in p105scrm-treated arteries to ~118% of p105scrm, and in p105siRNAs-treated arteries from ~53 to 65% of p105scrm (~124% of p105siRNAs) (**Fig. 4-19A,B**). These data indicate that p105siRNAs did not alter the ET-1-induced relative increase in p105 and p50 expression (**Fig. 4-19A,B**).

Collectively, these data indicate that IP_3R-mediated SR Ca^{2+} release activates p105/p50 expression via a mitochondria-, ROS-, and NF-κB-independent pathway. Data also indicate that rotenone, MnTMPyP, and p105siRNAs do not cause general inhibition of gene transcription.

4.9. NF-κB Stimulates Functional $Ca_V1.2$ Expression in Cerebral Artery Smooth Muscle Cells

To investigate NF-κB regulation of functional $Ca_V1.2$ expression, diameter regulation of pressurized (60 mmHg) endothelium-denuded arteries was studied.

4.9.1. Myogenic tone development in arteries

In resistance-size cerebral arteries, an elevation of intravascular pressure from 10 to 60 mmHg stretches the smooth muscle cells of the arterial wall, leading to activation of mechanosensitive ion channels (Hill *et al.*, 2001). Stimulation of stretch-activated cation channels induces a graded membrane depolarization of smooth muscle cells from ~-60 to -40 mV (Jaggar, 2001), which increases the steady-state open probability of $Ca_V1.2$ channels on smooth muscle cells (Knot & Nelson, 1998). This leads to increased Ca^{2+} influx through $Ca_V1.2$ channels to elevate steady-state arterial wall $[Ca^{2+}]_i$. Increased arterial wall $[Ca^{2+}]_i$ activates myosin light chain kinase, which leads to maintained constriction ('myogenic tone') (**Fig. 4-20**).

4.9.2. ET-1-stimulates functional $Ca_V1.2$ expression via NF-κB activation

Arteries were treated with either p105scrm or p105siRNAs and then exposed to either no further treatment or to ET-1 for 24 hours. At 60 mm Hg, control arteries (p105scrm) developed ~21% myogenic tone and membrane depolarization with 60 mM K^+ elevated tone to ~45%. p105 knockdown (p105siRNAs) reduced myogenic tone and depolarization-induced vasoconstriction to ~14 and 31%, respectively (**Fig. 4-21A,B**). A 24-hour exposure to ET-1 elevated mean myogenic tone and depolarization-induced tone in control arteries to ~32 and 55%, respectively (**Fig. 4-21A,B**). p105siRNAs attenuated

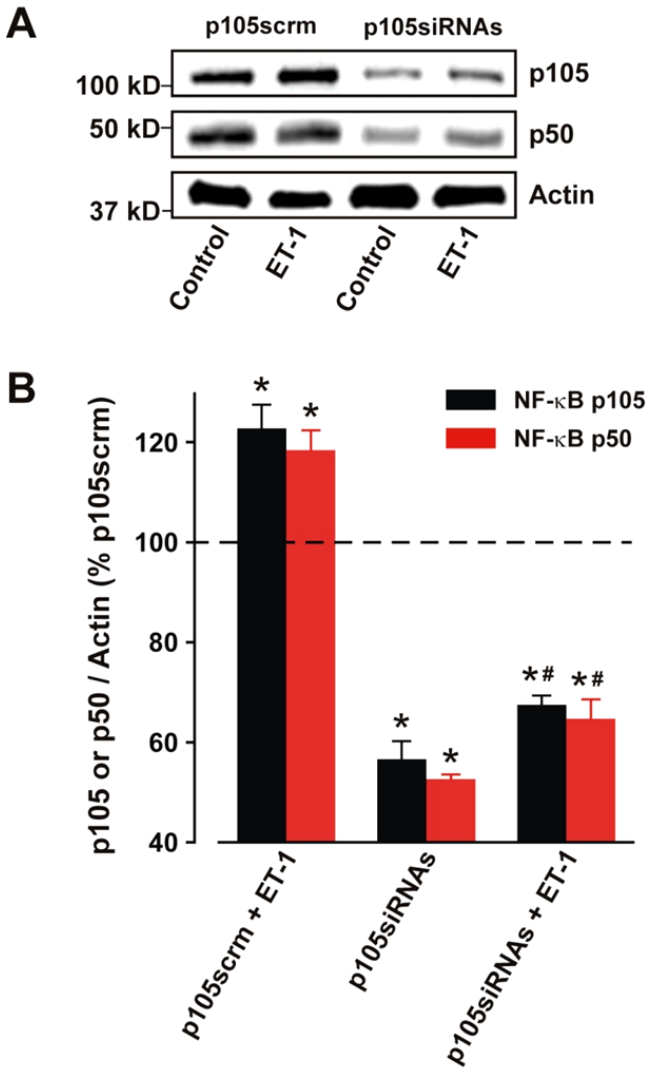

Figure 4-19. ET-1 elevates p105/p50 expression via an NF-κB-independent pathway in cerebral arteries

Notes: A, Western blot illustrating effects of p105siRNAs (10 μg/ml each) on p105 and p50 expression and regulation by ET-1. B, Mean data for p105 (black) (n=5 for each) and p50 (red) expression (n=4 for each). ET-1 concentration was 10 nM in all experiments. Values are expressed as mean±SEM. * indicates $P<0.05$ compared to arteries reverse permeabilized with p105scrm. # indicates $P<0.05$ compared to arteries reverse permeabilized with p105siRNAs.

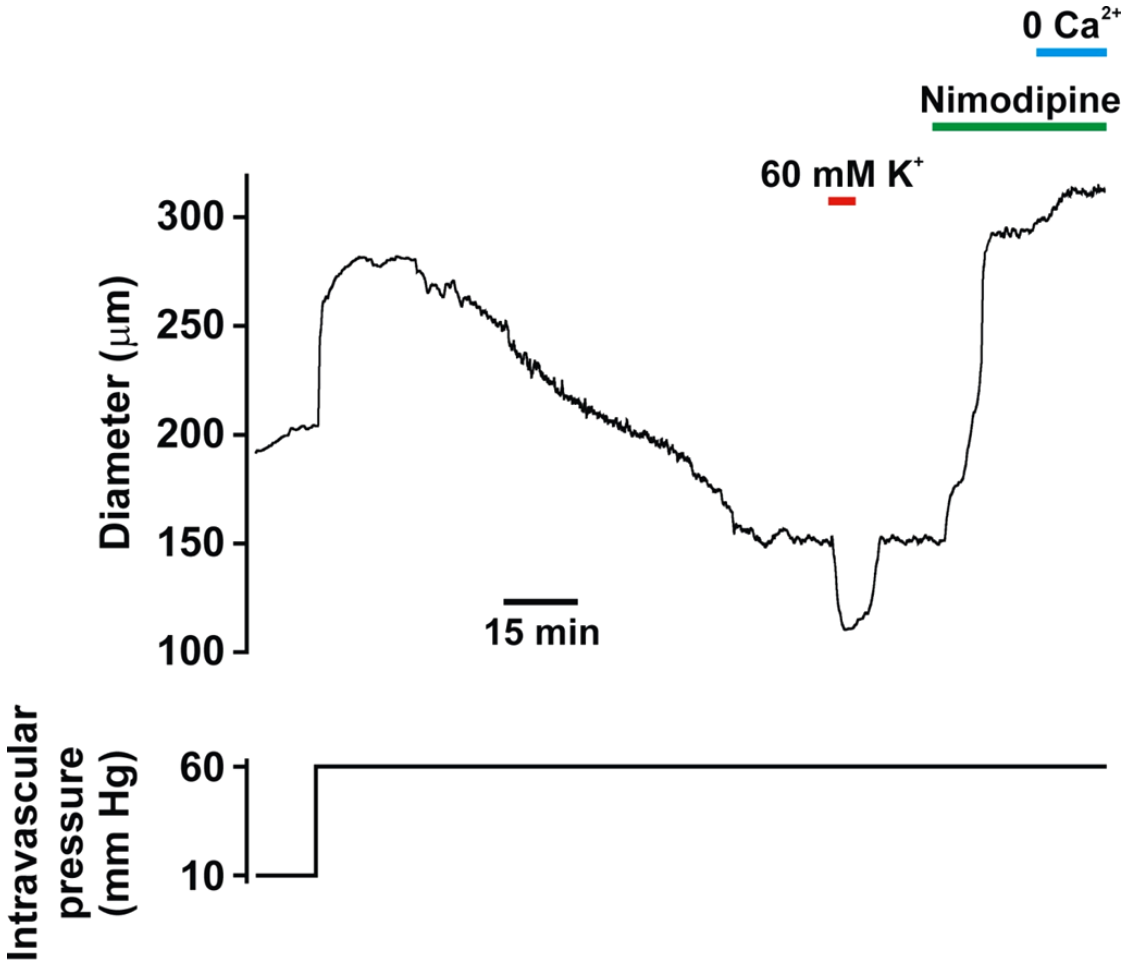

Figure 4-20. Myogenic tone development in cerebral arteries

Notes: Respresentative trace illustrating that an elevation of intravascular pressure from 10 to 60 mm Hg induces nimodipine-sensitive myogenic tone in a cerebral artery. Addition of 60 mM K^+ causes massive depolarization leading to further vasoconstriction.

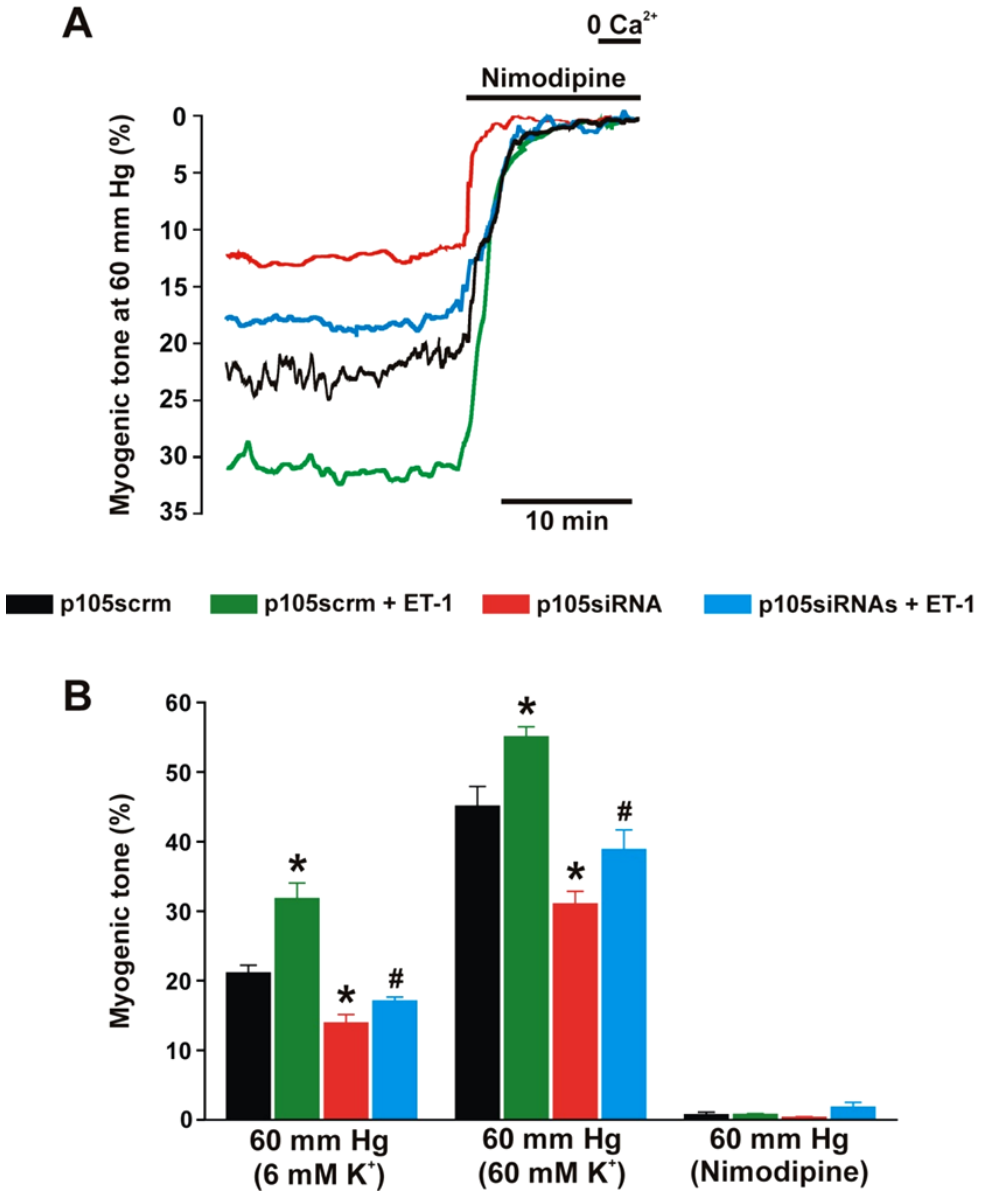

Figure 4-21. p105 knockdown reduces myogenic tone and attenuates ET-1-induced elevation in myogenic tone in cerebral arteries

Notes: A, Representative traces illustrating diameter in arteries pressurized to 60 mm Hg (6 mM K^+). Nimodipine (1 μM) fully dilated p105scrm- and p105siRNAs-treated arteries. B, Mean myogenic tone at 60 mm Hg (p105scrm, n=5, p105scrm + ET-1, n=6, p105siRNAs, n=6, p105siRNAs + ET-1, n=6), in 60 mM K^+ at 60 mm Hg (p105scrm, n=5, p105scrm + ET-1, n=5, p105siRNAs, n=5, p105siRNAs + ET-1, n=5), or nimodipine (1 μM) at 60 mm Hg (p105scrm, n=5, p105scrm + ET-1, n=6, p105siRNAs, n=5, p105siRNAs + ET-1, n=5). Values are expressed as mean±SEM. * indicates $P<0.05$ compared to arteries reverse permeabilized with p105scrm. # indicates $P<0.05$ compared to arteries reverse permeabilized with p105siRNAs.

the ET-1-induced elevation in myogenic tone and depolarization-induced vasoconstriction to ~17 and 39%, respectively (**Fig. 4-21A,B**). Nimodipine fully dilated arteries regardless of treatment, indicating that vasoconstriction occurred due to $Ca_V1.2$ channel activation (**Fig. 4-21A,B**). These data indicate that NF-κB is essential for functional basal $Ca_V1.2$ expression in cerebral artery smooth muscle cells and that ET-1-induced NF-κB activation elevates $Ca_V1.2$ expression and vasoconstriction.

CHAPTER 5. DISCUSSION*

5.1. Summary of Findings

Here, we investigated physiological signaling mechanisms that regulate $[Ca^{2+}]_{mito}$, functional consequences of changes in $[Ca^{2+}]_{mito}$, and mitochondrial regulation of ion channel gene expression in arterial smooth muscle cells. This study was performed using small, resistance-size cerebral arteries that regulate blood pressure and regional blood flow to the brain. In this study, we have used state-of-art techniques, including genetically-encoded fluorescent indicators and laser-scanning confocal microscopy to measure $[Ca^{2+}]_{mito}$ and ROS, fluorescence imaging and luciferase reporter gene assays to examine NF-κB activity, molecular biology and biochemical techniques to examine $Ca_V1.2$ expression, and pressurized artery diameter measurements to study the functional significance of elevated $Ca_V1.2$ channel expression.

A schematic diagram summarizing major findings of this study is provided in **Figs. 5-1** and **5-2**. Under resting conditions, basal levels of IP_3 activate IP_3R, leading to SR Ca^{2+} release. IP_3R-mediated SR Ca^{2+} release and constitutively produced mitoROS activate NF-κB. NF-κB controls basal $Ca_V1.2$ expression in cerebral artery smooth muscle cells and NF-κB knockdown leads to vasodilation.

ET-1-induced IP_3R-mediated SR Ca^{2+} release generates Ca^{2+} waves, elevates $[Ca^{2+}]_{mito}$, and depolarizes mitochondria, leading to an increase in mitoROS generation. ET-1-induced IP_3R-mediated mitoROS elevate cytosolic ROS that increase NF-κB nuclear translocation and transcriptional activity. ET-1-induced NF-κB activation stimulates $Ca_V1.2$ expression, leading to an elevation in $Ca_V1.2$-dependent pressure- and depolarization-induced vasoconstriction. ET-1-induced IP_3R-mediated SR Ca^{2+} release also elevates NF-κB p105/p50 subunit expression via a mitochondria-, ROS-, and NF-κB-independent pathway. Collectively, these data indicate that IP_3R-mediated SR Ca^{2+} release elevates $[Ca^{2+}]_{mito}$, stimulating mitoROS which activate NF-κB-dependent $Ca_V1.2$ channel expression. Thus, mitochondria sense IP_3R-mediated SR Ca^{2+} release to control functional $Ca_V1.2$ channel transcription in arterial smooth muscle cells, thereby regulating arterial contractility.

5.2. Ca^{2+} Signaling in Vascular Smooth Muscle Cells by PLC-Coupled Agonists

Several vasoconstrictors, including UTP, Ang II, and ET-1 activate PLC (Rosendorff, 1997; Ralevic & Burnstock, 1998; Touyz & Schiffrin, 2000; Zhang *et al.*, 2003), leading to PIP_2 hydrolysis and the generation of IP_3 and DAG. IP_3 stimulates

* Portions of this chapter adapted with permission. Narayanan D, Xi Q, Pfeffer LM, & Jaggar JH (2010). Mitochondria control functional $Ca_V1.2$ expression in smooth muscle cells of cerebral arteries. *Circ Res* **107**, 631-641.

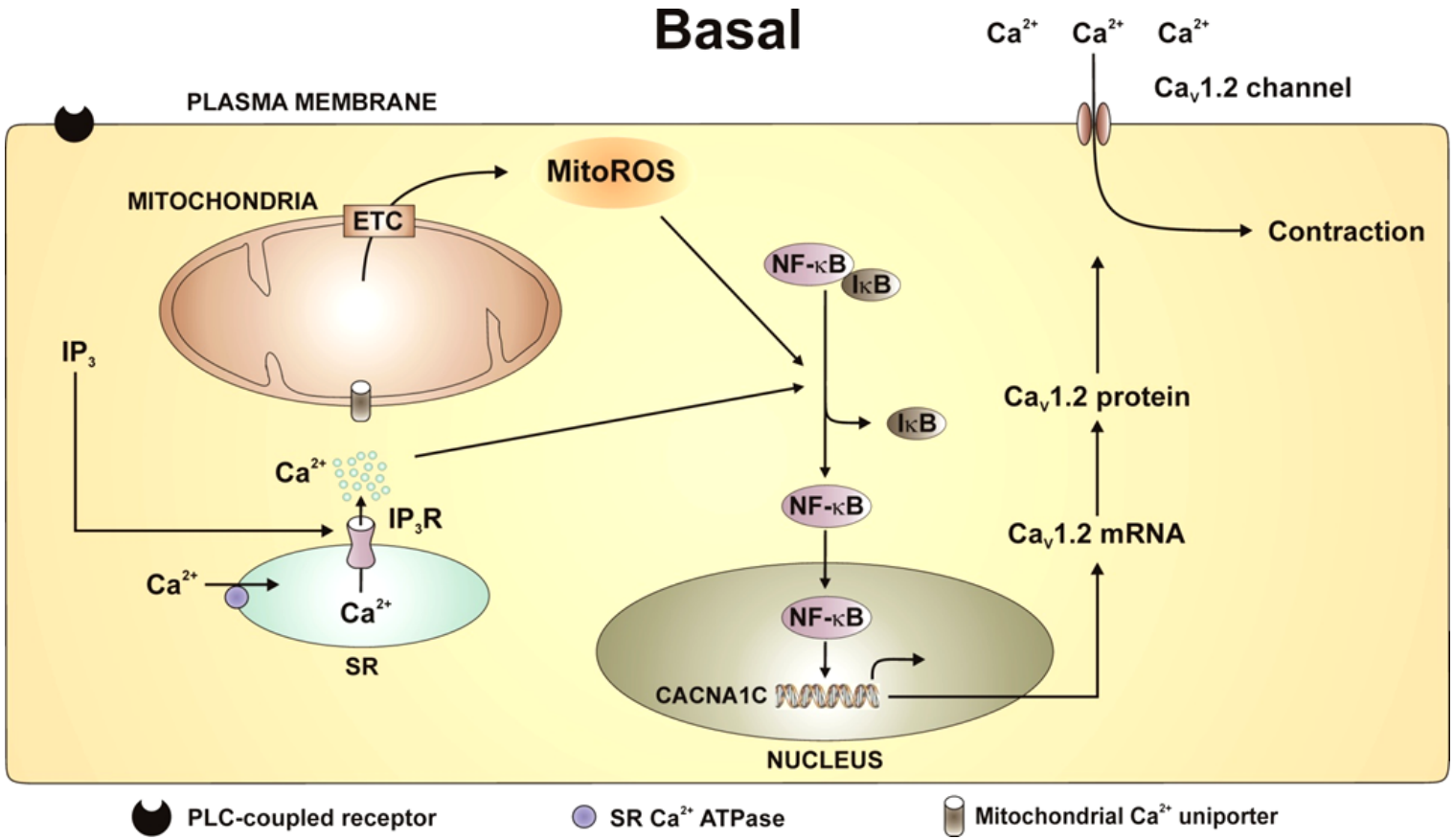

Figure 5-1. Proposed signaling pathways that control basal $Ca_V1.2$ expression in smooth muscle cells of cerebral arteries

Notes: Basal levels of IP_3R-mediated SR Ca^{2+} release and constitutively produced mitoROS activate NF-κB leading to $Ca_V1.2$ expression. IP_3 indicates inositol 1,4,5-trisphosphate, ETC indicates mitochondrial electron transport chain, and ψ_m indicates mitochondrial membrane potential.

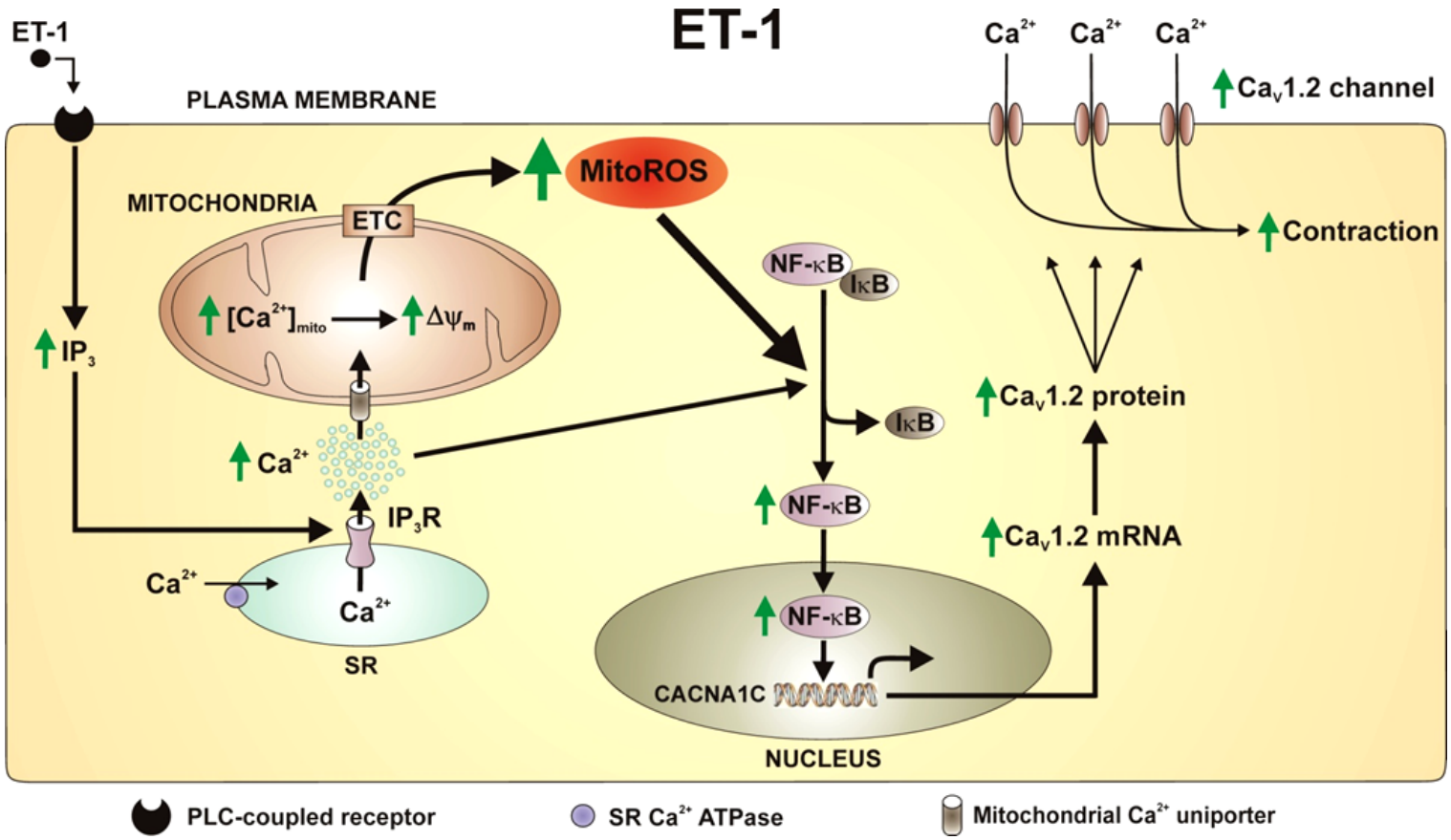

Figure 5-2. Proposed signaling pathways that control ET-1-induced $Ca_V1.2$ expression in smooth muscle cells of cerebral arteries

Notes: ET-1-induced IP_3R-mediated SR Ca^{2+} release activates NF-κB: (a) primarily by stimulating a mitochondrial ROS elevation and (b) via a secondary mitochondria-independent pathway, leading to $Ca_V1.2$ expression. IP_3 indicates inositol 1,4,5-trisphosphate, ETC indicates mitochondrial electron transport chain, and ψ_m indicates mitochondrial membrane potential.

IP_3Rs, and DAG activates PKC. Activation of IP_3R1, the major isoform expressed in smooth muscle cells of resistance-size cerebral arteries stimulates SR Ca^{2+} release in the form of Ca^{2+} waves, which contribute to global $[Ca^{2+}]_i$ elevation (Jaggar & Nelson, 2000; Zhao *et al.*, 2008). IP_3R1 activation also induces physical coupling of the N-terminus of IP_3R1 and the C-terminus of plasma membrane TRPC3 channel, leading to I_{Cat} activation. IP_3R-dependent I_{Cat} activation produces membrane depolarization, $Ca_V1.2$ channel activation, a global $[Ca^{2+}]_i$ elevation, and vasoconstriction (Xi *et al.*, 2008; Zhao *et al.*, 2008; Adebiyi *et al.*, 2010). Therefore, vasoconstrictor-induced IP_3R activation elevates $[Ca^{2+}]_i$ in cerebral artery smooth muscle cells via SR Ca^{2+} release-dependent and -independent mechanisms. In contrast, vasoconstrictor-activated PKC inhibits Ca^{2+} sparks, which leads to membrane depolarization, $Ca_V1.2$ channel activation, and a global $[Ca^{2+}]_i$ elevation (Jaggar & Nelson, 2000).

5.3. Regulation of $[Ca^{2+}]_{mito}$ by Cytosolic Ca^{2+} Signals

The regulation of arterial smooth muscle cell $[Ca^{2+}]_{mito}$ by vasoconstrictor-induced intracellular Ca^{2+} signals is unclear. Electron microscopy studies indicate that mitochondria can be located in close proximity (~20 nm) to the SR membrane in many cell types, including cultured arterial smooth muscle cells (Rizzuto *et al.*, 1999; Duchen, 2000b; Szado *et al.*, 2003; Pacher *et al.*, 2008). Such localization should place mitochondria within the vicinity of SR Ca^{2+} release channels that generate micromolar cytosolic Ca^{2+} elevations. Given that the MCU is sensitive to Ca^{2+} only within the micromolar concentration range (Gunter & Pfeiffer, 1990), such structural orientation allows local signaling between SR Ca^{2+} release channels and mitochondria. In cultured vascular smooth muscle cells, SR Ca^{2+} release elicited a $[Ca^{2+}]_{mito}$ elevation (Pacher *et al.*, 2008) and a delayed $[Ca^{2+}]_{mito}$ elevation occurred when $[Ca^{2+}]_i$ increased >1 μM, but not when the $[Ca^{2+}]_i$ elevation was <500 nM (Monteith & Blaustein, 1999). Ca^{2+} influx via the plasma membrane Na^+/Ca^{2+} exchanger also elevated $[Ca^{2+}]_{mito}$ in cultured vascular smooth muscle cells (Poburko *et al.*, 2009). In non-cultured, voltage-clamped colonic smooth muscle cells, uncaging IP_3 leads to mitochondrial Ca^{2+} uptake that feeds back to regulate IP_3R activity (Olson *et al.*, 2010).

Previous studies have used inorganic Ca^{2+} indicators to measure $[Ca^{2+}]_{mito}$ in cultured arterial smooth muscle cells (Monteith & Blaustein, 1999; Pacher *et al.*, 2008; Poburko *et al.*, 2009). These fluorophores are not designed to target to specific cellular locations, which inevitably leads to non-specific Ca^{2+} measurements. To our knowledge, our study is the first to use a genetically-encoded, mitochondria-targeted, fluorescent indicator to measure $[Ca^{2+}]_{mito}$ in contractile arterial smooth muscle cells. Furthermore, we studied cerebral artery smooth muscle cells in their native, contractile phenotype, while previous studies primarily used cultured, proliferating vascular smooth muscle cells. *In vitro* cultivation of vascular smooth muscle cells results in phenotypic alterations, characterized by changes in cell morphology, receptor expression, and contractile-cytoskeletal protein profiles, and switches arterial smooth muscle cell phenotype from a contractile state to an invasive, proliferative state (Absher *et al.*, 1989; Campbell *et al.*, 1989; Eguchi *et al.*, 1994). Therefore, it is highly likely that

physiological functions of mitochondria differ in these different cell phenotypes, particularly since spatial proximity to Ca^{2+} channels and transporters are critical for mitochondrial Ca^{2+} uptake.

Our data indicate that in contractile cerebral artery smooth muscle cells, thapsigargin, XeC, and Ru360 did not alter resting $[Ca^{2+}]_{mito}$, ψ_m, or mitoROS. In contrast, mitochondrial inhibitors reduced basal $[Ca^{2+}]_{mito}$, depolarized mitochondria, and reduced mitoROS levels. These data indicate that in resting arterial smooth muscle cells, mitochondria contain Ca^{2+} and generate low levels of ROS through mechanisms that are independent of IP_3R-mediated SR Ca^{2+} release. Therefore, basal mitochondrial Ca^{2+} levels appear to be maintained by Ca^{2+} uptake through transporters other than the MCU, which is sensitive to micromolar Ca^{2+} as that produced by SR Ca^{2+} release (Gunter & Pfeiffer, 1990). Apart from the MCU, several mitochondrial pumps and exchangers, including RaM (Gunter *et al.*, 2000) and reversal mode of mNCX (Griffiths *et al.*, 1998) have been speculated to be responsible for mitochondrial Ca^{2+} uptake and the maintenance of resting $[Ca^{2+}]_{mito}$ levels (Gunter *et al.*, 2000).

ET-1-induced IP_3R-mediated SR Ca^{2+} release stimulated Ca^{2+} waves and elevated $[Ca^{2+}]_{mito}$, leading to mitochondrial depolarization and mitoROS generation. Here, thapsigargin and XeC blocked the ET-1-induced $[Ca^{2+}]_{mito}$ elevation, mitochondrial depolarization, and mitoROS generation. In contrast, membrane depolarization, which elevates global $[Ca^{2+}]_i$, did not alter $[Ca^{2+}]_{mito}$, ψ_m, or mitoROS generation. These data are consistent with the hypothesis that IP_3R-mediated SR Ca^{2+} release stimulates mitochondrial Ca^{2+} uptake, leading to a $[Ca^{2+}]_{mito}$ elevation, mitochondrial depolarization, and mitoROS generation.

5.4. Ca^{2+} Waves May Be the Cytosolic Ca^{2+} Signal Regulating Mitochondrial Events

Consistent with imaging data indicating that vasoconstrictor-induced Ca^{2+} waves occur due to IP_3R activation in smooth muscle cells (Zhao *et al.*, 2008), our data suggest that Ca^{2+} waves specifically regulate $[Ca^{2+}]_{mito}$ and mitoROS generation in arterial smooth muscle cells. Given that Ca^{2+} waves are propagating Ca^{2+} signals, $[Ca^{2+}]_{mito}$ and mitoROS may also oscillate. Here, $[Ca^{2+}]_{mito}$ and mitoROS was measured within multiple smooth muscle cells in the arterial wall. $[Ca^{2+}]_{mito}$ and mitoROS within individual mitochondria may oscillate. In our experiments, 2mt8CG2 and mt-cpYFP fluorescence in each field was measured from mitochondria within ~25 smooth muscle cells within the arterial wall. Therefore, any asynchronous $[Ca^{2+}]_{mito}$ or mitoROS oscillations within individual mitochondria would have been averaged out by the imaging protocol. This protocol was necessary to measure sufficient 2mt8CG2 or mt-cpYFP fluorescence and to reduce the effects of indicator bleaching on measurements in cerebral artery smooth muscle cells. It would be interesting to study spatial and temporal relationships between ET-1-induced Ca^{2+} waves and $[Ca^{2+}]_{mito}$ or mitoROS changes within individual mitochondria in arterial smooth muscle cells. However, such an examination of millisecond changes in $[Ca^{2+}]_{mito}$ or mitoROS is more suitable for a future

investigation, and may require the use of a different mitochondria-targeted Ca^{2+} or ROS indicator that better suits the type of experiment. Future studies should be designed to examine spatial and temporal relationships between Ca^{2+} waves and $[Ca^{2+}]_{mito}$ or mitoROS signals within individual mitochondria in arterial smooth muscle cells.

5.5. Regulation of MitoROS Generation by $[Ca^{2+}]_{mito}$ and Mitochondrial Potential

ET-1-induced mitoROS elevation was blocked by XeC, Ru360, rotenone, and CCCP, indicating that IP_3R-mediated SR Ca^{2+} release, mitochondrial Ca^{2+} uptake, and mitochondrial depolarization stimulate mitoROS generation. The mechanism by which mitochondrial Ca^{2+} uptake induces mitochondrial depolarization and elevates ETC-generated mitoROS was not determined. A $[Ca^{2+}]_{mito}$ elevation may stimulate mitoROS generation at complexes I, III, and via $QH\cdot$ generation through multiple mechanisms (Brookes *et al.*, 2004): 1) stimulation of the tricarboxylic acid cycle enhancing electron flow through the ETC complexes; 2) inhibition of complex I; 3) dissociation and release cytochrome c from inner mitochondrial membrane; and 4) mPTP opening (Brookes *et al.*, 2004).

Mitochondrial depolarization has been demonstrated to increase or decrease ROS in a variety of different cell types, including smooth muscle cells of anatomically diverse blood vessels (Brookes *et al.*, 2004; Xi *et al.*, 2005; Belousov *et al.*, 2006; Wang *et al.*, 2008a). ψ_m is another important regulator of mPTP opening. Mitochondrial depolarization can induce mPTP opening by shifting the threshold potential to higher levels (Petronilli *et al.*, 1993; Bernardi, 1999). mPTP opening can in turn depolarize the mitochondria further, thereby enhancing the mitochondrial Ca^{2+} uptake-induced depolarization (Brookes *et al.*, 2004; Wang *et al.*, 2008a). Therefore, as suggested by a previous study, mitochondrial Ca^{2+} uptake may depolarize mitochondria due to (a) flow of Ca^{2+} ions into the mitochondrial matrix, and (b) mPTP opening (Duchen, 2004).

mPTP opening also elevates mitoROS generation via several pathways, including dissipation of chemical gradients across the mitochondrial membrane, and by changing the fluidity and rigidity of the inner mitochondrial membrane, leading to diversion of electrons in the ETC to mitoROS generation (Wang *et al.*, 2008a). Therefore, a $[Ca^{2+}]_{mito}$ elevation and mitochondrial depolarization may stimulate mitoROS generation by opening the mPTP.

In the present study, a small mitochondrial depolarization increased mitoROS generation, whereas a large mitochondrial depolarization inhibited mitoROS production, consistent with an earlier report in cerebral artery smooth muscle cells (Xi *et al.*, 2005). A small mitochondrial depolarization induced by nanomolar CCCP may increase mitoROS generation by shifting the mPTP threshold potential to higher levels (Petronilli *et al.*, 1993; Bernardi, 1999). Micromolar CCCP, which causes massive uncoupling of ETC, and disrupts the regulation of ψ_m, may severely affect electron transfer through the ETC complexes, resulting in a reduction in mitoROS generation. ETC uncoupling has

been shown to decrease mitoROS generation in many cell types, including vascular smooth muscle cells (Okuda *et al.*, 1992; Negre-Salvayre *et al.*, 1997; Xi *et al.*, 2005).

MitoROS production is also regulated by additional factors, including redox status of respiratory substrates, permeability of the inner mitochondrial membrane, and proton pumping by ETC complexes (Starkov & Fiskum, 2003). Future investigations should examine the mechanisms by which a vasoconstrictor-induced $[Ca^{2+}]_{mito}$ elevation and mitochondrial depolarization stimulate mitoROS generation.

5.6. Characterization of ET-1-Induced ROS Elevation

Endothelial denudation did not alter the ET-1-induced HyPer-CYTO and DCF fluorescence elevations, indicating that ROS were generated within smooth muscle cells and not by endothelial cells. This is in agreement with a previous study in pulmonary arteries suggesting that ET-1 elevates ROS in the arterial smooth muscle cells and not endothelial cells (Wedgwood *et al.*, 2001). Our data with mt-cpYFP suggest that ET-1 elevates mitochondrial $O_2^{-}\cdot$ production in arterial smooth muscle cells. Rotenone blocked the ET-1-induced elevations in mt-cpYFP and HyPer-CYTO fluorescence suggesting that ET-1-induced mitoROS elevation leads to an increase in cytosolic H_2O_2 levels. Dismutation of $O_2^{-}\cdot$ to H_2O_2 may occur both in the mitochondrial matrix and in the intermembrane space by mitochondrial SOD (Turrens, 2003; Li *et al.*, 2005; Archer *et al.*, 2010). Therefore, ET-1 elevates generation of mitochondrial $O_2^{-}\cdot$ and cytosolic H_2O_2. However, ET-1-induced elevations in $O^{2-}\cdot$ and H_2O_2 may also result in generation of $OH\cdot$, NO, and $ONOO\cdot$ through various pathways, including Fenton reaction (Turrens, 2003). ROS regulation of cellular signaling depends on the reactivity, and stability of the species. H_2O_2 which is more stable than $O_2^{-}\cdot$, can diffuse for a longer distance allowing it to serve as a signaling molecule (Archer *et al.*, 2010). H_2O_2 modulates the activity of several ROS-sensitive transcription factors such as HIF-1α (Huang *et al.*, 1996) and NF-κB (Takada *et al.*, 2003; Oliveira-Marques *et al.*, 2009).

5.7. ROS–Dependent and –Independent Pathways Which Activate NF-κB

Physiological functions and mechanisms of regulation of NF-κB in contractile arterial smooth muscle cells are poorly understood. Our data indicate that thapsigargin, XeC, rotenone, and MnTMPyP reduced basal NF-κB-dependent luciferase activity. Therefore, under basal conditions, NF-κB activation is regulated by both IP_3R-mediated SR Ca^{2+} release and constitutively produced mitoROS. This is consistent with studies in neurons, indicating that Ca^{2+} influx through VDCCs and IP_3R-mediated Ca^{2+} release are responsible for the basal NF-κB activity (Lilienbaum & Israel, 2003).

ET-1-induced NF-κB activation was blocked by XeC, and inhibited by rotenone and MnTMPyP. This indicates that ET-1-induced NF-κB activation occurs primarily via IP_3R-mediated mitoROS generation in cerebral artery smooth muscle cells. MitoROS activate NF-κB in several cell types, including in cultured vascular smooth muscle cells

(Lee *et al.*, 2008). However, alternate ROS-mediated mechanisms have also been demonstrated to activate NF-κB in arterial smooth muscle cells. For example, following arterial balloon injury, ROS derived from NO and NAD(P)H oxidase are primarily responsible for the elevated NF-κB activity in arterial smooth muscle cells (Souza *et al.*, 2000; Ialenti *et al.*, 2001). The mechanisms by which ROS activate NF-κB are unclear, with reports suggesting that ROS stimulate IKK, leading to serine phosphorylation and proteasomal degradation of IκB (Gloire *et al.*, 2006). Studies also indicate that ROS activate other kinases, such as tyrosine kinase to cause IκB tyrosine phosphorylation rather than the classical serine phosphorylation (Takada *et al.*, 2003; Brzoska & Szumiel, 2009). Additional studies will be necessary to identify the specific mechanisms by which ROS activate NF-κB in contractile arterial smooth muscle cells.

Rotenone and MnTMPyP abolished the ET-1-induced mitoROS elevation, but did not completely block ET-1-induced NF-κB activation. Therefore, ET-1-induced IP_3R-mediated SR Ca^{2+} release may activate NF-κB via a secondary mitoROS-independent pathway. Ca^{2+}-dependent, redox-independent NF-κB activation mechanisms may be mediated by calcineurin, PI3K/Akt, and/or PKC, as demonstrated in neurons (Lilienbaum & Israel, 2003). Calcineurin activation occurs due to Ca^{2+} binding to CaM, leading to the dissociation of the two proteins, allowing the catalytic site of calcineurin to become accessible (Lilienbaum & Israel, 2003). In addition to CaM, Ca^{2+} activate NF-κB via Ca^{2+}-sensitive PKC isoforms, including PKCα and PKCβ1, and PI3K/Akt (Lilienbaum & Israel, 2003). Supporting bi-modal activation, ER Ca^{2+} release activates NF-κB through both calcineurin- and redox-dependent mechanisms in U937 cells (Shatrov *et al.*, 1997). In addition to ET-1, Ang II, another PLC-coupled receptor agonist activates transcription factors, including NF-κB through ROS-dependent and -independent mechanisms (Iadecola & Gorelick, 2004). Binding of Ang II to AT1 receptors leads to PLC activation, $[Ca^{2+}]_i$ elevation, and PKC activation (Iadecola & Gorelick, 2004). PKC-mediated phosphorylation of $p47^{phox}$ stimulates ROS generation via NAD(P)H oxidase (Iadecola & Gorelick, 2004). Activated PKC could also stimulate cellular effectors in a ROS-independent manner (Iadecola & Gorelick, 2004).

In whole artery immunofluorescence experiments to study NF-κB localization, it is interesting to note that p50 nuclear translocation occurred in nuclei of some smooth muscle cells but not others. These experiments were performed on fixed arteries after 1 hour of ET-1 treatment, therefore, representing a snapshot of the cellular events occurring in the arterial smooth muscle cells at that time point. NF-κB activation and nuclear translocation may not occur at the same time in all smooth muscle cells of the artery due to a variety of reasons. The time taken for ET-1 to reach individual smooth muscle cells and stimulate its receptors will depend upon the location of the smooth muscle cell in the arterial wall. ET-1 will stimulate receptors of smooth muscle cells located on the periphery of the arterial wall prior to activating those cells in deeper layers. In some cells, ET-1 may have stimulated SR Ca^{2+} release but there may not be mitochondria in close proximity to the SR to stimulate mitoROS elevation and NF-κB activation. It is also possible that NF-κB nuclear translocation and activation of transcription may have already taken place and NF-κB may have recycled back to the cytosol within 1 hour. Nevertheless, our data suggests that ET-1 increases p50 nuclear translocation, thereby

activating NF-κB in cerebral artery smooth muscle cells. Transcriptional studies performed using NF-κB-dependent luciferase constructs confirm the finding that ET-1 activates NF-κB.

5.8. Regulation of Basal and ET-1-Induced Elevation in $Ca_V1.2$ Expression

$Ca_V1.2$ channels are the principal functional Ca^{2+} influx pathway in smooth muscle cells of resistance-size arteries (Jaggar *et al.*, 2000; Jaggar, 2001; Cheng *et al.*, 2007). $Ca_V1.2$ channels regulate multiple physiological functions in arterial smooth muscle cells, including contractility and gene expression, but signaling mechanisms and transcription factors that regulate their expression in these cells are unclear.

Our data indicate that IP_3R-mediated NF-κB activity controls basal $Ca_V1.2$ expression through both mitoROS generation and via a mitochondria-independent pathway. XeC, rotenone, and MnTMPyP slightly reduced basal $Ca_V1.2$ expression. In the absence of PLC-coupled receptor ligands, $[IP_3]_i$ and thus, IP_3R activity should be low. However, in the intact artery preparation studied here, basal release of receptor ligands, including ET-1, by endothelial cells may generate low levels of $[IP_3]_i$ in smooth muscle cells. Even though this basal IP_3R-mediated SR Ca^{2+} release was insufficient to elevate $[Ca^{2+}]_{mito}$, depolarize mitochondria, or stimulate mitoROS and cytosolic ROS, it was sufficient to activate NF-κB and stimulate $Ca_V1.2$ expression. IP_3R-independent basal mitoROS generation also activates NF-κB, leading to stimulation of basal $Ca_V1.2$ expression. Thus, IP_3Rs contribute to basal $Ca_V1.2$ expression through mitochondria-dependent and -independent NF-κB activation. In our experiments, the degree of p105 knockdown and the reduction in basal $Ca_V1.2$ expression were similar, indicating that NF-κB is a major transcriptional factor regulating $Ca_V1.2$ gene expression in arterial smooth muscle cells.

Data indicate that ET-1-induced IP_3R-mediated Ca^{2+} release stimulates $Ca_V1.2$ expression by causing a $[Ca^{2+}]_{mito}$ elevation, leading to mitoROS generation that activate NF-κB. Consistent with effects on NF-κB transcriptional activity, rotenone and MnTMPyP did not fully block the ET-1-induced elevation in $Ca_V1.2$ expression. Thus, IP_3R activation may also stimulate $Ca_V1.2$ expression via a secondary mitochondria- and ROS-independent pathway that also involves NF-κB. Therefore, ET-1-induced IP_3R activation stimulates NF-κB-dependent elevation in $Ca_V1.2$ expression primarily via a mitoROS-dependent pathway and through a secondary mitochondria- and ROS-independent pathway. Consistent with our finding that NF-κB controls $Ca_V1.2$ expression, TNF-α-induced NF-κB activation elevated L-type Ca^{2+} current in cultured rat hippocampal neurons (Furukawa & Mattson, 1998). In contrast, in human colonic smooth muscle cells NF-κB p50 and p65 subunit activation reduced $Ca_V1.2$ channel expression (Shi *et al.*, 2005). Opposing regulation of $Ca_V1.2$ transcription by NF-κB in these different smooth muscle cell types may occur through interaction with different κB binding motifs, of which there are several upstream of the $Ca_V1.2$ gene (Shi *et al.*, 2005). Furthermore, the presence or absence of additional transcriptional activators and/or repressors may explain differential regulation of $Ca_V1.2$ expression by NF-κB.

Ang II, a vasoconstrictor caused an endothelium-dependent increase in $Ca_V1.2$ expression in primary culture of rat mesenteric artery smooth muscle cells although it is unclear if depolarization of the smooth muscle cells is involved in this upregulation (Wang *et al.*, 2008b). Ang II has been shown to stimulate endothelial cells and induces ET-1 gene expression and secretion (Dohi *et al.*, 1992; Morey *et al.*, 1998). Therefore, the Ang II-induced ET-1 elevation may stimulate the pathway described here, resulting in an elevation in $Ca_V1.2$ expression in mesenteric artery smooth muscle cells. In cultured ventricular myocytes, global $[Ca^{2+}]_i$ elevation stimulated transcription of $Ca_V1.2$ α_1 subunit (Davidoff *et al.*, 1997). In rat renal arteries, membrane depolarization which elevates global $[Ca^{2+}]_i$, increased $Ca_V1.2$ protein (Pesic *et al.*, 2004). Here, IP_3R-mediated SR Ca^{2+} release stimulated $Ca_V1.2$ expression. Data from these studies raise several possibilities, including that local and global Ca^{2+} signals regulate $Ca_V1.2$ expression by different mechanisms in cerebral and renal artery smooth muscle cells and ventricular myocytes. Conceivably, this could occur at many levels in the pathway described here, including that global $[Ca^{2+}]_i$ may elevate $[Ca^{2+}]_{mito}$ in renal artery smooth muscle cells and ventricular myocytes, leading to mitoROS generation and NF-κB activation.

5.9. Regulation of p105/p50 Expression by IP_3R-Mediated SR Ca^{2+} Release

Factors that regulate p105 gene expression in arterial smooth muscle cells are poorly understood. Our data indicate that XeC reduced the basal p105/p50 expression and blocked the ET-1-induced elevation in p105/p50 expression. However, rotenone and MnTMPyP did not affect the basal and ET-1-induced elevation in p105/p50 expression. In addition, p105 knockdown did not alter the ET-1-induced relative increase in p105/p50 expression. These data indicate that ET-1-induced IP_3R-mediated SR Ca^{2+} release stimulated p105/p50 subunit expression via a mitochondria-, ROS-, and p105/p50-independent pathway. This is in contrast to the mitoROS- and p105/p50-dependence of $Ca_V1.2$ expression. Thus, ET-1-induced IP_3R-mediated SR Ca^{2+} release regulates $Ca_V1.2$ and NF-κB subunit expression through mitoROS- and p105/p50-dependent and -independent pathways, respectively.

The p105 promoter has binding sites for several transcription factors, including NF-κB, Sp1, Egr-1, and PEA3 (Cogswell *et al.*, 1993). In our study, using siRNA we specifically suppressed expression of only one NF-κB protein, namely p105, and its product p50. Expression of other NF-κB proteins, including p100/p52, p65, RelB, and c-Rel were not studied. Our data indicate that IP_3R-mediated SR Ca^{2+} release regulates p105 expression through a p105/p50-independent pathway. p105 gene transcription could be regulated by other members of the NF-κB family, as previously shown (Cogswell *et al.*, 1993). In addition, other Ca^{2+}-activated transcription factors, including Sp1 (Santini *et al.*, 2001) and Egr-1 (Thiel *et al.*, 2010) may also regulate p105 expression in the cerebral artery smooth muscle cells.

ET-1-induced IP_3R-mediated SR Ca^{2+} release activates NF-κB and also elevates NF-κB subunit expression. It is interesting to determine the relative contribution of each

of these signaling events in the ET-1-induced NF-κB-dependent elevation in $Ca_V1.2$ expression. Our data indicate that rotenone and MnTMPyP reduced the ET-1-induced elevation in NF-κB-dependent luciferase activity and $Ca_V1.2$ expression but did not affect the ET-1-induced elevation in p105/p50 expression. This suggests that ET-1 regulation of $Ca_V1.2$ expression is dependent on NF-κB activation and not an elevation in p105 expression. However, the ET-1-induced elevation in NF-κB subunit expression may amplify the elevation in NF-κB-dependent $Ca_V1.2$ transcription.

5.10. ET-1 and Vascular Function

ET-1 belongs to the endothelin (ET) peptide family, which have three more isoforms (Masaki, 2004). ET synthesis begins with production of preproET, which is cleaved by peptidases to yield big-ET, a biologically inactive intermediate (Masaki, 2004). Big-ET undergoes further cleavage by ET converting enzymes to produce ET (Masaki, 2004). Endothelial cell is the major source of ET-1 produced. In addition to endothelial cells, ET-1 is also produced by airway epithelial cells, macrophages, fibroblasts, cardiomyocytes, and neurons (Kedzierski & Yanagisawa, 2001). ET-1 released from the endothelial cells acts in a paracrine and autocrine manner by interacting with receptors on vascular smooth muscle cells and endothelial cells, respectively, and thereby modifying vascular contractility, growth, and proliferation (Kedzierski & Yanagisawa, 2001). Arterial smooth muscle cells express ET_A and ET_{B2} receptors (Masaki, 2004; Dammanahalli & Sun, 2008a), and endothelial cells express ET_{B1} receptors (Dammanahalli & Sun, 2008a). Stimulation of ET_A and ET_{B2} receptor activation stimulates Ca^{2+} waves, increases global $[Ca^{2+}]_i$, and vasoconstriction. ET_{B1} receptor activation leads to endothelial release of NO and prostaglandins, resulting in arterial vasodilation (Dammanahalli & Sun, 2008b).

ET-1 was used in this study to elicit local and global Ca^{2+} signals in cerebral artery smooth muscle cells. ET-1 plasma levels in rats and normal human subjects is ~20 pg/ml (8 pM) and 3.6 pg/ml (1.44 pM), respectively (Loffler *et al.*, 1993; Parlapiano *et al.*, 1999). Circulating levels of ET-1 in the plasma represent merely the "spillover" by endothelial cells (Zhu *et al.*, 1994; Maeda *et al.*, 1998). Vascular smooth muscle cells are exposed to ET-1 concentrations which are much higher than its plasma level (Zhu *et al.*, 1994; Maeda *et al.*, 1998). In this study, concentrations of ET-1 used for different experiments ranged from 10-100 nM based on the experimental preparations and conditions. Experiments designed to study mRNA and protein levels, required exposure of arteries to ET-1 over a long period of time. In these experiments, smooth muscle cell ET-1 receptors were intact and using higher concentrations over a long period of time could have desensitized the receptors. Therefore, a low concentration of ET-1 (10 nM) was used. ψ_m measurements were performed using isolated smooth muscle cells. The enzymes and trituration procedure used during the dissociation process could also result in damaging a few ET-1 receptors on the surface of arterial smooth muscle cells, resulting in a reduction of healthy ET-1 receptors. Therefore, a moderately high concentration of ET-1 (30 nM) was used. $[Ca^{2+}]_{mito}$, mitoROS, and cytosolic ROS measurements were obtained using moderately expressed amounts of genetically-encoded

fluorescent indicators. Therefore, a higher concentration of ET-1 (100 nM) was used for these experiments to elicit fluorescence changes from these indicators. ψ_m measurements using TMRM suggested that the different concentrations of ET-1 (10, 30, and 100 nM) used are within the slope of the sigmoidal curve. This indicates that the ET-1 concentrations used in this study neither understimulated nor saturated the receptors.

5.11. Regulation of Gene Expression by Ca^{2+} Signals

Vasoconstrictors, including purinergic and adrenergic receptor agonists modulate local and global Ca^{2+} signals similarly to ET-1 in smooth muscle cells of cerebral and systemic resistance-size arteries (Jaggar & Nelson, 2000; Mauban *et al.*, 2001). Therefore, IP_3R regulation of Ca^{2+} waves, $[Ca^{2+}]_{mito}$, and mitoROS generation may be a common mechanism by which vasoconstrictors regulate smooth muscle cell NF-κB activity, and thus control functional $Ca_V1.2$ expression and arterial contractility. Identification of this transcriptional pathway expands knowledge of Ca^{2+} signaling mechanisms regulating ion channel expression in vascular smooth muscle cells. Local and global Ca^{2+} signals have been shown to activate transcription factors and regulate ion channel gene expression in arterial smooth muscle cells. IP_3R-mediated SR Ca^{2+} release and local Ca^{2+} influx through $Ca_V1.2$ channels also stimulates calcineurin-dependent nuclear translocation of NFATc3 in cerebral artery smooth muscle cells (Gomez *et al.*, 2002; Nieves-Cintron *et al.*, 2008). However, Ca^{2+} sparks suppress calcineurin-dependent NFATc3 activation (Gomez *et al.*, 2002). NFATc3 activation downregulates expression of the K_{Ca} channel β1 subunit and Kv2.1, leading to hypertension (Amberg *et al.*, 2004; Nieves-Cintron *et al.*, 2007). In arterial smooth muscle cells, voltage-dependent Ca^{2+} influx and Ca^{2+} spark inhibition activate CREB leading to an increase in *c-fos* expression (Cartin *et al.*, 2000). Our data not only demonstrate that mitochondria are essential for mediating Ca^{2+}-dependent gene expression in arterial smooth muscle cells, but indicate that these organelles do so by sensing IP_3R-mediated Ca^{2+} release.

5.12. Conclusion

In native cerebral artery smooth muscle cells, SR Ca^{2+} release through IP_3R-gated Ca^{2+} channels elevates $[Ca^{2+}]_{mito}$, leading to mitochondrial depolarization and mitoROS generation. An IP_3R-mediated elevation in mitoROS generation activates NF-κB, leading to an elevation in $Ca_V1.2$ expression and vasoconstriction. In summary, this study indicates that mitochondria sense IP_3R-mediated SR Ca^{2+} release to control NF-κB activity, and thereby, functional $Ca_V1.2$ expression in cerebral artery smooth muscle cells.

A previous study has shown that mitochondria are involved in acute regulation of arterial contractility by activating Ca^{2+} sparks (Xi *et al.*, 2005). This study identifies another physiological function for mitochondria in arterial smooth muscle cells and shows that mitochondria can control ion channel gene expression and regulate arterial contractility on a more long-term basis. This study also highlights an important signaling

cascade wherein intracellular local Ca^{2+} signals modulate functional expression of plasma membrane Ca^{2+} channels and thereby regulate Ca^{2+} influx and arterial contractility.

5.13. Restoration of Homeostasis – Possible Negative Feedback Mechanisms

The pathway studied here begins with ET-1 binding to its receptors on arterial smooth muscle cells, and eventually results in elevated $Ca_V1.2$ expression and enhanced arterial contractility. Under normal conditions, various negative feedback mechanisms could regulate individual signaling events in the pathway described here leading to restoration of homeostasis. 1) ET-1 binding to endothelial ET_B receptors decreases the circulating ET-1 available to bind smooth muscle cell receptors thereby buffering the circulating ET-1 levels (Sanchez *et al.*, 2002), preventing overstimulation of smooth muscle cell receptors. 2) Increased ET-1 secretion can exert a negative feedback on ET-1 gene transcription in endothelial cells, through activation of ET_B receptors and internalization of the ET-1/ET_B receptor complex, as previously demonstrated in cultured porcine aortic endothelial cells (Sanchez *et al.*, 2002). Inhibition of ET-1 gene transcription would result in decreased ET-1 synthesis and therefore, result in a reduction in ET-1 secretion. 3) ET-1-induced $[IP_3]_i$ elevation stimulates IP_3R-mediated SR Ca^{2+} release. IP_3 and Ca^{2+} have been suggested to inhibit IP_3R (Hajnoczky & Thomas, 1994), thereby maintaining cytosolic IP_3R-mediated Ca^{2+} elevations. 4) Mitochondrial depolarization which occurs due to $[Ca^{2+}]_{mito}$ elevation, reduces the driving force for further mitochondrial Ca^{2+} uptake (Gunter *et al.*, 2000) and therefore could limit $[Ca^{2+}]_{mito}$ and mitoROS elevation. 5) NF-κB activation leads to nuclear translocation and stimulation of gene transcription. One of the mechanisms by which NF-κB autoregulates its activity is by stimulating transcription of IκBα, which causes cytosolic retention of NF-κB and reduces its activation (Chen & Greene, 2004). 6) As previously reported in cultured neurons, an elevation in $[Ca^{2+}]_i$, can internalize $Ca_V1.2$ channels reducing Ca^{2+} influx and $[Ca^{2+}]_i$ elevation.

Presence of these negative feedback loops may be essential for normal vascular physiology. Deregulation of these regulatory mechanisms could contribute to the development and maintenance of cardiovascular diseases.

5.14. Clinical Significance

Functional integrity of the endothelium is responsible for Ca^{2+} channel availability in vascular smooth muscle cells (Simard & Li, 2000). Dysfunctional endothelium is associated with a variety of diseases including hypertension and atherosclerosis (Ogita & Liao, 2004; Ray & Shah, 2005). Cardiovascular diseases, including systemic (Shichiri *et al.*, 1990) and pulmonary hypertension (Stewart *et al.*, 1991b) are associated with an elevation in circulating vasoconstrictors, including ET-1 (Ishikawa *et al.*, 1995; Abdel-Sayed *et al.*, 2003). Hypertension is also associated with an increase in vascular ROS, NF-κB activity, $Ca_V1.2$ protein, and Ca^{2+} currents (Wang *et al.*, 2006; Sawada *et al.*, 2007; Touyz & Schiffrin, 2008). These disease-associated

alterations may occur through activation of the IP_3R/mitoROS/NF-κB/$Ca_V1.2$ pathway.

Apart from hypertension, circulating plasma levels of ET-1 are elevated in other cardiovascular diseases, including cardiogenic shock (Cernacek & Stewart, 1989), myocardial infarction (Stewart *et al.*, 1991a), atherosclerosis (Luscher & Barton, 2000), and ischemic stroke (Estrada *et al.*, 1994). In addition, TNF-α, interferon-γ, Ang II, and thrombin increase ET-1 release from endothelial cells (Delerive *et al.*, 1999). Elevated levels of ET-1 receptors on arterial smooth muscle cells are observed in cardiovascular diseases, including pulmonary hypertension (Masaki, 2004), ischemic heart disease (Wackenfors *et al.*, 2004), and atherosclerosis (Pernow *et al.*, 2000). Enhancement of the ET-1-induced signaling pathways in arterial smooth muscle cells may occur due to endothelial injury resulting in increased ET-1 secretion, elevated ET-1 plasma levels, and/or enhanced ET-1 receptor expression levels. Pathological changes related to increased activation of ET-1 receptors may occur due to triggering of the IP_3R/mitoROS/NF-κB activation pathway. Therefore, targeting this pathway may provide a better understanding of the disease-related pathological changes and could be beneficial in developing therapeutic strategies to treat cardiovascular diseases.

5.15. Future Directions

This study shows that mitochondria control functional ion channel expression in native contractile cerebral artery smooth muscle cells. Future studies could be performed in several parts of the proposed signaling cascade to better characterize the individual events in the pathway. Potential investigations could be designed to explore:

1. The spatial and temporal relationships between Ca^{2+} waves and $[Ca^{2+}]_{mito}$ or mitoROS signals within individual mitochondria in arterial smooth muscle cells to determine if $[Ca^{2+}]_{mito}$ and mitoROS oscillate within individual mitochondria. It would also be interesting to examine whether propagation of Ca^{2+} waves induces waves of $[Ca^{2+}]_{mito}$ and mitoROS originating from mitochondria located along the path of propagation of the Ca^{2+} wave.

2. The precise mechanisms by which a $[Ca^{2+}]_{mito}$ elevation and mitochondrial depolarization stimulate mitoROS generation.

3. The pathways by which mitoROS and IP_3R-mediated SR Ca^{2+} release activate NF-κB in arterial smooth muscle cells.

4. The involvement of other members of the NF-κB family, including p52, p65, c-Rel, and RelB in regulating $Ca_V1.2$ expression.

5. The role(s) played by additional ROS-sensitive transcription factors, including AP-1, CREB, and Kruppel-like factor transcription factor(s) in the regulation of $Ca_V1.2$ gene expression.

6. If the proposed pathway is common to most G_q-protein coupled receptor agonists, including UTP and Ang II.

7. The regulation of expression of $\alpha_2\delta$, β, and γ subunits of $Ca_V1.2$, and other NF-κB proteins, including p52, p65, c-Rel, and RelB by IP_3R-mediated SR Ca^{2+} release, mitoROS, and NF-κB.

8. The importance and relevance of this pathway in the maintenance of hypertension by administration of pharmacological inhibitors of NF-κB and smooth muscle cell ET-1 receptors to hypertensive rodent models, followed by monitoring the blood pressure.

LIST OF REFERENCES

Aalkjaer C & Nilsson H (2005). Vasomotion: cellular background for the oscillator and for the synchronization of smooth muscle cells. *Br J Pharmacol* **144**, 605-616.

Abdel-Sayed S, Nussberger J, Aubert JF, Gohlke P, Brunner HR, & Brakch N (2003). Measurement of plasma endothelin-1 in experimental hypertension and in healthy subjects. *Am J Hypertens* **16**, 515-521.

Abo A, Pick E, Hall A, Totty N, Teahan CG, & Segal AW (1991). Activation of the NAD(P)H oxidase involves the small GTP-binding protein p21rac1. *Nature* **353**, 668-670.

Abramowitz J, Aydemir-Koksoy A, Helgason T, Jemelka S, Odebunmi T, Seidel CL, & Allen JC (2000). Expression of plasma membrane calcium ATPases in phenotypically distinct canine vascular smooth muscle cells. *J Mol Cell Cardiol* **32**, 777-789.

Absher M, Woodcock-Mitchell J, Mitchell J, Baldor L, Low R, & Warshaw D (1989). Characterization of vascular smooth muscle cell phenotype in long-term culture. *In Vitro Cell Dev Biol* **25**, 183-192.

Adebiyi A, McNally EM, & Jaggar JH (2008). Sulfonylurea receptor-dependent and -independent pathways mediate vasodilation induced by ATP-sensitive K^+ channel openers. *Mol Pharmacol* **74**, 736-743.

Adebiyi A, Zhao G, Narayanan D, Thomas-Gatewood CM, Bannister JP, & Jaggar JH (2010). Isoform-selective physical coupling of TRPC3 channels to IP_3 receptors in smooth muscle cells regulates arterial contractility. *Circ Res* **106**, 1603-1612.

Afzal M, Matsugo S, Sasai M, Xu B, Aoyama K, & Takeuchi T (2003). Method to overcome photoreaction, a serious drawback to the use of dichlorofluorescin in evaluation of reactive oxygen species. *Biochem Biophys Res Commun* **304**, 619-624.

Ago T, Kitazono T, Ooboshi H, Iyama T, Han YH, Takada J, Wakisaka M, Ibayashi S, Utsumi H, & Iida M (2004). Nox4 as the major catalytic component of an endothelial NAD(P)H oxidase. *Circulation* **109**, 227-233.

Ahn SY, Choi YS, Koo HJ, Jeong JH, Park WH, Kim M, Piao Y, & Pak YK (2010). Mitochondrial dysfunction enhances the migration of vascular smooth muscles cells via suppression of Akt phosphorylation. *Biochim Biophys Acta* **1800**, 275-281.

Ambasta RK, Kumar P, Griendling KK, Schmidt HH, Busse R, & Brandes RP (2004). Direct interaction of the novel Nox proteins with $p22^{phox}$ is required for the formation of a functionally active NAD(P)H oxidase. *J Biol Chem* **279**, 45935-45941.

Amberg GC, Navedo MF, Nieves-Cintron M, Molkentin JD, & Santana LF (2007). Calcium sparklets regulate local and global calcium in murine arterial smooth muscle. *J Physiol* **579**, 187-201.

Amberg GC, Rossow CF, Navedo MF, & Santana LF (2004). NFATc3 regulates Kv2.1 expression in arterial smooth muscle. *J Biol Chem* **279**, 47326-47334.

American Veterinary Medical Association Panel on Euthanasia (2001). 2000 Report of the AVMA Panel on Euthanasia. *J Am Vet Med Assoc* **218**, 669-696.

Archer SL, Marsboom G, Kim GH, Zhang HJ, Toth PT, Svensson EC, Dyck JR, Gomberg-Maitland M, Thebaud B, Husain AN, Cipriani N, & Rehman J (2010). Epigenetic attenuation of mitochondrial superoxide dismutase 2 in pulmonary arterial hypertension: a basis for excessive cell proliferation and a new therapeutic target. *Circulation* **121**, 2661-2671.

Arnaudeau S, Kelley WL, Walsh JV, Jr., & Demaurex N (2001). Mitochondria recycle Ca^{2+} to the endoplasmic reticulum and prevent the depletion of neighboring endoplasmic reticulum regions. *J Biol Chem* **276**, 29430-29439.

Arsura M, Panta GR, Bilyeu JD, Cavin LG, Sovak MA, Oliver AA, Factor V, Heuchel R, Mercurio F, Thorgeirsson SS, & Sonenshein GE (2003). Transient activation of NF-κB through a TAK1/IKK kinase pathway by TGF-β1 inhibits AP-1/SMAD signaling and apoptosis: implications in liver tumor formation. *Oncogene* **22**, 412-425.

Asehnoune K, Strassheim D, Mitra S, Kim JY, & Abraham E (2004). Involvement of reactive oxygen species in Toll-like receptor 4-dependent activation of NF-κB. *J Immunol* **172**, 2522-2529.

Baeuerle PA & Baltimore D (1996). NF-κB: ten years after. *Cell* **87**, 13-20.

Bailey SR, Mitra S, Flavahan S, & Flavahan NA (2005). Reactive oxygen species from smooth muscle mitochondria initiate cold-induced constriction of cutaneous arteries. *Am J Physiol Heart Circ Physiol* **289**, H243-H250.

Baines DL, Janes M, Newman DJ, & Best OG (2002). Oxygen-evoked changes in transcriptional activity of the 5'-flanking region of the human amiloride-sensitive sodium channel (αENaC) gene: role of nuclear factor κB. *Biochem J* **364**, 537-545.

Basuroy S, Bhattacharya S, Leffler CW, & Parfenova H (2009). Nox4 NAD(P)H oxidase mediates oxidative stress and apoptosis caused by TNF-α in cerebral vascular endothelial cells. *Am J Physiol Cell Physiol* **296**, C422-C432.

Beech DJ, Muraki K, & Flemming R (2004). Non-selective cationic channels of smooth muscle and the mammalian homologues of Drosophila TRP. *J Physiol* **559**, 685-706.

Belousov VV, Fradkov AF, Lukyanov KA, Staroverov DB, Shakhbazov KS, Terskikh AV, & Lukyanov S (2006). Genetically encoded fluorescent indicator for intracellular hydrogen peroxide. *Nat Methods* **3**, 281-286.

Bernardi P (1999). Mitochondrial transport of cations: channels, exchangers, and permeability transition. *Physiol Rev* **79**, 1127-1155.

Bernardi P & Petronilli V (1996). The permeability transition pore as a mitochondrial calcium release channel: a critical appraisal. *J Bioenerg Biomembr* **28**, 131-138.

Berridge MJ (2001). The versatility and complexity of calcium signalling. *Novartis Found Symp* **239**, 52-64.

Berridge MJ (2004). Calcium signal transduction and cellular control mechanisms. *Biochim Biophys Acta* **1742**, 3-7.

Berridge MJ, Bootman MD, & Lipp P (1998). Calcium - a life and death signal. *Nature* **395**, 645-648.

Berridge MJ, Bootman MD, & Roderick HL (2003). Calcium signalling: dynamics, homeostasis and remodelling. *Nat Rev Mol Cell Biol* **4**, 517-529.

Bezprozvanny I & Ehrlich BE (1995). The inositol 1,4,5-trisphosphate ($InsP_3$) receptor. *J Membr Biol* **145**, 205-216.

Birukov KG (2009). Cyclic stretch, reactive oxygen species, and vascular remodeling. *Antioxid Redox Signal* **11**, 1651-1667.

Blanck J, Ristau O, Zhukov AA, Archakov AI, Rein H, & Ruckpaul K (1991). Cytochrome P-450 spin state and leakiness of the monooxygenase pathway. *Xenobiotica* **21**, 121-135.

Blatter LA & Wier WG (1992). Agonist-induced $[Ca^{2+}]_i$ waves and Ca^{2+}-induced Ca^{2+} release in mammalian vascular smooth muscle cells. *Am J Physiol* **263**, H576-H586.

Boittin FX, Galione A, & Evans AM (2002). Nicotinic acid adenine dinucleotide phosphate mediates Ca^{2+} signals and contraction in arterial smooth muscle via a two-pool mechanism. *Circ Res* **91**, 1168-1175.

Boittin FX, Macrez N, Halet G, & Mironneau J (1999). Norepinephrine-induced Ca^{2+} waves depend on $InsP_3$ and ryanodine receptor activation in vascular myocytes. *Am J Physiol* **277**, C139-C151.

Bolton TB, Gordienko DV, Povstyan OV, Harhun MI, & Pucovsky V (2004). Smooth muscle cells and interstitial cells of blood vessels. *Cell Calcium* **35**, 643-657.

Bonizzi G & Karin M (2004). The two NF-$_k$B activation pathways and their role in innate and adaptive immunity. *Trends Immunol* **25**, 280-288.

Bootman MD, Collins TJ, Peppiatt CM, Prothero LS, MacKenzie L, De Smet P, Travers M, Tovey SC, Seo JT, Berridge MJ, Ciccolini F, & Lipp P (2001). Calcium signalling - an overview. *Semin Cell Dev Biol* **12**, 3-10.

Bourcier T, Sukhova G, & Libby P (1997). The nuclear factor κ-B signaling pathway participates in dysregulation of vascular smooth muscle cells *in vitro* and in human atherosclerosis. *J Biol Chem* **272**, 15817-15824.

Brayden JE & Nelson MT (1992). Regulation of arterial tone by activation of calcium-dependent potassium channels. *Science* **256**, 532-535.

Brookes PS (2005). Mitochondrial H^+ leak and ROS generation: an odd couple. *Free Radic Biol Med* **38**, 12-23.

Brookes PS, Yoon Y, Robotham JL, Anders MW, & Sheu SS (2004). Calcium, ATP, and ROS: a mitochondrial love-hate triangle. *Am J Physiol* **287**, C817-C833.

Brzoska K & Szumiel I (2009). Signalling loops and linear pathways: NF-κB activation in response to genotoxic stress. *Mutagenesis* **24**, 1-8.

Bubici C, Papa S, Dean K, & Franzoso G (2006). Mutual cross-talk between reactive oxygen species and nuclear factor-kappa B: molecular basis and biological significance. *Oncogene* **25**, 6731-6748.

Campbell JH, Kocher O, Skalli O, Gabbiani G, & Campbell GR (1989). Cytodifferentiation and expression of alpha-smooth muscle actin mRNA and protein during primary culture of aortic smooth muscle cells. Correlation with cell density and proliferative state. *Arteriosclerosis* **9**, 633-643.

Cartin L, Lounsbury KM, & Nelson MT (2000). Coupling of Ca^{2+} to CREB activation and gene expression in intact cerebral arteries from mouse: roles of ryanodine receptors and voltage- dependent Ca^{2+} channels. *Circ Res* **86**, 760-767.

Catterall WA (2000). Structure and regulation of voltage-gated Ca^{2+} channels. *Annu Rev Cell Dev Biol* **16**, 521-555.

Cernacek P & Stewart DJ (1989). Immunoreactive endothelin in human plasma: marked elevations in patients in cardiogenic shock. *Biochem Biophys Res Commun* **161**, 562-567.

Chalmers S, Olson ML, MacMillan D, Rainbow RD, & McCarron JG (2007). Ion channels in smooth muscle: regulation by the sarcoplasmic reticulum and mitochondria. *Cell Calcium* **42**, 447-466.

Chandel NS, Trzyna WC, McClintock DS, & Schumacker PT (2000). Role of oxidants in NF-κB activation and TNF-α gene transcription induced by hypoxia and endotoxin. *J Immunol* **165**, 1013-1021.

Chang HY & Yang X (2000). Proteases for cell suicide: functions and regulation of caspases. *Microbiol Mol Biol Rev* **64**, 821-846.

Chen LF & Greene WC (2004). Shaping the nuclear action of NF-kappaB. *Nat Rev Mol Cell Biol* **5**, 392-401.

Chen XL, Tummala PE, Olbrych MT, Alexander RW, & Medford RM (1998). Angiotensin II induces monocyte chemoattractant protein-1 gene expression in rat vascular smooth muscle cells. *Circ Res* **83**, 952-959.

Cheng H, Lederer WJ, & Cannell MB (1993). Calcium sparks: elementary events underlying excitation-contraction coupling in heart muscle. *Science* **262**, 740-744.

Cheng X, Liu J, Asuncion-Chin M, Blaskova E, Bannister JP, Dopico AM, & Jaggar JH (2007). A novel $Ca_V1.2$ N terminus expressed in smooth muscle cells of resistance size arteries modifies channel regulation by auxiliary subunits. *J Biol Chem* **282**, 29211-29221.

Cheranov SY & Jaggar JH (2004). Mitochondrial modulation of Ca^{2+} sparks and transient K_{Ca} currents in smooth muscle cells of rat cerebral arteries. *J Physiol* **556**, 755-771.

Cheranov SY & Jaggar JH (2006). TNF-α dilates cerebral arteries via NAD(P)H oxidase-dependent Ca^{2+} spark activation. *Am J Physiol Cell Physiol* **290**, C964-C971.

Clapham DE (1995). Calcium signaling. *Cell* **80**, 259-268.

Clempus RE & Griendling KK (2006). Reactive oxygen species signaling in vascular smooth muscle cells. *Cardiovasc Res* **71**, 216-225.

Cogswell PC, Scheinman RI, & Baldwin AS, Jr. (1993). Promoter of the human NF-κB p50/p105 gene. Regulation by NF-κB subunits and by c-REL. *J Immunol* **150**, 2794-2804.

Collins TJ, Lipp P, Berridge MJ, & Bootman MD (2001). Mitochondrial Ca^{2+} uptake depends on the spatial and temporal profile of cytosolic Ca^{2+} signals. *J Biol Chem* **276**, 26411-26420.

Colombini M (2004). VDAC: the channel at the interface between mitochondria and the cytosol. *Mol Cell Biochem* **256-257**, 107-115.

Csordas G & Hajnoczky G (2009). SR/ER-mitochondrial local communication: calcium and ROS. *Biochim Biophys Acta* **1787**, 1352-1362.

Dai B, Saada N, Echetebu C, Dettbarn C, & Palade P (2002). A new promoter for α_{1C} subunit of human L-type cardiac calcium channel $Ca_V1.2$. *Biochem Biophys Res Commun* **296**, 429-433.

Dai J, Lee CH, Poburko D, Szado T, Kuo KH, & van Breemen C (2007). Endothelin-1-mediated wave-like $[Ca^{2+}]_i$ oscillations in intact rabbit inferior vena cava. *J Vasc Res* **44**, 495-503.

Dammanahalli JK & Sun Z (2008a). Endothelin (ET)-1 inhibits nicotinamide adenine dinucleotide phosphate oxidase activity in human abdominal aortic endothelial cells: a novel function of ET_{B1} receptors. *Endocrinology* **149**, 4979-4987.

Dammanahalli KJ & Sun Z (2008b). Endothelins and NAD(P)H oxidases in the cardiovascular system. *Clin Exp Pharmacol Physiol* **35**, 2-6.

Davidoff AJ, Maki TM, Ellingsen O, & Marsh JD (1997). Expression of calcium channels in adult cardiac myocytes is regulated by calcium. *J Mol Cell Cardiol* **29**, 1791-1803.

De Brito OM & Scorrano L (2008). Mitofusin 2 tethers endoplasmic reticulum to mitochondria. *Nature* **456**, 605-610.

De Martin R, Hoeth M, Hofer-Warbinek R, & Schmid JA (2000). The transcription factor NF-κB and the regulation of vascular cell function. *Arterioscler Thromb Vasc Biol* **20**, E83-E88.

Delerive P, Martin-Nizard F, Chinetti G, Trottein F, Fruchart JC, Najib J, Duriez P, & Staels B (1999). Peroxisome proliferator-activated receptor activators inhibit thrombin-induced endothelin-1 production in human vascular endothelial cells by inhibiting the activator protein-1 signaling pathway. *Circ Res* **85**, 394-402.

Detmer K, Wang Z, Warejcka D, Leeper-Woodford SK, & Newman WH (2001). Endotoxin stimulated cytokine production in rat vascular smooth muscle cells. *Am J Physiol Heart Circ Physiol* **281**, H661-H668.

Dohi Y, Hahn AW, Boulanger CM, Buhler FR, & Luscher TF (1992). Endothelin stimulated by angiotensin II augments contractility of spontaneously hypertensive rat resistance arteries. *Hypertension* **19**, 131-137.

Drummond RM & Tuft RA (1999). Release of Ca^{2+} from the sarcoplasmic reticulum increases mitochondrial $[Ca^{2+}]$ in rat pulmonary artery smooth muscle cells. *J Physiol* **516 Pt 1**, 139-147.

Duchen MR (2000a). Mitochondria and Ca^{2+} in cell physiology and pathophysiology. *Cell Calcium* **28**, 339-348.

Duchen MR (2000b). Mitochondria and calcium: from cell signalling to cell death. *J Physiol* **529 Pt 1**, 57-68.

Duchen MR (2004). Roles of mitochondria in health and disease. *Diabetes* **53 Suppl 1**, S96-S102.

Duchen MR, Leyssens A, & Crompton M (1998). Transient mitochondrial depolarizations reflect focal sarcoplasmic reticular calcium release in single rat cardiomyocytes. *J Cell Biol* **142**, 975-988.

Dupont WD & Plummer WD, Jr. (1990). Power and sample size calculations. A review and computer program. *Control Clin Trials* **11**, 116-128.

Earley S (2006). Molecular diversity of receptor operated channels in vascular smooth muscle: a role for heteromultimeric TRP channels? *Circ Res* **98**, 1462-1464.

Earley S & Brayden JE (2010). Transient receptor potential channels and vascular function. *Clin Sci (Lond)* **119**, 19-36.

Earley S, Heppner TJ, Nelson MT, & Brayden JE (2005). TRPV4 forms a novel Ca^{2+} signaling complex with ryanodine receptors and BK_{Ca} channels. *Circ Res* **97**, 1270-1279.

Eguchi S, Hirata Y, Imai T, Kanno K, & Marumo F (1994). Phenotypic change of endothelin receptor subtype in cultured rat vascular smooth muscle cells. *Endocrinology* **134**, 222-228.

Elion GB, Yu TF, Gutman AB, & Hitchings GH (1968). Renal clearance of oxipurinol, the chief metabolite of allopurinol. *Am J Med* **45**, 69-77.

Endo M (2006). Calcium ion as a second messenger with special reference to excitation-contraction coupling. *J Pharmacol Sci* **100**, 519-524.

Ertel EA, Campbell KP, Harpold MM, Hofmann F, Mori Y, Perez-Reyes E, Schwartz A, Snutch TP, Tanabe T, Birnbaumer L, Tsien RW, & Catterall WA (2000). Nomenclature of voltage-gated calcium channels. *Neuron* **25**, 533-535.

Estrada V, Tellez MJ, Moya J, Fernandez-Durango R, Egido J, & Fernandez Cruz AF (1994). High plasma levels of endothelin-1 and atrial natriuretic peptide in patients with acute ischemic stroke. *Am J Hypertens* **7**, 1085-1089.

Faulkner KM, Liochev SI, & Fridovich I (1994). Stable Mn(III) porphyrins mimic superoxide dismutase *in vitro* and substitute for it *in vivo*. *J Biol Chem* **269**, 23471-23476.

Fawell S, Seery J, Daikh Y, Moore C, Chen LL, Pepinsky B, & Barsoum J (1994). Tat-mediated delivery of heterologous proteins into cells. *Proc Natl Acad Sci USA* **91**, 664-668.

Fernie AR, Carrari F, & Sweetlove LJ (2004). Respiratory metabolism: glycolysis, the TCA cycle and mitochondrial electron transport. *Curr Opin Plant Biol* **7**, 254-261.

Filippin L, Abad MC, Gastaldello S, Magalhaes PJ, Sandona D, & Pozzan T (2005). Improved strategies for the delivery of GFP-based Ca^{2+} sensors into the mitochondrial matrix. *Cell Calcium* **37**, 129-136.

Filippin L, Magalhaes PJ, Di BG, Colella M, & Pozzan T (2003). Stable interactions between mitochondria and endoplasmic reticulum allow rapid accumulation of calcium in a subpopulation of mitochondria. *J Biol Chem* **278**, 39224-39234.

Floyd R & Wray S (2007). Calcium transporters and signalling in smooth muscles. *Cell Calcium* **42**, 467-476.

Forstermann U, Closs EI, Pollock JS, Nakane M, Schwarz P, Gath I, & Kleinert H (1994). Nitric oxide synthase isozymes. Characterization, purification, molecular cloning, and functions. *Hypertension* **23**, 1121-1131.

Friedl HP, Till GO, Ryan US, & Ward PA (1989). Mediator-induced activation of xanthine oxidase in endothelial cells. *FASEB J* **3**, 2512-2518.

Fukami JI, Yamamoto I, & Casida JE (1967). Metabolism of rotenone *in vitro* by tissue homogenates from mammals and insects. *Science* **155**, 713-716.

Furukawa K & Mattson MP (1998). The transcription factor NF-κB mediates increases in calcium currents and decreases in NMDA- and AMPA/kainate-induced currents induced by tumor necrosis factor-α in hippocampal neurons. *J Neurochem* **70**, 1876-1886.

Gafni J, Munsch JA, Lam TH, Catlin MC, Costa LG, Molinski TF, & Pessah IN (1997). Xestospongins: potent membrane permeable blockers of the inositol 1,4,5-trisphosphate receptor. *Neuron* **19**, 723-733.

Gerasimenko O & Tepikin A (2005). How to measure Ca^{2+} in cellular organelles? *Cell Calcium* **38**, 201-211.

Gerhardstein BL, Gao T, Bunemann M, Puri TS, Adair A, Ma H, & Hosey MM (2000). Proteolytic processing of the C terminus of the α_{1C} subunit of L-type calcium channels and the role of a proline-rich domain in membrane tethering of proteolytic fragments. *J Biol Chem* **275**, 8556-8563.

Gloire G, Legrand-Poels S, & Piette J (2006). NF-κB activation by reactive oxygen species: fifteen years later. *Biochem Pharmacol* **72**, 1493-1505.

Goldsby RA & Heytler PG (1963). Uncoupling of oxidative phosphorylation by carbonyl cyanide phenylhydrazones. II. Effects of carbonyl cyanide m-chlorophenylhydrazone on mitochondrial respiration. *Biochemistry* **2**, 1142-1147.

Gollasch M & Nelson MT (1997). Voltage-dependent Ca^{2+} channels in arterial smooth muscle cells. *Kidney Blood Press Res* **20**, 355-371.

Gomez MF, Stevenson AS, Bonev AD, Hill-Eubanks DC, & Nelson MT (2002). Opposing actions of inositol 1,4,5-trisphosphate and ryanodine receptors on nuclear factor of activated T-cells regulation in smooth muscle. *J Biol Chem* **277**, 37756-37764.

Gorlach A, Brandes RP, Nguyen K, Amidi M, Dehghani F, & Busse R (2000). A $gp91^{phox}$ containing NAD(P)H oxidase selectively expressed in endothelial cells is a major source of oxygen radical generation in the arterial wall. *Circ Res* **87**, 26-32.

Gorsky LD, Koop DR, & Coon MJ (1984). On the stoichiometry of the oxidase and monooxygenase reactions catalyzed by liver microsomal cytochrome P-450. Products of oxygen reduction. *J Biol Chem* **259**, 6812-6817.

Gouw MA, Wilffert B, Wermelskirchen D, & van Zwieten PA (1990). Ca^{2+} influx insensitive to organic Ca^{2+} entry blockers contributes to noradrenaline-induced contractions of the isolated guinea pig aorta. *Pharmacology* **40**, 277-287.

Graier WF, Frieden M, & Malli R (2007). Mitochondria and Ca^{2+} signaling: old guests, new functions. *Pflugers Arch* **455**, 375-396.

Griendling KK & FitzGerald GA (2003). Oxidative stress and cardiovascular injury: Part I: basic mechanisms and *in vivo* monitoring of ROS. *Circulation* **108**, 1912-1916.

Griendling KK, Minieri CA, Ollerenshaw JD, & Alexander RW (1994). Angiotensin II stimulates NADH and NAD(P)H oxidase activity in cultured vascular smooth muscle cells. *Circ Res* **74**, 1141-1148.

Griesbeck O, Baird GS, Campbell RE, Zacharias DA, & Tsien RY (2001). Reducing the environmental sensitivity of yellow fluorescent protein. Mechanism and applications. *J Biol Chem* **276**, 29188-29194.

Griffiths EJ, Ocampo CJ, Savage JS, Rutter GA, Hansford RG, Stern MD, & Silverman HS (1998). Mitochondrial calcium transporting pathways during hypoxia and reoxygenation in single rat cardiomyocytes. *Cardiovasc Res* **39**, 423-433.

Gros R, Afroze T, You XM, Kabir G, Van WR, Kalair W, Hoque AE, Mungrue IN, & Husain M (2003). Plasma membrane calcium ATPase overexpression in arterial smooth muscle increases vasomotor responsiveness and blood pressure. *Circ Res* **93**, 614-621.

Guibert C, Ducret T, & Savineau JP (2008). Voltage-independent calcium influx in smooth muscle. *Prog Biophys Mol Biol* **98**, 10-23.

Gunter TE, Buntinas L, Sparagna G, Eliseev R, & Gunter K (2000). Mitochondrial calcium transport: mechanisms and functions. *Cell Calcium* **28**, 285-296.

Gunter TE & Gunter KK (2001). Uptake of calcium by mitochondria: transport and possible function. *IUBMB Life* **52**, 197-204.

Gunter TE & Pfeiffer DR (1990). Mechanisms by which mitochondria transport calcium. *Am J Physiol* **258**, C755-C786.

Hajnoczky G, Csordas G, Madesh M, & Pacher P (2000). The machinery of local Ca^{2+} signalling between sarco-endoplasmic reticulum and mitochondria. *J Physiol* **529 Pt 1**, 69-81.

Hajnoczky G, Csordas G, & Yi M (2002). Old players in a new role: mitochondria-associated membranes, VDAC, and ryanodine receptors as contributors to calcium signal propagation from endoplasmic reticulum to the mitochondria. *Cell Calcium* **32**, 363-377.

Hajnoczky G, Robb-Gaspers LD, Seitz MB, & Thomas AP (1995). Decoding of cytosolic calcium oscillations in the mitochondria. *Cell* **82**, 415-424.

Hajnoczky G & Thomas AP (1994). The inositol trisphosphate calcium channel is inactivated by inositol trisphosphate. *Nature* **370**, 474-477.

Halling DB, Aracena-Parks P, & Hamilton SL (2005). Regulation of voltage-gated Ca^{2+} channels by calmodulin. *Sci STKE* **2005**, re15.

Han Y, Runge MS, & Brasier AR (1999). Angiotensin II induces interleukin-6 transcription in vascular smooth muscle cells through pleiotropic activation of nuclear factor-κB transcription factors. *Circ Res* **84**, 695-703.

Harrison R (2002). Structure and function of xanthine oxidoreductase: where are we now? *Free Radic Biol Med* **33**, 774-797.

Hayashi T & Su TP (2007). Sigma-1 receptor chaperones at the ER-mitochondrion interface regulate Ca^{2+} signaling and cell survival. *Cell* **131**, 596-610.

Hayden MS & Ghosh S (2008). Shared principles in NF-κB signaling. *Cell* **132**, 344-362.

Hensley K, Robinson KA, Gabbita SP, Salsman S, & Floyd RA (2000). Reactive oxygen species, cell signaling, and cell injury. *Free Radic Biol Med* **28**, 1456-1462.

Heppner TJ, Bonev AD, Santana LF, & Nelson MT (2002). Alkaline pH shifts Ca^{2+} sparks to Ca^{2+} waves in smooth muscle cells of pressurized cerebral arteries. *Am J Physiol Heart Circ Physiol* **283**, H2169-H2176.

Heytler PG (1963). Uncoupling of oxidative phosphorylation by carbonyl cyanide phenylhydrazones. I. Some characteristics of m-Cl-CCP action on mitochondria and chloroplasts. *Biochemistry* **2**, 357-361.

Hilenski LL, Clempus RE, Quinn MT, Lambeth JD, & Griendling KK (2004). Distinct subcellular localizations of Nox1 and Nox4 in vascular smooth muscle cells. *Arterioscler Thromb Vasc Biol* **24**, 677-683.

Hill MA, Zou H, Potocnik SJ, Meininger GA, & Davis MJ (2001). Invited review: arteriolar smooth muscle mechanotransduction: Ca^{2+} signaling pathways underlying myogenic reactivity. *J Appl Physiol* **91**, 973-983.

Hogg RC, Wang Q, Helliwell RM, & Large WA (1993). Properties of spontaneous inward currents in rabbit pulmonary artery smooth muscle cells. *Pflugers Arch* **425**, 233-240.

Holland PM, Abramson RD, Watson R, & Gelfand DH (1991). Detection of specific polymerase chain reaction product by utilizing the 5' -> 3' exonuclease activity of *Thermus aquaticus* DNA polymerase. *Proc Natl Acad Sci USA* **88**, 7276-7280.

Huang LE, Arany Z, Livingston DM, & Bunn HF (1996). Activation of hypoxia-inducible transcription factor depends primarily upon redox-sensitive stabilization of its α subunit. *J Biol Chem* **271**, 32253-32259.

Huser J, Rechenmacher CE, & Blatter LA (1998). Imaging the permeability pore transition in single mitochondria. *Biophys J* **74**, 2129-2137.

Iadecola C & Gorelick PB (2004). Hypertension, angiotensin, and stroke: beyond blood pressure. *Stroke* **35**, 348-350.

Ialenti A, Ianaro A, Maffia P, Carnuccio R, D'Acquisto F, Maiello FM, & Di RM (2001). Role of nuclear factor-κB in a rat model of vascular injury. *Naunyn Schmiedebergs Arch Pharmacol* **364**, 343-350.

Inesi G (1987). Sequential mechanism of calcium binding and translocation in sarcoplasmic reticulum adenosine triphosphatase. *J Biol Chem* **262**, 16338-16342.

Irani K (2000). Oxidant signaling in vascular cell growth, death, and survival: a review of the roles of reactive oxygen species in smooth muscle and endothelial cell mitogenic and apoptotic signaling. *Circ Res* **87**, 179-183.

Ishida Y & Paul RJ (2005). Ca^{2+} clearance in smooth muscle: lessons from gene-altered mice. *J Smooth Muscle Res* **41**, 235-245.

Ishikawa S, Miyauchi T, Sakai S, Ushinohama H, Sagawa K, Fusazaki N, Kado H, Sunagawa H, Honda S, Ueno H, Yamaguchi I, Sugishita Y, & Goto K (1995). Elevated levels of plasma endothelin-1 in young patients with pulmonary hypertension caused by congenital heart disease are decreased after successful surgical repair. *J Thorac Cardiovasc Surg* **110**, 271-273.

Iwamoto T, Kita S, & Katsuragi T (2005). Salt-sensitive hypertension, Na^+/Ca^{2+} exchanger, and vascular smooth muscle. *Trends Cardiovasc Med* **15**, 273-277.

Jaggar JH (2001). Intravascular pressure regulates local and global Ca^{2+} signaling in cerebral artery smooth muscle cells. *Am J Physiol Cell Physiol* **281**, C439-C448.

Jaggar JH (2007). Smooth muscle sparklet Ca_V channels defined: 1.2 is the number. *Am J Physiol Heart Circ Physiol* **293**, H1317-H1319.

Jaggar JH & Nelson MT (2000). Differential regulation of Ca^{2+} sparks and Ca^{2+} waves by UTP in rat cerebral artery smooth muscle cells. *Am J Physiol Cell Physiol* **279**, C1528-C1539.

Jaggar JH, Porter VA, Lederer WJ, & Nelson MT (2000). Calcium sparks in smooth muscle. *Am J Physiol Cell Physiol* **278**, C235-C256.

Jaggar JH, Stevenson AS, & Nelson MT (1998). Voltage dependence of Ca^{2+} sparks in intact cerebral arteries. *Am J Physiol* **274**, C1755-C1761.

Jakubowski W & Bartosz G (2000). 2,7-dichlorofluorescin oxidation and reactive oxygen species: what does it measure? *Cell Biol Int* **24**, 757-760.

Kaftan EJ, Xu T, Abercrombie RF, & Hille B (2000). Mitochondria shape hormonally induced cytoplasmic calcium oscillations and modulate exocytosis. *J Biol Chem* **275**, 25465-25470.

Karihtala P & Soini Y (2007). Reactive oxygen species and antioxidant mechanisms in human tissues and their relation to malignancies. *APMIS* **115**, 81-103.

Karin M (1999). How NF-κB is activated: the role of the IκB kinase (IKK) complex. *Oncogene* **18**, 6867-6874.

Kaur S, Wang F, Venkatraman M, & Arsura M (2005). X-linked inhibitor of apoptosis (XIAP) inhibits c-Jun N-terminal kinase 1 (JNK1) activation by transforming growth factor β1 (TGF-β1) through ubiquitin-mediated proteosomal degradation of the TGF-β1-activated kinase 1 (TAK1). *J Biol Chem* **280**, 38599-38608.

Kedzierski RM & Yanagisawa M (2001). Endothelin system: the double-edged sword in health and disease. *Annu Rev Pharmacol Toxicol* **41**, 851-876.

Kibbe M, Billiar T, & Tzeng E (1999). Inducible nitric oxide synthase and vascular injury. *Cardiovasc Res* **43**, 650-657.

Knot HJ & Nelson MT (1998). Regulation of arterial diameter and wall [Ca^{2+}] in cerebral arteries of rat by membrane potential and intravascular pressure. *J Physiol* **508 Pt 1**, 199-209.

Kunsch C & Medford RM (1999). Oxidative stress as a regulator of gene expression in the vasculature. *Circ Res* **85**, 753-766.

Kuthan H & Ullrich V (1982). Oxidase and oxygenase function of the microsomal cytochrome P450 monooxygenase system. *Eur J Biochem* **126**, 583-588.

Kye MJ, Spiess J, & Blank T (2007). Transcriptional regulation of intronic calcium-activated potassium channel SK2 promoters by nuclear factor-κB and glucocorticoids. *Mol Cell Biochem* **300**, 9-17.

Lamont C & Wier WG (2004). Different roles of ryanodine receptors and inositol (1,4,5)-trisphosphate receptors in adrenergically stimulated contractions of small arteries. *Am J Physiol Heart Circ Physiol* **287**, H617-H625.

Lander HM (1997). An essential role for free radicals and derived species in signal transduction. *FASEB J* **11**, 118-124.

Landolfi B, Curci S, Debellis L, Pozzan T, & Hofer AM (1998). Ca^{2+} homeostasis in the agonist-sensitive internal store: functional interactions between mitochondria and the ER measured In situ in intact cells. *J Cell Biol* **142**, 1235-1243.

Landry DB, Couper LL, Bryant SR, & Lindner V (1997). Activation of the NF-κB and IκB system in smooth muscle cells after rat arterial injury. Induction of vascular cell adhesion molecule-1 and monocyte chemoattractant protein-1. *Am J Pathol* **151**, 1085-1095.

Large WA (2002). Receptor-operated Ca^{2+}-permeable nonselective cation channels in vascular smooth muscle: a physiologic perspective. *J Cardiovasc Electrophysiol* **13**, 493-501.

Lassegue B & Clempus RE (2003). Vascular NAD(P)H oxidases: specific features, expression, and regulation. *Am J Physiol Regul Integr Comp Physiol* **285**, R277-R297.

Le Bail O, Schmidt-Ullrich R, & Israel A (1993). Promoter analysis of the gene encoding the IκB-α/MAD3 inhibitor of NF-κB: positive regulation by members of the rel/NF-κB family. *EMBO J* **12**, 5043-5049.

Lee CH, Kuo KH, Dai J, & van Breemen C (2005). Asynchronous calcium waves in smooth muscle cells. *Can J Physiol Pharmacol* **83**, 733-741.

Lee CH, Poburko D, Kuo KH, Seow CY, & van Breemen C (2002). Ca^{2+} oscillations, gradients, and homeostasis in vascular smooth muscle. *Am J Physiol Heart Circ Physiol* **282**, H1571-H1583.

Lee SJ, Seo KW, Yun MR, Bae SS, Lee WS, Hong KW, & Kim CD (2008). 4-Hydroxynonenal enhances MMP-2 production in vascular smooth muscle cells via mitochondrial ROS-mediated activation of the Akt/NF-κB signaling pathways. *Free Radic Biol Med* **45**, 1487-1492.

Lesh RE, Somlyo AP, Owens GK, & Somlyo AV (1995). Reversible permeabilization. A novel technique for the intracellular introduction of antisense oligodeoxynucleotides into intact smooth muscle. *Circ Res* **77**, 220-230.

Levy D, Seigneuret M, Bluzat A, & Rigaud JL (1990). Evidence for proton countertransport by the sarcoplasmic reticulum Ca^{2+}-ATPase during calcium transport in reconstituted proteoliposomes with low ionic permeability. *J Biol Chem* **265**, 19524-19534.

Li L, Mamputu JC, Wiernsperger N, & Renier G (2005). Signaling pathways involved in human vascular smooth muscle cell proliferation and matrix metalloproteinase-2 expression induced by leptin: inhibitory effect of metformin. *Diabetes* **54**, 2227-2234.

Li YP, Atkins CM, Sweatt JD, & Reid MB (1999). Mitochondria mediate tumor necrosis factor-α/NF-κB signaling in skeletal muscle myotubes. *Antioxid Redox Signal* **1**, 97-104.

Liao P, Yong TF, Liang MC, Yue DT, & Soong TW (2005). Splicing for alternative structures of $Ca_V1.2$ Ca^{2+} channels in cardiac and smooth muscles. *Cardiovasc Res* **68**, 197-203.

Lilienbaum A & Israel A (2003). From calcium to NF-κB signaling pathways in neurons. *Mol Cell Biol* **23**, 2680-2698.

Lin L, DeMartino GN, & Greene WC (1998). Cotranslational biogenesis of NF-κB p50 by the 26S proteasome. *Cell* **92**, 819-828.

Liu C & Hermann TE (1978). Characterization of ionomycin as a calcium ionophore. *J Biol Chem* **253**, 5892-5894.

Livak KJ & Schmittgen TD (2001). Analysis of relative gene expression data using real-time quantitative PCR and the $2^{-\Delta\Delta CT}$ Method. *Methods* **25**, 402-408.

Loffler BM, Breu V, & Clozel M (1993). Effect of different endothelin receptor antagonists and of the novel non-peptide antagonist Ro 46-2005 on endothelin levels in rat plasma. *FEBS Lett* **333**, 108-110.

Lotzer K, Funk CD, & Habenicht AJ (2005). The 5-lipoxygenase pathway in arterial wall biology and atherosclerosis. *Biochim Biophys Acta* **1736**, 30-37.

Lukyanenko V, Gyorke I, Wiesner TF, & Gyorke S (2001). Potentiation of Ca^{2+} release by cADP-ribose in the heart is mediated by enhanced SR Ca^{2+} uptake into the sarcoplasmic reticulum. *Circ Res* **89**, 614-622.

Luscher TF & Barton M (2000). Endothelins and endothelin receptor antagonists: therapeutic considerations for a novel class of cardiovascular drugs. *Circulation* **102**, 2434-2440.

Lytton J, Westlin M, & Hanley MR (1991). Thapsigargin inhibits the sarcoplasmic or endoplasmic reticulum Ca-ATPase family of calcium pumps. *J Biol Chem* **266**, 17067-17071.

Maddali KK, Korzick DH, Tharp DL, & Bowles DK (2005). PKCδ mediates testosterone-induced increases in coronary smooth muscle $Ca_V1.2$. *J Biol Chem* **280**, 43024-43029.

Maeda S, Miyauchi T, Kobayashi T, Goto K, & Matsuda M (1998). Exercise causes tissue-specific enhancement of endothelin-1 mRNA expression in internal organs. *J Appl Physiol* **85**, 425-431.

Maruyama Y, Nakanishi Y, Walsh EJ, Wilson DP, Welsh DG, & Cole WC (2006). Heteromultimeric TRPC6-TRPC7 channels contribute to arginine vasopressin-induced cation current of A7r5 vascular smooth muscle cells. *Circ Res* **98**, 1520-1527.

Masaki T (2004). Historical review: Endothelin. *Trends Pharmacol Sci* **25**, 219-224.

Matlib MA, Zhou Z, Knight S, Ahmed S, Choi KM, Krause-Bauer J, Phillips R, Altschuld R, Katsube Y, Sperelakis N, & Bers DM (1998). Oxygen-bridged dinuclear ruthenium amine complex specifically inhibits Ca^{2+} uptake into mitochondria *in vitro* and *in situ* in single cardiac myocytes. *J Biol Chem* **273**, 10223-10231.

Mauban JR, Lamont C, Balke CW, & Wier WG (2001). Adrenergic stimulation of rat resistance arteries affects Ca^{2+} sparks, Ca^{2+} waves, and Ca^{2+} oscillations. *Am J Physiol Heart Circ Physiol* **280**, H2399-H2405.

McCarron JG, Chalmers S, Bradley KN, MacMillan D, & Muir TC (2006). Ca^{2+} microdomains in smooth muscle. *Cell Calcium* **40**, 461-493.

McCarron JG & Muir TC (1999). Mitochondrial regulation of the cytosolic Ca^{2+} concentration and the $InsP_3$-sensitive Ca^{2+} store in guinea-pig colonic smooth muscle. *J Physiol* **516 Pt 1**, 149-161.

Miller FJ, Jr., Filali M, Huss GJ, Stanic B, Chamseddine A, Barna TJ, & Lamb FS (2007). Cytokine activation of nuclear factor κB in vascular smooth muscle cells requires signaling endosomes containing Nox1 and ClC-3. *Circ Res* **101**, 663-671.

Miriel VA, Mauban JR, Blaustein MP, & Wier WG (1999). Local and cellular Ca^{2+} transients in smooth muscle of pressurized rat resistance arteries during myogenic and agonist stimulation. *J Physiol* **518**, 815-824.

Monteith GR & Blaustein MP (1999). Heterogeneity of mitochondrial matrix free Ca^{2+}: resolution of Ca^{2+} dynamics in individual mitochondria *in situ*. *Am J Physiol* **276**, C1193-C1204.

Montero M, Lobaton CD, Hernandez-Sanmiguel E, Santodomingo J, Vay L, Moreno A, & Alvarez J (2004). Direct activation of the mitochondrial calcium uniporter by natural plant flavonoids. *Biochem J* **384**, 19-24.

Moreau B, Nelson C, & Parekh AB (2006). Biphasic regulation of mitochondrial Ca^{2+} uptake by cytosolic Ca^{2+} concentration. *Curr Biol* **16**, 1672-1677.

Morey AK, Razandi M, Pedram A, Hu RM, Prins BA, & Levin ER (1998). Oestrogen and progesterone inhibit the stimulated production of endothelin-1. *Biochem J* **330 Pt 3**, 1097-1105.

Mueller CF, Laude K, McNally JS, & Harrison DG (2005). ATVB in focus: redox mechanisms in blood vessels. *Arterioscler Thromb Vasc Biol* **25**, 274-278.

Narayanan D, Xi Q, Pfeffer LM, & Jaggar JH (2010). Mitochondria control functional $Ca_V1.2$ expression in smooth muscle cells of cerebral arteries. *Circ Res* **107**, 631-641.

Navedo MF, Amberg GC, Nieves M, Molkentin JD, & Santana LF (2006). Mechanisms underlying heterogeneous Ca^{2+} sparklet activity in arterial smooth muscle. *J Gen Physiol* **127**, 611-622.

Navedo MF, Amberg GC, Votaw VS, & Santana LF (2005). Constitutively active L-type Ca^{2+} channels. *Proc Natl Acad Sci USA* **102**, 11112-11117.

Navedo MF, Nieves-Cintron M, Amberg GC, Yuan C, Votaw VS, Lederer WJ, McKnight GS, & Santana LF (2008). AKAP150 is required for stuttering persistent Ca^{2+} sparklets and angiotensin II-induced hypertension. *Circ Res* **102**, E1-E11.

Navedo MF, Takeda Y, Nieves-Cintron M, Molkentin JD, & Santana LF (2010). Elevated Ca^{2+} sparklet activity during acute hyperglycemia and diabetes in cerebral arterial smooth muscle cells. *Am J Physiol Cell Physiol* **298**, C211-C220.

Negre-Salvayre A, Hirtz C, Carrera G, Cazenave R, Troly M, Salvayre R, Penicaud L, & Casteilla L (1997). A role for uncoupling protein-2 as a regulator of mitochondrial hydrogen peroxide generation. *FASEB J* **11**, 809-815.

Nelson MT, Cheng H, Rubart M, Santana LF, Bonev AD, Knot HJ, & Lederer WJ (1995). Relaxation of arterial smooth muscle by calcium sparks. *Science* **270**, 633-637.

Nelson MT, Standen NB, Brayden JE, & Worley JF, III (1988). Noradrenaline contracts arteries by activating voltage-dependent calcium channels. *Nature* **336**, 382-385.

Nieves-Cintron M, Amberg GC, Navedo MF, Molkentin JD, & Santana LF (2008). The control of Ca^{2+} influx and NFATc3 signaling in arterial smooth muscle during hypertension. *Proc Natl Acad Sci USA* **105**, 15623-15628.

Nieves-Cintron M, Amberg GC, Nichols CB, Molkentin JD, & Santana LF (2007). Activation of NFATc3 down-regulates the β1 subunit of large conductance, calcium-activated K^+ channels in arterial smooth muscle and contributes to hypertension. *J Biol Chem* **282**, 3231-3240.

Nishio E & Watanabe Y (1997). The involvement of reactive oxygen species and arachidonic acid in alpha 1-adrenoceptor-induced smooth muscle cell proliferation and migration. *Br J Pharmacol* **121**, 665-670.

Ogita H & Liao J (2004). Endothelial function and oxidative stress. *Endothelium* **11**, 123-132.

Okuda M, Lee HC, Kumar C, & Chance B (1992). Comparison of the effect of a mitochondrial uncoupler, 2,4-dinitrophenol and adrenaline on oxygen radical production in the isolated perfused rat liver. *Acta Physiol Scand* **145**, 159-168.

Oliveira-Marques V, Marinho HS, Cyrne L, & Antunes F (2009). Role of hydrogen peroxide in NF-κB activation: from inducer to modulator. *Antioxid Redox Signal* **11**, 2223-2243.

Olson ML, Chalmers S, & McCarron JG (2010). Mitochondrial Ca^{2+} uptake increases Ca^{2+} release from inositol 1,4,5-trisphosphate receptor clusters in smooth muscle cells. *J Biol Chem* **285**, 2040-2050.

Pacher P, Sharma K, Csordas G, Zhu Y, & Hajnoczky G (2008). Uncoupling of ER-mitochondrial calcium communication by transforming growth factor-β. *Am J Physiol Renal Physiol* **295**, F1303-F1312.

Pacher P, Thomas AP, & Hajnoczky G (2002). Ca^{2+} marks: miniature calcium signals in single mitochondria driven by ryanodine receptors. *Proc Natl Acad Sci USA* **99**, 2380-2385.

Paravicini TM & Touyz RM (2006). Redox signaling in hypertension. *Cardiovasc Res* **71**, 247-258.

Parfenova H & Leffler CW (2008). Cerebroprotective functions of HO-2. *Curr Pharm Des* **14**, 443-453.

Paria BC, Bair AM, Xue J, Yu Y, Malik AB, & Tiruppathi C (2006). Ca^{2+} influx induced by protease-activated receptor-1 activates a feed-forward mechanism of TRPC1 expression via nuclear factor-κB activation in endothelial cells. *J Biol Chem* **281**, 20715-20727.

Parlapiano C, Paoletti V, Campana E, Giovanniello T, Pantone P, Labbadia G, Califano F, Donnarumma L, & Musca A (1999). CGRP and ET-1 plasma levels in normal subjects. *Eur Rev Med Pharmacol Sci* **3**, 139-141.

Patterson RL, Boehning D, & Snyder SH (2004). Inositol 1,4,5-trisphosphate receptors as signal integrators. *Annu Rev Biochem* **73**, 437-465.

Perez GJ, Bonev AD, & Nelson MT (2001). Micromolar Ca^{2+} from sparks activates Ca^{2+}-sensitive K^+ channels in rat cerebral artery smooth muscle. *Am J Physiol Cell Physiol* **281**, C1769-C1775.

Pernow J, Bohm F, Johansson BL, Hedin U, & Ryden L (2000). Enhanced vasoconstrictor response to endothelin-B-receptor stimulation in patients with atherosclerosis. *J Cardiovasc Pharmacol* **36**, S418-S420.

Pesic A, Madden JA, Pesic M, & Rusch NJ (2004). High blood pressure upregulates arterial L-type Ca^{2+} channels: is membrane depolarization the signal? *Circ Res* **94**, E97-E104.

Petronilli V, Cola C, Massari S, Colonna R, & Bernardi P (1993). Physiological effectors modify voltage sensing by the cyclosporin A-sensitive permeability transition pore of mitochondria. *J Biol Chem* **268**, 21939-21945.

Petronilli V, Miotto G, Canton M, Brini M, Colonna R, Bernardi P, & Di LF (1999). Transient and long-lasting openings of the mitochondrial permeability transition pore can be monitored directly in intact cells by changes in mitochondrial calcein fluorescence. *Biophys J* **76**, 725-734.

Pitts KR, Yoon Y, Krueger EW, & McNiven MA (1999). The dynamin-like protein DLP1 is essential for normal distribution and morphology of the endoplasmic reticulum and mitochondria in mammalian cells. *Mol Biol Cell* **10**, 4403-4417.

Plant TD & Schaefer M (2003). TRPC4 and TRPC5: receptor-operated Ca^{2+}-permeable nonselective cation channels. *Cell Calcium* **33**, 441-450.

Poburko D, Lee CH, & van Breemen C (2004). Vascular smooth muscle mitochondria at the cross roads of Ca^{2+} regulation. *Cell Calcium* **35**, 509-521.

Poburko D, Liao CH, van Breemen C, & Demaurex N (2009). Mitochondrial regulation of sarcoplasmic reticulum Ca^{2+} content in vascular smooth muscle cells. *Circ Res* **104**, 104-112.

Poot M, Zhang YZ, Kramer JA, Wells KS, Jones LJ, Hanzel DK, Lugade AG, Singer VL, & Haugland RP (1996). Analysis of mitochondrial morphology and function with novel fixable fluorescent stains. *J Histochem Cytochem* **44**, 1363-1372.

Quednau BD, Nicoll DA, & Philipson KD (1997). Tissue specificity and alternative splicing of the Na^{+}/Ca^{2+} exchanger isoforms NCX1, NCX2, and NCX3 in rat. *Am J Physiol* **272**, C1250-C1261.

Ralevic V & Burnstock G (1998). Receptors for purines and pyrimidines. *Pharmacol Rev* **50**, 413-492.

Rapizzi E, Pinton P, Szabadkai G, Wieckowski MR, Vandecasteele G, Baird G, Tuft RA, Fogarty KE, & Rizzuto R (2002). Recombinant expression of the voltage-dependent anion channel enhances the transfer of Ca^{2+} microdomains to mitochondria. *J Cell Biol* **159**, 613-624.

Ray R & Shah AM (2005). NAD(P)H oxidase and endothelial cell function. *Clin Sci (Lond)* **109**, 217-226.

Rey FE, Cifuentes ME, Kiarash A, Quinn MT, & Pagano PJ (2001). Novel competitive inhibitor of NAD(P)H oxidase assembly attenuates vascular O^{2-} and systolic blood pressure in mice. *Circ Res* **89**, 408-414.

Rizzuto R, Bernardi P, & Pozzan T (2000). Mitochondria as all-round players of the calcium game. *J Physiol* **529 Pt 1**, 37-47.

Rizzuto R, Brini M, Murgia M, & Pozzan T (1993). Microdomains with high Ca^{2+} close to IP_3-sensitive channels that are sensed by neighboring mitochondria. *Science* **262**, 744-747.

Rizzuto R, Duchen MR, & Pozzan T (2004). Flirting in little space: the ER/mitochondria Ca^{2+} liaison. *Sci STKE* **2004**, re1.

Rizzuto R, Marchi S, Bonora M, Aguiari P, Bononi A, De Stefani D, Giorgi C, Leo S, Rimessi A, Siviero R, Zecchini E, & Pinton P (2009). Ca^{2+} transfer from the ER to mitochondria: when, how and why. *Biochim Biophys Acta* **1787**, 1342-1351.

Rizzuto R, Pinton P, Brini M, Chiesa A, Filippin L, & Pozzan T (1999). Mitochondria as biosensors of calcium microdomains. *Cell Calcium* **26**, 193-199.

Rizzuto R & Pozzan T (2006). Microdomains of intracellular Ca^{2+}: molecular determinants and functional consequences. *Physiol Rev* **86**, 369-408.

Rosendorff C (1997). Endothelin, vascular hypertrophy, and hypertension. *Cardiovasc Drugs Ther* **10**, 795-802.

Ruegg UT, Wallnofer A, Weir S, & Cauvin C (1989). Receptor-operated calcium-permeable channels in vascular smooth muscle. *J Cardiovasc Pharmacol* **14 Suppl 6**, S49-S58.

Saada N, Dai B, Echetebu C, Sarna SK, & Palade P (2003). Smooth muscle uses another promoter to express primarily a form of human $Ca_V1.2$ L-type calcium channel different from the principal heart form. *Biochem Biophys Res Commun* **302**, 23-28.

Sakuma S, Fujimoto Y, Sakamoto Y, Uchiyama T, Yoshioka K, Nishida H, & Fujita T (1997). Peroxynitrite induces the conversion of xanthine dehydrogenase to oxidase in rabbit liver. *Biochem Biophys Res Commun* **230**, 476-479.

Sanchez R, MacKenzie A, Farhat N, Nguyen TD, Stewart DJ, Mercier I, Calderone A, & Thorin E (2002). Endothelin B receptor-mediated regulation of endothelin-1 content and release in cultured porcine aorta endothelial cell. *J Cardiovasc Pharmacol* **39**, 652-659.

Sanders KM (2001). Invited review: mechanisms of calcium handling in smooth muscles. *J Appl Physiol* **91**, 1438-1449.

Santana LF & Navedo MF (2009). Molecular and biophysical mechanisms of Ca^{2+} sparklets in smooth muscle. *J Mol Cell Cardiol* **47**, 436-444.

Santini MP, Talora C, Seki T, Bolgan L, & Dotto GP (2001). Cross talk among calcineurin, Sp1/Sp3, and NFAT in control of $p21^{WAF1/CIP1}$ expression in keratinocyte differentiation. *Proc Natl Acad Sci USA* **98**, 9575-9580.

Sato H, Sato M, Kanai H, Uchiyama T, Iso T, Ohyama Y, Sakamoto H, Tamura J, Nagai R, & Kurabayashi M (2005). Mitochondrial reactive oxygen species and c-Src play a critical role in hypoxic response in vascular smooth muscle cells. *Cardiovasc Res* **67**, 714-722.

Sawada H, Mitani Y, Maruyama J, Jiang BH, Ikeyama Y, Dida FA, Yamamoto H, Imanaka-Yoshida K, Shimpo H, Mizoguchi A, Maruyama K, & Komada Y (2007). A nuclear factor-κB inhibitor pyrrolidine dithiocarbamate ameliorates pulmonary hypertension in rats. *Chest* **132**, 1265-1274.

Scaduto RC, Jr. & Grotyohann LW (1999). Measurement of mitochondrial membrane potential using fluorescent rhodamine derivatives. *Biophys J* **76**, 469-477.

Schuh K, Uldrijan S, Telkamp M, Rothlein N, & Neyses L (2001). The plasmamembrane calmodulin-dependent calcium pump: a major regulator of nitric oxide synthase I. *J Cell Biol* **155**, 201-205.

Schumacker PT (2003). Current paradigms in cellular oxygen sensing. *Adv Exp Med Biol* **543**, 57-71.

Senftleben U, Cao Y, Xiao G, Greten FR, Krahn G, Bonizzi G, Chen Y, Hu Y, Fong A, Sun SC, & Karin M (2001). Activation by IKKα of a second, evolutionary conserved, NF-κB signaling pathway. *Science* **293**, 1495-1499.

Sharma VK, Ramesh V, Franzini-Armstrong C, & Sheu SS (2000). Transport of Ca^{2+} from sarcoplasmic reticulum to mitochondria in rat ventricular myocytes. *J Bioenerg Biomembr* **32**, 97-104.

Shatrov VA, Lehmann V, & Chouaib S (1997). Sphingosine-1-phosphate mobilizes intracellular calcium and activates transcription factor NF-κB in U937 cells. *Biochem Biophys Res Commun* **234**, 121-124.

Shi XZ, Choudhury BK, Pasricha PJ, & Sarna SK (2007). A novel role of VIP in colonic motility function: induction of excitation-transcription coupling in smooth muscle cells. *Gastroenterology* **132**, 1388-1400.

Shi XZ, Pazdrak K, Saada N, Dai B, Palade P, & Sarna SK (2005). Negative transcriptional regulation of human colonic smooth muscle $Ca_V1.2$ channels by p50 and p65 subunits of nuclear factor-κB. *Gastroenterology* **129**, 1518-1532.

Shichiri M, Hirata Y, Ando K, Emori T, Ohta K, Kimoto S, Ogura M, Inoue A, & Marumo F (1990). Plasma endothelin levels in hypertension and chronic renal failure. *Hypertension* **15**, 493-496.

Shimamura K, Sekiguchi F, & Sunano S (1999). Tension oscillation in arteries and its abnormality in hypertensive animals. *Clin Exp Pharmacol Physiol* **26**, 275-284.

Simard JM & Li X (2000). Functional integrity of endothelium determines Ca^{2+} channel availability in smooth muscle: involvement of nitric oxide. *Pflugers Arch* **439**, 752-758.

Simpson PB, Mehotra S, Lange GD, & Russell JT (1997). High density distribution of endoplasmic reticulum proteins and mitochondria at specialized Ca^{2+} release sites in oligodendrocyte processes. *J Biol Chem* **272**, 22654-22661.

Sitsapesan R, McGarry SJ, & Williams AJ (1995). Cyclic ADP-ribose, the ryanodine receptor and Ca^{2+} release. *Trends Pharmacol Sci* **16**, 386-391.

Souza HP, Souza LC, Anastacio VM, Pereira AC, Junqueira ML, Krieger JE, da Luz PL, Augusto O, & Laurindo FR (2000). Vascular oxidant stress early after balloon injury: evidence for increased NAD(P)H oxidoreductase activity. *Free Radic Biol Med* **28**, 1232-1242.

Spat A, Szanda G, Csordas G, & Hajnoczky G (2008). High- and low-calcium-dependent mechanisms of mitochondrial calcium signalling. *Cell Calcium* **44**, 51-63.

Starkov AA & Fiskum G (2003). Regulation of brain mitochondrial H_2O_2 production by membrane potential and NAD(P)H redox state. *J Neurochem* **86**, 1101-1107.

Stewart DJ, Kubac G, Costello KB, & Cernacek P (1991a). Increased plasma endothelin-1 in the early hours of acute myocardial infarction. *J Am Coll Cardiol* **18**, 38-43.

Stewart DJ, Levy RD, Cernacek P, & Langleben D (1991b). Increased plasma endothelin-1 in pulmonary hypertension: marker or mediator of disease? *Ann Intern Med* **114**, 464-469.

Sun Z & Andersson R (2002). NF-κB activation and inhibition: a review. *Shock* **18**, 99-106.

Sward K, Dreja K, Lindqvist A, Persson E, & Hellstrand P (2002). Influence of mitochondrial inhibition on global and local $[Ca^{2+}]_i$ in rat tail artery. *Circ Res* **90**, 792-799.

Szabadkai G, Bianchi K, Varnai P, De Stefani D, Wieckowski MR, Cavagna D, Nagy AI, Balla T, & Rizzuto R (2006). Chaperone-mediated coupling of endoplasmic reticulum and mitochondrial Ca^{2+} channels. *J Cell Biol* **175**, 901-911.

Szado T, Kuo KH, Bernard-Helary K, Poburko D, Lee CH, Seow C, Ruegg UT, & van Breemen C (2003). Agonist-induced mitochondrial Ca^{2+} transients in smooth muscle. *FASEB J* **17**, 28-37.

Takada Y, Mukhopadhyay A, Kundu GC, Mahabeleshwar GH, Singh S, & Aggarwal BB (2003). Hydrogen peroxide activates NF-κB through tyrosine phosphorylation of IκBα and serine phosphorylation of p65: evidence for the involvement of IκBα kinase and Syk protein-tyrosine kinase. *J Biol Chem* **278**, 24233-24241.

Takei K, Stukenbrok H, Metcalf A, Mignery GA, Sudhof TC, Volpe P, & De Camilli P (1992). Ca^{2+} stores in Purkinje neurons: endoplasmic reticulum subcompartments demonstrated by the heterogeneous distribution of the $InsP_3$ receptor, Ca^{2+}-ATPase, and calsequestrin. *J Neurosci* **12**, 489-505.

Tan W & Colombini M (2007). VDAC closure increases calcium ion flux. *Biochim Biophys Acta* **1768**, 2510-2515.

Tang ZZ, Liang MC, Lu S, Yu D, Yu CY, Yue DT, & Soong TW (2004). Transcript scanning reveals novel and extensive splice variations in human L-type voltage-gated calcium channel, $Ca_V1.2$ α_1 subunit. *J Biol Chem* **279**, 44335-44343.

Ten RM, Paya CV, Israel N, Le BO, Mattei MG, Virelizier JL, Kourilsky P, & Israel A (1992). The characterization of the promoter of the gene encoding the p50 subunit of NF-κB indicates that it participates in its own regulation. *EMBO J* **11**, 195-203.

Thiel G, Mayer SI, Muller I, Stefano L, & Rossler OG (2010). Egr-1-A Ca^{2+}-regulated transcription factor. *Cell Calcium* **47**, 397-403.

Touyz RM, Chen X, Tabet F, Yao G, He G, Quinn MT, Pagano PJ, & Schiffrin EL (2002). Expression of a functionally active $gp91^{phox}$-containing neutrophil-type NAD(P)H oxidase in smooth muscle cells from human resistance arteries: regulation by angiotensin II. *Circ Res* **90**, 1205-1213.

Touyz RM & Schiffrin EL (2000). Signal transduction mechanisms mediating the physiological and pathophysiological actions of angiotensin II in vascular smooth muscle cells. *Pharmacol Rev* **52**, 639-672.

Touyz RM & Schiffrin EL (2008). Reactive oxygen species and hypertension: a complex association. *Antioxid Redox Signal* **10**, 1041-1044.

Trenker M, Malli R, Fertschai I, Levak-Frank S, & Graier WF (2007). Uncoupling proteins 2 and 3 are fundamental for mitochondrial Ca^{2+} uniport. *Nat Cell Biol* **9**, 445-452.

Triggle DJ (2006). L-type calcium channels. *Curr Pharm Des* **12**, 443-457.

Trollinger DR, Cascio WE, & Lemasters JJ (2000). Mitochondrial calcium transients in adult rabbit cardiac myocytes: inhibition by ruthenium red and artifacts caused by lysosomal loading of Ca^{2+}-indicating fluorophores. *Biophys J* **79**, 39-50.

Turrens JF (2003). Mitochondrial formation of reactive oxygen species. *J Physiol* **552**, 335-344.

Vaithianathan T, Narayanan D, Asuncion-Chin MT, Jeyakumar LH, Liu J, Fleischer S, Jaggar JH, & Dopico AM (2010). Subtype identification and functional characterization of ryanodine receptors in rat cerebral artery myocytes. *Am J Physiol Cell Physiol* **299**, C264-C278.

Vangheluwe P, Schuermans M, Zador E, Waelkens E, Raeymaekers L, & Wuytack F (2005). Sarcolipin and phospholamban mRNA and protein expression in cardiac and skeletal muscle of different species. *Biochem J* **389**, 151-159.

Wackenfors A, Emilson M, Ingemansson R, Hortobagyi T, Szok D, Tajti J, Vecsei L, Edvinsson L, & Malmsjo M (2004). Ischemic heart disease induces upregulation of endothelin receptor mRNA in human coronary arteries. *Eur J Pharmacol* **484**, 103-109.

Wang H, Liu J, & Wu L (2009). Methylglyoxal-induced mitochondrial dysfunction in vascular smooth muscle cells. *Biochem Pharmacol* **77**, 1709-1716.

Wang HD, Pagano PJ, Du Y, Cayatte AJ, Quinn MT, Brecher P, & Cohen RA (1998). Superoxide anion from the adventitia of the rat thoracic aorta inactivates nitric oxide. *Circ Res* **82**, 810-818.

Wang Q, Hogg RC, & Large WA (1992). Properties of spontaneous inward currents recorded in smooth muscle cells isolated from the rabbit portal vein. *J Physiol* **451**, 525-537.

Wang W, Fang H, Groom L, Cheng A, Zhang W, Liu J, Wang X, Li K, Han P, Zheng M, Yin J, Wang W, Mattson MP, Kao JP, Lakatta EG, Sheu SS, Ouyang K, Chen J, Dirksen RT, & Cheng H (2008a). Superoxide flashes in single mitochondria. *Cell* **134**, 279-290.

Wang WZ, Pang L, & Palade P (2008b). Angiotensin II causes endothelial-dependent increase in expression of $Ca_V1.2$ protein in cultured arteries. *Eur J Pharmacol* **599**, 117-120.

Wang WZ, Saada N, Dai B, Pang L, & Palade P (2006). Vascular-specific increase in exon 1B-encoded $Ca_v1.2$ channels in spontaneously hypertensive rats. *Am J Hypertens* **19**, 823-831.

Wang YX, Zheng YM, Abdullaev I, & Kotlikoff MI (2003). Metabolic inhibition with cyanide induces calcium release in pulmonary artery myocytes and Xenopus oocytes. *Am J Physiol Cell Physiol* **284**, C378-C388.

Wedgwood S, Dettman RW, & Black SM (2001). ET-1 stimulates pulmonary arterial smooth muscle cell proliferation via induction of reactive oxygen species. *Am J Physiol Lung Cell Mol Physiol* **281**, L1058-L1067.

Wellman GC & Nelson MT (2003). Signaling between SR and plasmalemma in smooth muscle: sparks and the activation of Ca^{2+}-sensitive ion channels. *Cell Calcium* **34**, 211-229.

Welsh DG, Morielli AD, Nelson MT, & Brayden JE (2002). Transient receptor potential channels regulate myogenic tone of resistance arteries. *Circ Res* **90**, 248-250.

Wilkerson MK, Heppner TJ, Bonev AD, & Nelson MT (2006). Inositol trisphosphate receptor calcium release is required for cerebral artery smooth muscle cell proliferation. *Am J Physiol Heart Circ Physiol* **290**, H240-H247.

Wolin MS, Ahmad M, & Gupte SA (2005). Oxidant and redox signaling in vascular oxygen sensing mechanisms: basic concepts, current controversies, and potential importance of cytosolic NAD(P)H. *Am J Physiol Lung Cell Mol Physiol* **289**, L159-L173.

Wong RK, Pettit AI, Quinn PA, Jennings SC, Davies JE, & Ng LL (2003). Advanced glycation end products stimulate an enhanced neutrophil respiratory burst mediated through the activation of cytosolic phospholipase A2 and generation of arachidonic acid. *Circulation* **108**, 1858-1864.

Worley PF, Baraban JM, Supattapone S, Wilson VS, & Snyder SH (1987). Characterization of inositol trisphosphate receptor binding in brain. Regulation by pH and calcium. *J Biol Chem* **262**, 12132-12136.

Wray S & Burdyga T (2010). Sarcoplasmic reticulum function in smooth muscle. *Physiol Rev* **90**, 113-178.

Wray S, Burdyga T, & Noble K (2005). Calcium signalling in smooth muscle. *Cell Calcium* **38**, 397-407.

Wu KD, Bungard D, & Lytton J (2001). Regulation of SERCA Ca^{2+} pump expression by cytoplasmic Ca^{2+} in vascular smooth muscle cells. *Am J Physiol Cell Physiol* **280**, C843-C851.

Xi Q, Adebiyi A, Zhao G, Chapman KE, Waters CM, Hassid A, & Jaggar JH (2008). IP_3 constricts cerebral arteries via IP_3 receptor-mediated TRPC3 channel activation and independently of sarcoplasmic reticulum Ca^{2+} release. *Circ Res* **102**, 1118-1126.

Xi Q, Cheranov SY, & Jaggar JH (2005). Mitochondria-derived reactive oxygen species dilate cerebral arteries by activating Ca^{2+} sparks. *Circ Res* **97**, 354-362.

Xu CB, Zheng JP, Zhang W, Zhang Y, & Edvinsson L (2008). Lipid-soluble smoke particles upregulate vascular smooth muscle ET_B receptors via activation of mitogen-activating protein kinases and NF-κB pathways. *Toxicol Sci* **106**, 546-555.

Yatomi Y (2006). Sphingosine 1-phosphate in vascular biology: possible therapeutic strategies to control vascular diseases. *Curr Pharm Des* **12**, 575-587.

Zangar RC, Davydov DR, & Verma S (2004). Mechanisms that regulate production of reactive oxygen species by cytochrome P450. *Toxicol Appl Pharmacol* **199**, 316-331.

Zhang WM, Yip KP, Lin MJ, Shimoda LA, Li WH, & Sham JS (2003). ET-1 activates Ca^{2+} sparks in PASMC: local Ca^{2+} signaling between inositol trisphosphate and ryanodine receptors. *Am J Physiol Lung Cell Mol Physiol* **285**, L680-L690.

Zhao G, Adebiyi A, Blaskova E, Xi Q, & Jaggar JH (2008). Type 1 inositol 1,4,5-trisphosphate receptors mediate UTP-induced cation currents, Ca^{2+} signals, and vasoconstriction in cerebral arteries. *Am J Physiol Cell Physiol* **295**, C1376-C1384.

Zhu ZG, Wang MS, Jiang ZB, Jiang Z, Xu SX, Ren CY, & Shi MX (1994). The dynamic change of plasma endothelin-1 during the perioperative period in patients with rheumatic valvular disease and secondary pulmonary hypertension. *J Thorac Cardiovasc Surg* **108**, 960-968.

Zhuge R, Fogarty KE, Tuft RA, & Walsh JV, Jr. (2002). Spontaneous transient outward currents arise from microdomains where BK channels are exposed to a mean Ca^{2+} concentration on the order of 10 μM during a Ca^{2+} spark. *J Gen Physiol* **120**, 15-27.

Zou AP, Ma YH, Sui ZH, Ortiz De Montellano PR, Clark JE, Masters BS, & Roman RJ (1994). Effects of 17-octadecynoic acid, a suicide-substrate inhibitor of cytochrome P450 fatty acid ω-hydroxylase, on renal function in rats. *J Pharmacol Exp Ther* **268**, 474-481.

VITA

Damodaran Narayanan was born on December 25, 1979 in Chennai, India. He graduated from high school in 1997. He obtained his Bachelor of Medicine, Bachelor of Surgery (M.B.,B.S.) degree from Madras Medical College, affiliated to The Tamil Nadu Dr. M.G.R. Medical University in June 2004. He joined the Integrated Program in Biomedical Sciences (IPBS) at the University of Tennessee Health Science Center (UTHSC), Memphis in August 2005. He is a member of American Physiological Society and a founding member of Tennessee Physiological Society. He received the Dorothy K. and Daniel L. Gerwin Graduate Scholarship, awarded to the most outstanding Ph.D. student from the Department of Physiology, UTHSC in July 2008. He was also a recipient of a predoctoral fellowship (July 2009 – June 2010) from the American Heart Association (Greater Southeast Affiliate). He has also received two travel awards (John Autian Student Enrichment Fund) in 2009 and 2010 from the College of Graduate Health Sciences, UTHSC to present his research at Experimental Biology Meeting, an international scientific research conference. He was also awarded for best poster presentation by a senior Ph.D. graduate student at the Graduate Research Day, UTHSC in 2009 and 2010. He was awarded his Ph.D. in December 2010.